Human centered assistive control strategies for lower limb wearable robotic devices

Mohamed Amine Alouane

UNIVERSITÉ PARIS-EST

École Doctorale MSTIC

Laboratoire Images, Signaux et Systèmes Intelligents

Thèse

Présentée pour l'obtention du grade de

Docteur de l'Université Paris Est

En "Robotique, Automatique"

par

Mohamed Amine ALOUANE

Commandes orientées assistance d'un exosquelette de membres inférieurs

Human centered assistive control strategies for lower limb wearable robotic devices

Soutenue le: 23/10/2020

Devant le jury composé de:

Mr. Antoine FERREIRA,	Rapporteur	Professeur, INSA Centre Val de Loire, France
Mr. Yannick AOUSTIN,	Rapporteur	Professeur, Université de Nantes, France
Mrs. Véronique PERDEREAU,	Président du jury	Professeure, Sorbonne Université, France
Mr. Mohamed GUIATNI,	Examinateur	Professeur, Ecole Militaire Polytechnique, Algerie
Mrs. Hala RIFAI,	Examinateur	Maîtresse de conférence, Université Paris Est Créteil (UPEC), France
Mr. Samer MOHAMMED,	Co-directeur de thèse	Professeur, Université Paris Est Créteil (UPEC), France
Mr. Yacine AMIRAT,	Directeur de thèse	Professeur, Université Paris Est Créteil (UPEC), France

Abstract

REHABILITATION engineering and assistive technologies are emerging as promising solutions to develop support systems to improve elderly and post-stroke people's independence when performing daily living activities such as walking, sitting down, getting up, ascending/descending stairs, etc. In the last years, many research projects were carried out worldwide to develop exoskeletons/orthoses intended to assist mobility, increase motor abilities of human subjects, or to be used as auxiliary devices for neuromuscular rehabilitation. Developing control strategies of human-in-the-loop robotic systems such as exoskeletons is an important challenge in robotics community. These strategies must guarantee good performance in terms of tracking accuracy, robustness with respect to parametric uncertainties, variability between subjects and external disturbances. At the same time, it should account for the wearer's motor ability and/or intention while ensuring his/her safety. In the context of rehabilitation, in addition to the wearable robot solutions, Functional Electrical Stimulation (FES) is another technology that allows to recover mobility and relative independence for injured people. However, this rehabilitation technology has limitations related to muscular fatigue, which leads to the use of FES for a short time and short-time ambulation. To overcome the above-mentioned drawbacks of FES and limit the patient's dependency on the use of wearable robots, hybrid robotic systems exploiting both FES and exoskeletons/orthoses have been proposed in the literature for rehabilitation purposes. In this thesis, we propose different control strategies to assist lower limb movements using orthoses/exoskeletons and Functional Electrical Stimulation (FES). The first strategy consists of a proxy-NDO-based force controller for three human-robot interaction modes: zero-impedance mode, force tracking mode, and high torque mode. A two-mass dynamic model-based nonlinear disturbance observer is used, on the one hand, to guarantee zero-impedance output, accurate estimation of

possible disturbances from the wearer and environment sides, and on the other hand, to ensure the wearer's safety when the interaction torque is relatively high. The second strategy is based on a hybrid controller of a knee joint hybrid orthosis for knee joint flexion/extension movements restoration. The generated stimulation torque, considered as an external disturbance, is estimated using a Non-linear Disturbance Observer (NDO). The torque provided by the wearer is complemented by a controlled torque provided by the orthosis and applied in such a way to guarantee an accurate tracking of the knee joint reference position trajectory. The third developed control strategy is an impedance modulation-based control strategy to assist the wearer when performing Sit-to-Stand (STS) movements. The impedance modulation-based control consists of an impedance compensation-based control complemented with a balance reinforcement-based control. A time-varying desired impedance model is developed to provide appropriate power assistance according to the wearer's ability. The impedance compensation-based control structure includes also a human joint torque observer aimed at estimating the human joint torques, and a Sliding Mode-based Controller (SMC) to guarantee good tracking accuracy and robustness with respect to modeling uncertainties and external disturbances. The fourth control strategy consists of an assistance-as-needed hybrid controller intended to assist knee joint flexion/extension and STS movements. A NDO is used to estimate the human involvement in movement achievement through FES. The estimated human torque is exploited in an impedance controller to generate the desired trajectory that will be tracked using a position controller while ensuring the desired compliance. The proposed control strategies were evaluated in simulations and/or experiments using different lower limb orthosis/exoskeleton prototypes. Results showed satisfactory performance in terms of accuracy, robustness with respect to modeling uncertainties and external disturbances, as well as, the consideration of the wearer's motor ability and/or intention while ensuring his/her safety.

Keywords: Lower limb exoskeleton, Proxy-based controller, NDO, FES, wearable hybrid robotic systems, STS, Assistance as needed, Impedance controller.

Résumé

LES technologies de rééducation et d'assistance sont des solutions prometteuses pour développer des systèmes d'aide aux personnes âgées et les personnes ayant subi un accident vasculaire cérébral afin d'améliorer leur autonomie durant les activités de la vie quotidienne e.g. marcher, se lever, monter et descendre les escaliers, etc. Beaucoup de recherches sont menés pour le développement d'exosquelettes d'aide à la mobilité, d'augmentation des capacités motrices, ou d'aide à la réhabilitation. L'un des défis liés à la recherche dans le domaine des exosquelettes est l'élaboration de stratégies de commande. Considérant l'aspect cognitif et physique de l'interaction exosquelette/ sujet, les stratégies de commande devraient assurer à la fois la précision et la robustesse vis à vis des incertitudes de modélisation et des perturbations externes. Elles doivent aussi tenir compte de la capacité sensorimotrice du porteur, tout en assurant sa sécurité. En outre, la stimulation électrique fonctionnelle (FES) est aussi l'une des technologies de rééducation permettant aux personnes de retrouver leur mobilité. Toutefois, ces approches présentent des limites liées à l'apparition de la fatigue musculaire, cela conduit à l'utilisation de la FES en une courte durée et/ou sur de courtes distances. Pour surmonter les inconvénients de la FES et limiter la dépendance liée à l'utilisation d'orthèses, les intentions se sont tournées vers les exosquelettes/orthèses hybride, où la FES et les exosquelettes/orthèses sont utilisés. Dans cette thèse, nous avons proposé différentes stratégies de commande pour assister les mouvements des membres inférieurs en utilisant des orthèses/exosquelettes et la stimulation électrique fonctionnelle.

Aperçu de la thèse

La vue d'ensemble de l'organisation par chapitre de la these est donnee ci-dessous :

Le chapitre 1 présente le contexte général et la structure de la thèse et souligne les contributions du travail de recherche.

Dans le deuxième chapitre, on présente et analyse l'état de l'art de la recherche en robotique portable en mettant l'accent sur les exosquelettes des membres inférieurs. Les prototypes les plus pertinents de ces robots sont d'abord décrits du point de vue de la conception mécanique ; ces prototypes sont destinés à être utilisés soit pour l'augmentation de la puissance, la rééducation ou l'assistance. Les aspects importants liés au développement de robots portables, tels que le mode d'actionnement, la stratégie de commande et l'évaluation des performances, sont ensuite abordés. En outre, la technologie FES, couramment utilisée en rééducation, est décrite et analysée dans un contexte clinique. Les systèmes hybrides combinant la technologie FES et les robots portables, utilisés à des fins d'assistance/rééducation, sont ensuite présentés. Enfin, les stratégies de commande en boucle ouverte ou fermée couramment utilisées pour ces systèmes sont analysées et les principaux défis en matière de contrôle sont discutés.

Le chapitre 3 décrit d'abord les différents capteurs, actionneurs et prototypes de robots portables (orthèse EICOSI, exosquelette EROWA et exosquelette ANGELEGS) utilisés pour évaluer les performances des stratégies de commande proposées. Les modèles dynamiques de l'actionneur (SEA (Serial Elastic Actuator)) utilisé comme mode d'actionnement de l'exosquelette EROWA, et des prototypes susmentionnés, ainsi que l'identification de leurs paramètres sont ensuite présentés. La modélisation des prototypes est effectuée pour deux types de mouvements : les mouvements de flexion/extension de l'articulation du genou et les mouvements de transfère Assis-Debout (STS).

Dans le chapitre 4, une stratégie de commande basée sur le Proxy (PNC) est proposée pour trois modes d'interaction homme-robot : le mode à impédance nulle, le mode de suivi en couple et le mode à couple élevé. Cette stratégie exploite à la fois une commande par mode glissant basé sur un proxy (PSMC) et une commande PD (Proportionnel-Dérivé) basé sur un observateur de perturbations non linéaires (NDO) de l'actionneur (SEA) pour assurer un suivi précis en couple, une robustesse par rapport aux incertitudes de modélisation et aux perturbations externes, et la sécurité du porteur. La stabilité du contrôleur proposé est analysée et la performance de ce dernier est évaluée par des sim-

ulations et des expériences dans le cas des mouvements de l'articulation du genou de l'exosquelette EROWA.

Le chapitre 5 présente le développement d'une stratégie de commande hybride pour la restauration des mouvements de flexion/extension de l'articulation du genou. La description générale du contrôleur hybride est d'abord présentée en détaillant ses deux composantes, à savoir le contrôle de l'orthèse EICOSI et le contrôleur FES. La stratégie de commande proposée est conçue pour améliorer l'implication du sujet pendant les mouvements de flexion/extension de l'articulation du genou. Dans ce chapitre, nous avons également exploré l'utilisation d'un observateur de perturbations non linéaires pour l'estimation en ligne du couple de stimulation généré. Enfin, le protocole expérimental et les performances du contrôleur hybride évaluées par des simulations et des expériences, sont présentés et discutés.

Dans le chapitre 6, on étudie le développement d'une stratégie de commande basée sur la modulation d'impédance pour aider les personnes effectuant des mouvements assis-debout (STS). La première partie du chapitre détaille les deux composantes de la structure de commande, c'est-à-dire le contrôleur basé sur la compensation d'impédance et le contrôleur basé sur le renforcement de l'équilibre. Un observateur de couple articulaire humain (HJTO) est utilisé pour estimer les couples développés par le porteur et une commande par modes glissants (SMC) est exploité pour assurer un suivi précis de la position. En outre, un modèle d'impédance souhaitée variant dans le temps est proposé pour assurer une assistance appropriée en fonction de la capacité motrice du porteur. La robustesse de la stratégie de commande proposée en ce qui concerne les incertitudes de modélisation est également analysée. La deuxième partie du chapitre présente et analyse les performances de la stratégie de commande proposée en simulation et en expérimentation avec un sujet sain.

Dans le septième chapitre une stratégie de commande hybride d'assistance selon le besoin (AAN) combinant l'utilisation d'une commande en impédance de l'exosquelette/orthèse avec la stimulation électrique fonctionnelle (FES) du quadriceps est développée. Cette stratégie de commande est évaluée dans deux types d'activités : i) les mouvements de flexion/extension de l'articulation du genou, ii) les mouvements assis-debout. La commande en impédance de l'orthèse/exosquelette et la commande de

la FES sont d'abord conçus pour chaque activité. Dans la deuxième partie du chapitre, pour chaque activité, le protocole expérimental utilisé et la performance de la stratégie de commande proposée sont présentés et discutés.

Le chapitre 8 résume les contributions de la thèse et discute des orientations futures de la recherche.

Conclusions et perspectives

Les stratégies de commande proposées ont été évaluées dans des simulations et/ou des expériences utilisant différents prototypes d'orthèses de membres inférieurs/exosquelettes. Les résultats ont montré des performances satisfaisantes en termes de précision, de robustesse par rapport aux incertitudes de modélisation et aux perturbations externes, ainsi que la prise en compte de la capacité motrice et/ou de l'intention du porteur tout en assurant sa sécurité.

La première stratégie proposée est une commande en couple par proxy de l'actionneur SEA de l'exosquelette EROWA pour trois modes d'interaction homme-robot. Un modèle dynamique à deux masses basées sur un NDO est exploité dans la couche interne du PSMC (Proxy based Sliding Mode Controller) conventionnelle afin d'améliorer la robustesse du contrôleur en ce qui concerne les incertitudes liées à la modélisation et celles liée à l'environnement. En plus de l'amélioration de la précision du suivi en couple, cette stratégie garantit la sécurité du porteur en utilisant un modèle de compliance en couple qui varie en fonction du couple d'interaction entre le porteur et l'exosquelette au niveau de l'articulation du genou. La stratégie de commande proposée, évaluée par des simulations et des expériences, a permis d'obtenir une plus grande précision de suivi par rapport aux contrôleurs PID et PSMC tout en garantissant la sécurité du porteur face à des situations inattendues.

La deuxième stratégie consiste en un contrôleur hybride d'une orthèse hybride de l'articulation du genou pour la restauration des mouvements de flexion/extension. Le couple de stimulation généré, considéré comme une perturbation externe, est estimé à l'aide d'un Observateur de Perturbations Non-Linéaires (NDO). Le couple fourni par le porteur est complété par un couple de contrôle adaptatif fourni par l'orthèse. La stabil-

ité entrée-état de l'ensemble du système par rapport au couple de stimulation estimé a été prouvée théoriquement au sens de Lyapunov. La simulation et les résultats expérimentaux ont montré la capacité de l'estimateur proposé à estimer le couple de stimulation musculaire sans nécessiter une modélisation musculosquelettique relativement complexe ou l'utilisation de capteurs de force/couple supplémentaires. Ils ont également montré la capacité du contrôleur hybride proposé à assurer un suivi précis de la trajectoire désirée.

La troisième stratégie de commande est basée sur la compensation d'impédance, complété par une commande pour le renforcement de l'équilibre afin d'aider un sujet à effectuer des mouvements assis-debout (STS). Cette stratégie permet d'adapter l'impédance du système porteur/exosquelette à celle souhaitée en utilisant un observateur de couple articulaire humain et un modèle d'impédance désiré variable dans le temps. De plus, une commande par modes glissants (SMC) est utilisée pour fournir une assistance suffisante pour la réalisation de la tâche désirée. Le contrôle basé sur le renforcement de l'équilibre a été développé pour empêcher l'échec lors de la réalisation du mouvement de STS. Les caractéristiques et la robustesse de la stratégie proposée ont été théoriquement analysées en simulation. La performance de la stratégie de commande proposée est évaluée en simulation et par des expériences. Les résultats obtenus ont montré l'efficacité de la stratégie de commande proposée pour estimer les couples articulaires du porteur, réduire l'impédance du système porteur/exosquelette et fournir une assistance appropriée au porteur pour la réduction de l'effort humain et le renforcement de l'équilibre.

La quatrième stratégie consiste en une stratégie de commande hybride pour l'assistance au besoin. Deux études de cas ont été envisagées ; la première concerne l'utilisation d'une orthèse de l'articulation du genou pour assurer les mouvements de flexion/extension du genou et la seconde étude concerne l'utilisation de l'exosquelette EROWA pour l'assistance aux mouvements STS. Les résultats expérimentaux ont montré la capacité de la stratégie de commande proposée à retarder l'apparition de la fatigue musculaire, et l'avantage d'utiliser une stratégie hybride par rapport aux deux types d'assistance utilisés séparément : FES et/ou exosquelette/orthèse. La stratégie de commande proposée permet de réduire l'assistance requise de l'exosquelette pour effectuer

un mouvement tout en assurant une meilleure implication du sujet.

Sur la base des résultats obtenus dans cette thèse, nous pensons que les stratégies de commande proposées contribuent efficacement pour assurer un contrôle des exosquelettes des membres inférieurs d'une manière pour que ces derniers permettent d'assister les personnes dépendantes dans leurs activités de la vie quotidienne. Les stratégies proposées peuvent être étendues dans de futures travaux de recherche. Une perspective à court terme consistera à étudier d'autres stratégies de commande avancées dans la structure de la couche interne de la commande à base de proxy. Un défi intéressant à relever, spécifique aux stratégies de commande en impédance, consistera à développer des approches permettant, d'une part, d'identifier la compliance du système porteur/exosquelette pour une activité de la vie quotidienne donnée, l'interaction avec l'environnement, le niveau d'incertitude, etc. et, d'autre part, de déterminer les paramètres d'impédance optimaux.

Pour mieux caractériser le contexte de mouvement du porteur, une perspective prometteuse est le développement des stratégies de commande exploitant des algorithmes de détection des modes de la marche basés sur des algorithmes d'apprentissage (marche en palier, montée/descente d'escaliers, montée/descente de rampes, etc. Ce type d'approche présentera les avantages de fournir une détection relativement rapide de l'intention humaine ou du mode de la marche, et un contrôle efficace des robots portables pour fournir à l'utilisateur l'assistance requise sans effets de latence.

Afin d'améliorer les performances des stratégies de commande hybrides FES/Exosquelette, il est important de développer des méthodes d'estimation du couple induit par la FES ainsi que des modèles réalistes d'estimation de la fatigue musculaire ; pour ces deux objectifs, les algorithmes d'apprentissage sont potentiellement intéressants. En pratique, même si l'activité musculaire peut être facilement mesurée à l'aide de signaux EMG, l'utilisation de la FES rend ces signaux inutilisables en raison des artefacts induits par la FES et des interférences des signaux des muscles voisins. Le développement d'un algorithme de traitement des signaux EMG qui permet de capturer le signal entre les trains d'impulsions de stimulation est une solution alternative intéressante pour évaluer qualitativement l'estimation du couple induit par la FES obtenue à partir d'un NDO. De plus, l'utilisation de stratégies de commande en boucle fermée de la FES

permettra d'améliorer la précision de suivi ainsi que de retarder l'apparition de la fatigue musculaire. Cependant, l'utilisation d'une commande FES en boucle fermée génère un problème de redondance des actionneurs pour lequel les approches d'allocation dynamique des commandes sont des solutions intéressantes à étudier. Ces approches, basées sur des algorithmes d'optimisation avancés, permettent de répartir les couples d'assistance entre les actionneurs de manière à minimiser et à retarder l'apparition de la fatigue musculaire.

Les stratégies de commande proposées dans cette thèse ont été principalement évaluées par des expériences impliquant des sujets sains et ont montré leur efficacité. Cependant, des expériences avec des patients parétiques doivent être menées pour évaluer le potentiel de ces stratégies de commande dans un cadre clinique. Nous pensons que ces stratégies seront très bénéfiques pour la rééducation, car elles peuvent réduire les efforts humains nécessaires tout en permettant au sujet d'effectuer le même mouvement.

Contents

Chapter 1

General introduction

"The secret of getting ahead is getting started."

Mark Twain

STANDING up, walking, running are basic examples of daily living activities of most people. However, such activities are very challenging for some populations who cannot provide sufficient efforts to perform successfully the required motions; these people are either elderly, survived a stroke or suffer from a Spinal Cord Injury (SCI). Recent statistics show that between 2015 and 2050, the proportion of the world's population over 60 years will nearly double (12 % in 2015 to 22 % in 2050) [1]. Several studies show that stroke is one of the leading causes of disabilities in the world. By 2030, scientist are expecting a prevalence of stroke and other neurological diseases to reach 350 million of people, which is approximately 5 % of the world's population. Nowadays, strokes are increasing by about 1.5 million of new cases each year with 0.5 million survivors [2]. Estimations show that the annual incidence of SCI is approximately 250 000 and 500 000 in the world every year [3].

Rehabilitation engineering and assistive technologies offer different practical solutions to assist individuals suffering from different forms of disabilities and help them recovering their physical and cognitive functions lost due to diseases, injuries or muscular weaknesses. In this thesis, we propose different human centered control strategies for assisting lower limb movements through the use of orthoses/exoskeletons and Functional Electrical Stimulation (FES).

The present chapter introduces the general context and structure of the thesis and highlights the contributions of this research work.

The second chapter presents and analyzes the state-of-the-art in wearable robotics research with a focus on lower limb exoskeletons. The most relevant prototypes of these robots are first described from the mechanical design point of view; these prototypes are intended to be used either for power augmentation, rehabilitation or daily assistance purposes. Important aspects related to the development of wearable robots, such as the actuation mode, control strategy, and performance assessment, are then discussed. Moreover, FES technology, commonly used in rehabilitation engineering, is described and analyzed in clinical context. Hybrid systems combining FES technology and wearable robots, used for assistive/rehabilitation purposes, are then overviewed. Finally, the commonly used

[1] https://www.who.int/news-room/fact-sheets/detail/ageing-and-health
[2] https://www.who.int/bulletin/volumes/94/9/16-181636/en/
[3] https://www.who.int/news-room/fact-sheets/detail/spinal-cord-injury

open-loop or closed-loop control strategies of these systems are analyzed and the main control challenges discussed.

Chapter 3 describes first the different sensors, actuators and wearable robot prototypes (EICOSI orthosis, EROWA exoskeleton, and ANGELEGS exoskeleton) used for evaluating the performance of the proposed assistive control strategies. The dynamic models of the Series Elastic Actuator (SEA) used as actuation mode of the EROWA exoskeleton, and of the above mentioned prototypes, along with their parameter identification, are then presented. The modeling of the prototypes is carried out for two types of movements: knee joint flexion/extension movements and STS movements.

In chapter 4, a Proxy-NDO-based Control (PNC) strategy is proposed for three human-robot interaction modes: zero-impedance mode, force tracking mode and high torque mode. This strategy exploits both a Proxy-based Sliding Mode Control (PSMC) and a Non-linear Disturbance Observer (NDO) based PD force control of the Series Elastic Actuator (SEA) to ensure an accurate force tracking, robustness with respect to modeling uncertainties and external disturbances, and wearer's safety. The stability of the proposed controller is analyzed and the performance of the latter evaluated through simulations and experiments in the case of knee joint movements of the EROWA exoskeleton.

Chapter 5 presents the development of a hybrid control strategy for knee joint flexion/extension movements restoration. Overall description of the hybrid controller is first presented by detailing its two components i.e. the control of the EICOSI orthosis and the FES controller. The proposed control strategy is designed to enhance the involvement of the subject during the knee joint flexion/extension movements. In this chapter, we also explored the use of a non-linear disturbance observer for on-line estimation of the generated stimulation torque. Finally, the experimental protocol and the performance of the hybrid controller evaluated through simulations and experiments, are presented and discussed .

Chapter 6 deals with the development of an impedance modulation-based control strategy to assist people performing Sit-To-Stand (STS) movements. The first part of the chapter details the two components of the control structure, i.e. the impedance compensation-based controller and the balance reinforcement-based controller. A human joint torque observer (HJTO) is used to estimate the torques developed by the wearer

and a Sliding Mode Controller (SMC) is exploited to ensure an accurate position tracking. Besides, a time-varying desired impedance model is proposed to ensure an appropriate assistance according to the wearer's motor ability. The robustness of the proposed control strategy with respect to modeling uncertainties is also analyzed. The second part of the chapter presents and analyzes the performance of the proposed controller in simulation and experiments with a healthy subject.

In chapter 7, a hybrid Assistance-As-Needed (AAN) control strategy combining the use of exoskeleton/orthosis impedance control with quadriceps FES, is developed. This control srategy is evaluted in two types of physical activities: i) flexion/extensionmovements of the knee joint, ii) Sit-To-Stand movements. The orthosis/exoskeleton impedance controller and the FES controller are first designed for each activity. In the second part of the chapter, for each activity, the used experimental protocol and performance of the proposed control strategy are presented and discussed.

Chapter 8 summarizes the contributions of the thesis and discusses future research directions.

Chapter 2

Review of wearable robotic systems

"Research is what I'm doing when I don't know what I'm doing."

Wernher von Braun

Contents

2.1 Introduction

THE purpose of the present chapter is to present and analyze the state-of-the-art in wearable robotics research with a focus on lower limb exoskeletons. The first part describes, from the mechanical design point of view, the most relevant prototypes of these robots reported in the literature and intended to be used either for power augmentation, rehabilitation or daily assistance purposes. Important aspects related to the development of wearable robots, such as the actuation mode, control strategy, and performance assessement, are then discussed. In the last part of the chapter, the FES technology, commonly used in rehabilitation engineering, is first introduced and its pros and cons analyzed in clinical context. Hybrid systems combining FES technology and wearable robots, used for assistive/rehabilitation purposes, are then overviewed. Open-loop or closed-loop control strategies of these systems, proposed in the literature, are then analyzed and the main control challenges discussed.

2.2 Lower limb wearable robots

In the literature, different definitions of powered or active wearable robots, and in particular exoskeletons and/or orthoses have been proposed. In [1], an exoksleton is defined as "a device that enhances the physical capabilities of an able-bodied user", meanwhile, an active or powered orthosis is "a device used to assist a person with an impairment of the limbs". However, the terms "active orthosis" and "exoskeleton" are often used interchangeably [1]. In the rest of the manuscript, the term orthosis/exoskeleton refers to active or powered orthosis/exoskeleton. In [2], Herr defines exoskeletons and orthoses as "mechanical devices that are essentially anthropomorphic in nature, are worn by an operator and fit closely to the body, and work in concert with the operator's movements".

Exoskeletons can be used either for rehabilitation, assistance, or/and power augmentation purposes. The main goal behind using exoskeletons for rehabilitation is to provide guided movements to restore the limb function (e.g., after a stroke). Exoskeletons intended for rehabilitation offer the ability to ensure repetitive training while facilitating labor intensiveness by decreasing the wearer's action load. Exoskeletons for daily assis-

[1] https://en.wikipedia.org/wiki/Neuromechanics_of_orthoses

tance are intended to be worn by people with a movement disorder (e.g. elderly, patients) to provide physical support when performing daily living activities such as walking, stairs ascending/descending, sitting down and standing up. The use of power augmentation wearable robots is motivated by the power provided to reduce worker's maneuverability while carrying loads during work tasks and operations; missions for soldiers holding significant loads for a long time represent a typical use case of exoskeletons in military applications. In this chapter, lower limb exoskeletons are classified into two major categories, i) power augmentation exoskeletons, and ii) assistance and rehabilitation exoskeletons.

2.2.1 Power augmentation exoskeletons

The first attempt to design an exoskeleton was in 1968, with the so-called Hardiman which is a huge full-body exoskeleton designed for military purposes [3]. Hardiman consists of 30 DoF and its weight is 680 Kg. Even though this exoskeleton was developed to increase significantly the wearer's ability in terms of strength and endurance, the project was abandoned and then followed by the development of many other prototypes.

Since 2000, the Defence Advanced Research Project Agency (DARPA) funded a project aiming to develop an exoskeleton for human performance augmentation called BLEEX (Berkley Lower Extremety EXoskeleton) [4] (see Figure 2.1). This prototype, actuated with hydraulic actuators, is equipped with several sensors such as encoders at the hip, knee and ankle joints, as well as force sensors placed under the feet. The mechanical frame consists of 7 DoF from which only four DoF are active at hip and knee joints. BLEEX allows a walking speed up to 1.3 m/s and permits the wearer squating, twisting and running over and under obstacles while carrying loads. Various versions of BLEEX were proposed on the market by the university of California under the names of ExoHicker, ExoClimber and Human Universal Load Carrier (HULC).

XOS, another DARPA funded exoskeleton developed by Sarcos Robotics, is a full exoskeleton suit which supports both lower and upper limbs. Like the BLEEX exoskeleton, XOS was developed to increase the speed, strength, and endurance with the minimal effort exerted by the wearer when carrying heavy loads. A single fuel-based engine empowers the servomotors of the XOS suit. XOS includes 30 actuated DoF, and is equipped with force sensors on both user and exoskeleton sides [5, 6, 7]. The first prototypes, XO and XO

Max, have achieved an autonomy of 4 hours and 8 hours, respectively.

Researchers at Kanagawa Institute of Technology in Japan designed a full-body exoskeleton to aid nurses at the hospital. The exoskeleton is driven by pneumatic actuators at elbows, hips and knees joints. The prototype is equipped with FSR (force sensing resistor) sensors attached above rectus femoris muscle to detect the wearer's intent [8] [9]. Several other exoskeleton prototypes have been developed worldwide in the last decade for human performance augmentation. Daewoo Shipbuilding and South Korean Marine Engineering companies designed together a wearable robot to assist shipbuilders carrying heavy loads [10]. In 2012, the french engineering company RB3D developed the Hercule Exoskeleton for the French army. The exoskeleton has a weight of 30 kg while its mechanical frame consists of 14 DoF with only four actuated ones at knee and hip joints [11].

The Body Extender (BE) system, developed at PERCRO laboratory of Scuola Superiore Sant'Anna (Italy), is an exoskeleton intended for augmenting the human strength while bearing heavy loads. The prototype is composed of four robotic limbs with anthropomorphic kinematics and has a total of 22 actuated DoF independently actuated by mean of electric actuators. The Body Extender is equipped with 22 incremental encoders at the actuated joints, 5 force/torque sensors at the connecting points between the user and the device, and 1 accelerometer placed in a backpack [12].

2.2.2 Assistance and rehabilitation exoskeletons

In the last decade, wearable robot prototypes for research and industrial purposes were developed to assist dependent people (elderly and stroke patients) in their daily living activities as well as in assisting therapists in clinical rehabilitation process. In particular, the use of wearable robots for rehabilitation purposes of patients suffering from physical disabilities, has shown a great interest [1, 13]. Several studies have shown how wearable robots could significantly improve physical therapies with respect to conventional clinical methods that often require important efforts from both patients and therapists. In [14], Mehrholz et al. note that robotic gait therapy in combination with conventional therapy is more effective than standard physiotherapy alone. Specifically, people in the first three months following stroke and those who are not able to walk seem to take more benefits

(a) (b) (c)

Figure 2.1: (a) BLEEX, (b) ExoHicker, (c) ExoClimber.

from such kind of intervention. A comparative study between robot assisted therapy and conventional therapy, conducted by Sale et al. [15] on 53 sub-acute post-stroke patients, has revealed significant improvement in motor functions obtained in short time when using robotic assisted therapy.

The oldest commercialized exoskeleton for stroke patients is the ReWalk exoskeleton which is electrically actuated at the hip and knee joint levels to assist walking and STS movements [16]. The battery and the control board are placed in a backpack. ReWalk was approved by the Food and Drug Administration (FDA) to be used with spinal cord injured patients. The limitations of this device are mainly its heavy mechanical structure and the time period needed to get used to wearing it.

HAL (Hybrid Assistive Limb), developed by the Japanese company Cyberdine, is one of the well-known exoskeletons designed to help patients to restore their walking functions after a Spinal Cord Injury (SCI) [17, 18, 19]. HAL uses the remaining lower limb muscular ability to assist knee and hip joint movements and exploits muscular activity signals (EMG) for this purpose. The major drawback related to the use of EMG is its sensitivity to electrode placement and skin impedance impacting therefore the robustness and adaptability of the robot for different subjects.

The company Ekso Bionics developed the Ekso exoskeleton intended to provide assistance for paraplegic patients [20]. Ekso is a full lower limb exoskeleton actuated at the knee and hip joints. It can be used under the supervision of a physical therapist having manual control over the device for security reasons. ExoNR is a new generation exoskeleton proposed by Ekso Bionics in 2019 to assist neuro-rehabilitation of subjects recovering from stroke and spinal cord injury. This new version, approved by the FDA, is equipped with a touchscreen controller allowing therapists to adapt the assistance provided by the exoskeleton to challenge patients with real-time feedback and perform outcome measurements during use [21]. In addition, ExoNR is featured with an optimized smart assist software which allows patients to learn walking with a more natural gait [2].

In [22], Kong et al present the Sogang University Biomedical Assistive Robot (SUBAR), which is an advanced version of the Exoskeleton for Patients and Old population by Sogang (EXPOS) [23]. SUBAR is a lower limb exoskeleton developed to assist physically impaired people. This prototype is powered by geared DC actuators at hip and knee joints, and equipped with incremental encoders to measure knee and hip joint angles.

Indego is another full lower limb exoskelton electrically actuated at the hip and knee joints. This prototype is dedicated to gait training and assistance of people with SCI during STS movements and other daily living activities[3]. REX is an exoskeleton developed by Rex Bionics to assist the wearer to go down or up a slope or stairs with low effort provided by the latter. The limitations of this prototype are mainly related to its bulky frame and low gait speed [24, 25] (see Figure 2.2). Mindwalker, developed by Twente university-Netherland, is a powered hip and knee exoskeleton intended to assist SCI patients using non-invasive brain control [26]. Each of the powered joints is actuated by a Series Elastic Actuator (SEA). A high-level controller is used to provide the wearer an assistance in the frontal and lateral planes during walking.

In [27], Bortole et al. present the H2 lower limb exoskeleton for gait rehabilitation of post-stroke subjects. The prototype has six actuated joints (hip, knee, and ankle of both legs), and is equipped with 6 potentiometers, 18 Hall effect sensors, 24 strain gauges and 4 foot switches are used to measure the joints position and velocity, as well as force and

[2]https://www.roboticsbusinessreview.com/health-medical/ekso-bionics-launches-new-exoskeleton-for-neurorehabilitation/

[3]https://exoskeletonreport.com/product/indego/

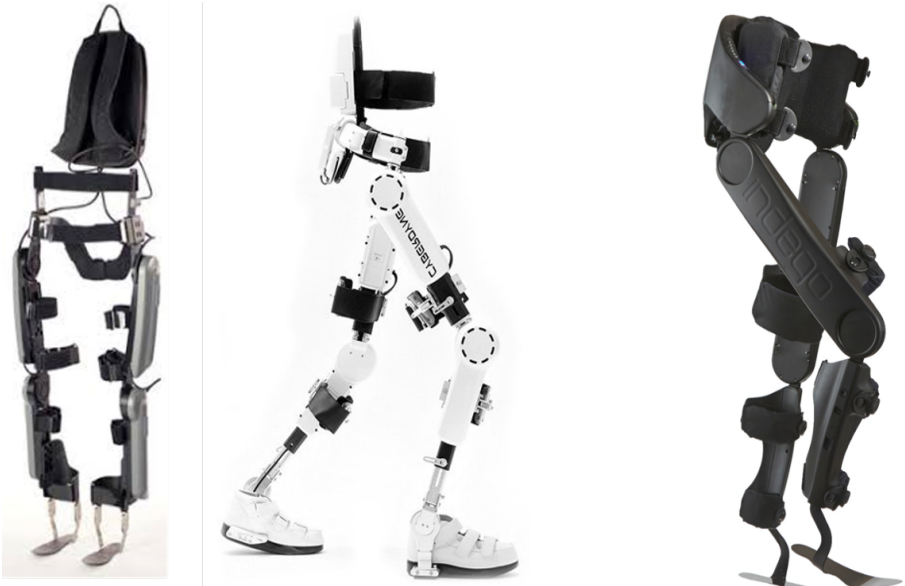

(a) (b) (c)

Figure 2.2: Some examples of assistive exoskeletons. (a): Rewalk, (b): HAL, (c): Indigo

interaction torque between wearer's limb and exoskeleton.

2.3 Actuation modes of lower limb wearable robots

Actuation of exoskeletons is of crucial significance since it directly impacts the latter in terms of portability, efficiency and safety. Electric actuators were firstly used as actuation mode for exoskeletons in 1974 by Vukobratovic et al. [28]. Since then, this actuation mode was widely used in lower limb exoskeletons such as HAL [19, 29, 30, 31, 32], ReWalk [33], etc. Electric actuators are more power-efficient in comparison with hydraulic or pneumatic actuators but show at the same time a relatively important size and a higher weight to achieve the same purpose. To achieve high torques, small size, and lightweight simultaneously, geared-drive and/or cable driven actuators are used instead of direct-drive actuators. The poor torque density at low speed as well as friction, backlash, torque ripple, and gears noise are some of the inherent limitations of electric actuators. To deal with these limitations, Series Elastic Actuators (SEAs) were introduced. The advantages of the latter in comparison with the standard electric actuators are their capability to deal with schock tolerance, low reflected inertia, accuracy, stable force control, and energy storage [34, 35]. Recently, SEAs have been used in many wearable robots such as: the Active Ankle-Foot Orthosis (AAFO) intended to compensate for patients' foot drop [36], the

MindWalker lower limb exoskeleton used to support SCI patients during walking [26]. In [37], Kong et al. describe the design of a compact Rotary Series Elastic Actuator (cRSEA) considering the following requirements: precise and large torque generation, back drivability, low output impedance, and hardware compactness.

Hydraulic or pneumatic actuators, usually used for wearer's motor ability augmentation [38], are characterized by their high power/weight ratio. BLEEX [4] and SARCOS [39] are typical examples of exoskeletons exploiting such an actuation mode and are intended to enhance the soldiers' capabilities [5]. The full-body exoskeleton, developed at Kanagawa Institue of Technology and used to assist nurses to carry patients in their arms [40, 41], is another prototype that uses pneumatic rotary actuators.

Pneumatic muscle actuators, used by McKibben for prosthetic application in 1950, is another efficient actuation mode for exoskeletons [42]. Pneumatic muscles are characterized by their ease of manufacturing and show similar behaviours as natural human skeletal muscles. In addition, they are safe and suitable for rehabilitation purposes due to their inherent compliance and their limited maximum contraction. These actuators are characterized by their relatively high power/weight ratio, and their relatively light weight [43]. The use of pneumatic artificial muscle actuators is reported in the work of Caldwell et al. [44] in which the design of a 10-DoF lower-body exoskeleton for actively assisting human walking is described. In [45, 46], Sawicki et al. describe the design of a powered lower limb orthosis for motor adaptation and rehabilitation purposes using artificial pneumatic muscles; this orthosis provides plantar flexion torque at the ankle joint. Due to the use of compressible air, artificial pneumatic muscles suffer from some limitations such as their low control bandwidth.

The above-mentionned systems show strong potential in assisting SCI patients walking or enabling soldiers to carry heavy loads. However, the rigid mechanical frame of the exoskeletons often fails to allow the wearer to perform natural joint movements due to its bulkiness and misalignment between the wearer's joints and those of the wearable robot, which create undesirable force interactions during movements.

Recently, researchers focused on the development of lightweight exoskeletons based on soft clothing-like materials called "exosuits"[4]. A suit, which is made of specially de-

[4]https://wyss.harvard.edu/technology/soft-exosuits-for-lower-extremity-mobility/

signed fabrics, is significantly lighter than a conventional exoskeleton; it also imposes less restrictions to the wearer's movements and avoids uncomfortable movements resulting from joints misalignment. In more recent studies, it has been demonstrated that the assistance delivered through an exosuit interface allows substantial reductions in terms of energy cost during walking [47, 48]. Although exosuits can only augment, not replace, wearer's existing functions, they can be exploited in synergy with the impaired individual's remaining abilities to assist his/her functional movements.

One of the most known research teams working on exosuits is the Wyss institute at Harvard university (see Figure 2.3). Their first efforts led to the development of wearable robots that could comfortably deliver assistive forces to healthy users during walking [49, 50]. In [51], Asbeck et al. present the design of an exoskeleton aligned with the human anatomical body structure. Soft modules located at joints are used as actuators. These soft actuators achieve compliant movements by exploiting pneumatic actuation and visco-elastic properties of soft materials such as plastic and rubber.

Even though they do not use rigid mechanical structure, are characterized by their lightweight and achieve an efficient alignment with the wearer's joints, soft exoskeleton or suits are limited by their inability to provide sufficient assistive torques, and challenges of calculating an accurate dynamic model to design appropriate control strategies.

Figure 2.3: Harvard Wyss institute soft exosuit[5]

2.4 Control strategies of lower limb wearable robots

The need of appropriate control strategies for wearable robots taking into account the presence of the human in the control loop for both human augmentation and assistance is of great importance ; developing such strategies constitutes one of the main challenges in the design of lower limb exoskeletons. Two major control strategies can be identified [52]: The first one concerns the tracking of predefined trajectories imposed by the wearer; and used as inputs to control the exoskeleton independently from the subject's movement. The second one, called Assistance-As-Needed (AAN) strategy, consists of assisting the wearer to achieve a given activity while taking into account his/her intention, and eventually his/her residual motor abilities [52].

According to [1], and based on the control paradigm of the central nervous system, a general framework for controlling a lower limb exoskeleton must include three levels of control strategies: i) a high-level control strategy where the subject intention is detected, ii) a medium-level control strategy where the detected human intention is converted into desired joint trajectory, and iii) a low-level control strategy which ensures the tracking of the trajectory issued from the mid-level layer. One of the most used low-level control strategies is the conventional Proportional-Integral-Derivative (PID) controller. However, this controller suffers from several limitations due mainly to the setting of appropriate control parameters. Even though these parameters may be optimal for particular subjects and for particular tasks, they might not be applicable for other subjects due to changes in the model parameters or even for the same subject in different time period of the day due for example to muscular fatigue.

To ensure a robust trajectory tracking with respect to model parameter uncertainties and external disturbances caused by the wearer, the exoskeleton or the environment, advanced control approaches are generally used. In [53], a Sliding Mode Control (SMC) strategy is used to control a 2-Dofs gait rehabilitation wearable robot intended to assist hip and knee joints movements. The same approach is exploited in [54] to control a knee joint orthosis for patients having stiff-legged. In [55, 56], adaptive controllers are used to control an Actuated Ankle Foot Orthosis (AAFO). The latter is driven by both, the

[5] https://biodesign.seas.harvard.edu/soft-exosuits

residual human torque at the ankle joint level and the torque of the AAFO actuator. The ankle reference position trajectory is updated online using cubic spline interpolations between the different key events of the gait cycle and adapted to the selected wearer's speed. The advantages of such a control strategy are its robustness with respect to the system (AAFO/wearer) model parameters uncertainties, and its self-adaption to the wearer's walking conditions and capabilities.

In a human-in-the-loop robotic system, considering force interactions between the wearer and the robot resulting from joints misalignment, constitutes a challenge for the good performance of the robot controller. This is due to the fact that these effects can be regarded as unexpected external disturbances. Many recent research studies have proposed the so-called disturbance-observer (DOB)-based control strategies where the disturbance is estimated using a model-based observer and directly compensated in the control scheme. In [37], Kong et al. propose a linear DOB-based PID controller for controlling a SEA actuator to achieve fast and accurate tracking of a reference torque. A nonlinear disturbance observer (NDO)-based nonlinear controller is proposed in [57] to control a multi-joint lower limb exoskeleton. NDO technique is exploited in [58] to estimate the human joint torque in impedance control of a knee joint orthosis.

In AAN-based strategies, the main goal is to provide assistance by taking into account the wearer's motor capabilities. It is then necessary to use a multi-level control paradigm that includes human intention detection algorithms, power assistance strategies as well as joint-level control [1]. To provide appropriate assistance to the wearer, a primary issue is to estimate the wearer's intention. To recognize the human intention, two types of sensors are usually used: cognitive-based sensors and physical-based sensors [59, 60]. The subject's intention, estimated by measuring muscular activity through EMG measurements or brain activity through EEG measurements using Brain Machine Interface (BMI), can be used as exoskeleton controller input. As examples, for the control of the HAL exoskeleton, the muscular activity of the wearer is measured using surface electromyography (sEMG) sensors [61]. In [62], a closed-loop BMI system is used to control a lower limb exoskeleton for SCI gait rehabilitation. The encephalographic signals of the subjects are exploited to detect their gait intention and trigger movements of the exoskeleton. The main advantage of using EMG or EEG modalities is that the wearer's intention can still be

estimated, even if the wearer cannot provide the necessary joint torques. However, these modalities can be affected by several noise artifacts in signals resulting from electrodes placement, interference due to signals from neighbouring muscles and/or brain areas, etc. An alternative solution for human intention recognition consists of using physical-based sensors. The Body Extender, a whole body exoskeleton designed for augmenting the human strength for handling heavy loads, uses force sensors mounted between the wearer and the exoskeleton to estimate the wearer's intention [12]. Impedance control is another well-known method used in AAN-based control strategies. Its principle consists of regulating the dynamic relation between the assistive device and the wearer by linking the position tracking error to the interaction force/torque through a mechanical impedance. In [63], the joint velocity is used as input of the impedance controller to infer the human intended action. In [22], Kong et al. use the angular deformation rate of the series elastic module of an SEA to estimate human joint torque. In [64], an impedance controller is used for controlling a lower limb exoskeleton to support the wearer as much as needed while encouraging him/her to produce maximal voluntary participation. In [65], Hussain et al. propose an adaptive impedance controller for gait training on treadmill for patients with neurologic impairments. In [27], an impedance control algorithm is used to create a force field along a desired trajectory and apply a correction torque when patients deviate from the desired walking movement using the H2 exoskeleton.

2.5 Performance assessment

In [66], Huo et al. propose three assessment metrics of lower limb exoskeletons performance: metabolic cost, gait analysis, and muscle activity analysis. However, cognitive assessment is of importance as well, since it expects that a symbiotic and usable exoskeleton does not limit the wearer's movements, and must stay compliant to them. Due to the complexity of evaluating the cognitive aspects, there are few works exploiting such assessment metrics in the literature [67]. Besides, very rare studies reported evaluations of assistance device safety since a large number of researchers tried to quantitatively assess the effectiveness of assistance strategies or how to tune it to maximize a certain performance metric [67]. In [27], to evaluate the safety and usability of the H2 exoskeleton, 12

training sessions corresponding to 4 weeks of training for 3 hemiparetic stroke patients have been performed. These training sessions allowed to measure the patients' feedback about the use of the exoskeleton by using the Likert scale[68].

Metabolic cost based metrics are used to compare the metabolic energy expenditure of the user during walking with and without the use of the exoskeleton. The oxygen consumption, the carbon dioxide production, the urinary nitrogen excretion and the Metabolic Cost of Transportation (MCoT) are the basic measurement means. Some studies reported a reduction in the metabolic cost of a user wearing an exoskeleton during walking. For instance, Sawicki et al. studied the metabolic cost of plantar flexor mechanical efforts generated during walking at different step lengths and at a constant frequency [45, 46]. In [69], Martini et al. report that a hip exoskeleton-based locomotion allows reducing oxygen consumption and MCoT in comparison with the treadmill walking at the same speed. Gait analysis, used especially for rehabilitation purposes, is also an important and useful assessment tool. Kinematic and dynamic variables, temporal-spatial gait variables, physiological cost variables, and other variables related to the gait function are frequently used as assessment indicators. In [70], biomechanical gait analysis (stability, gait speed, step length, etc.) is exploited to assess the performance of a 2-DoF motor-powered gait orthosis for SCI patients. In [71], C. Wu et al. evaluate the effect of gait training using a lower limb exoskeleton for individuals with SCI. The evaluation includes the timed up-and-go test, 10-m walk test, and 6-min walk test with an exoskeleton. The results showed that the participants walked faster and farther without any injury or fall incidence when using the exoskeleton. Gait analysis was also exploited for performance analysis of various assistive robots: HAL exoskeleton [61], the gait orthosis in [72], the Lokomat exoskeleton [73], etc. Muscle activity analysis allows assessing the wearer's contribution when performing a task, and consequently, the assistance performance. The muscular activity is evaluated by averaging the muscle activation levels using EMG analysis. This assessment metric was used for performance evaluation of the HAL-3 exoskeleton worn by healthy subjects during different activities: walking, standing up, ascending stairs, etc. [61]. In [74], Akahira et al. exploit the muscular activity of the wearer through EMG measurements to assess the effectiveness of a motor-assisted knee motion device during orthotic gait. In [58], the electromyographic activity of quadriceps muscles is used

to evaluate the performance of an impedance control strategy of a knee joint orthosis. The reported results show a decrease in the muscular activity of four healthy subjects when using the impedance controller in comparison with the case when the controller is unused.

In [75], Zhang et al. assess a neural oscillators based control approach applied to train and synchronize the movements of the assist suit with those of the wearer. Besides the decrease in the electromyographic activity of the thigh muscles, psychological evaluation with subjects showed that walking with the robot suit with mutual inhibition was considered easier and stable in comparison to walking without inhibition.

Despite the availability of metrics to evaluate improvements in terms of mobility for the user during rehabilitation, standards protocols for assessing the assistive and rehabilitative aspects of novel robotic devices are still lacking. The functional assessment must be a quantitative comparison of the accomplishments, in terms of daily living activity achievement, motion speed, subject involvement,etc., reached by the wearer with and without the assistive device.

2.6 Functional Electrical Stimulation (FES) and hybrid orthoses

Electrical stimulation for stroke patients offers a wide range of benefits from improving motor skills to reducing numbness [76]. It allows recovering from many side effects of stroke. This technique is often used during stroke rehabilitation when a patient is faced with post-stroke paralysis, weakness, pain, or sensory issues. FES consists of stimulating muscles to contract during an activity such as sitting down, standing up [77], or walking [78]. The perceived benefit of FES for post-stroke subjects is that it can facilitate the practice of exercises that could not be done due to hemiparesis [6]. Besides, FES allows motivating post-stroke patients and providing them sensory and visual feedback, while being repetitive and challenging.

FES is a useful technology in clinical context; however, it has drawbacks since it can cause muscular fatigue, skin irritation, etc. It is also subject to many uncertainties due to

[6] muscular weakness or partial paralysis restricted to one side of the body

the variability in muscle length and strength between subjects, and the placement of the electrodes, which results in different joint behaviours [79].

To overcome the above-mentioned drawbacks and limit the patient's dependency on the use of orthoses/exoskeletons, hybrid orthoses/exoskeletons were proposed in the literature [79] [80]. A hybrid orthosis/exoskeleton combines the use of an orthosis (also called robotic orthosis) or exoskeleton and FES acting as an electrical stimulation orthosis.

One of the major challenges regarding the development of controllers for hybrid orthoses/exoskeletons is related to the accurate estimation of the joint torques induced by stimulation, and the modeling of muscular fatigue [79, 81]. Different solutions have been proposed in the literature such as model-based and sensor-based approaches.

In [82, 83, 84], a Hill-based model is used to estimate the torque induced by stimulation as well as the muscular fatigue [85]. Nevertheless, model-based approaches generally require an accurate identification process which is a difficult task in a clinical context due to time constraints and continuous dynamic parameters variation (fatigue, muscle spasticity[7], etc.) as well as variable physiological and environmental factors such as skin impedance, temperature, and electrode placement [86]. To deal with the above-mentioned limitations, sensor-based approaches have been proposed [87, 88]. In [87], a force sensor is placed on a lower limb orthosis to measure the interaction forces between the wearer's shank and the orthosis, and thus, estimate the torque induced by stimulation. In [88, 89], FSR (force sensing resistor) sensors are placed on the inner side of a shank orthosis to measure the interaction torque between an orthosis and the wearer and estimate the muscular fatigue. Although this method does not require a model and is not subject-specific, the placement of torque/force sensors is constrained in the case of many compact exoskeletons or orthoses. Additionally, torque/force sensors have generally a relatively high cost [90].

In terms of control strategies of hybrid orthoses/exoskeletons, two major strategies can be distinguished: open loop and closed-loop hybrid control strategies [88]. In the rest of the manuscript, the term "hybrid control" refers to the control of hybrid systems

[7] Spasticity is a condition in which muscles stiffen or tighten, preventing normal fluid movement. The muscles remain contracted and resist being stretched, thus affecting movement, speech and gait.

combining FES technology and wearable robots.

2.6.1 Open-loop hybrid control strategies

Open-loop hybrid strategies consist of using preprogrammed stimulation pattern synchronized through the detection of gait events [91]. One of the first hybrid orthoses is described in [92]. It consists of six channels stimulation FES and a robotic orthosis actuated by a direct current servomotor and motor-driven drum brake. A finite state control algorithm synchronizes between the brake, motor and muscle stimulation to efficiently control the prototype. The comparison of walking performance of the hybrid orthosis, the active orthosis, and FES, used separately, showed small improvements in terms of gait velocity and metabolic cost in the case of the hybrid orthosis. However, it can be noticed, at the same time, a knee flexion deterioration after 10 min of walking, leading to a reduced gait duration. In [93], Durfee and Hausdorf describe the design of a hybrid FES/orthosis system which includes a long-legged brace with controllable friction brakes at the knee and hip joints. The purpose of this system is to achieve acceptable trajectory tracking by using FES to induce lower limb movements, while controlling the position and resulting velocity using joint brakes. This control strategy, evaluated with a paraplegic subject, allowed a reduction in the duty cycle of muscle stimulation, and improvement in the knee trajectory tracking compared to FES strategy used alone. In [94], Obinata et al. propose a hybrid orthosis where open-loop FES is applied to the quadriceps muscles of both legs while DC actuators are used to compensate for the joint moments. In [95], the authors describe a hybrid control strategy to provide enhanced hip extension in paraplegics during the stance phase of gait cycle. The proposed control strategy consists of using a constant stimulation current intensity and varying the timing of stimulation based on both a finite state machine and hip joint torques from previous iterations. The proposed approach was evaluated on a level-ground walking test with a complete T10 paraplegic subject. Results showed a 34% reduction in electrical power requirements at the hip joints during the stance phase of gait cycle with the hybrid approach compared to when using orthosis without FES. In [96], Buleae et al. study the effects of incorporating stance-controlled knee flexion during loading response and pre-swing phases on level-ground walking using a hybrid orthosis. In [97], a variable impedance knee mechanism with a 16-channel

percutaneous FES system for stair descent is proposed by the same authors. The muscle activation pattern was synthesized to descend in a step-by-step fashion. The obtained results showed a reduction of the stimulation duty cycle during the stance phase while allowing to restore stair descent at controllable and comfortable speeds for the user.

2.6.2 Closed-loop hybrid control strategies

Closed-loop strategies rely on indirect measurements of muscle performance (i.e. joint position and velocity [98], interaction force/torque between the leg and exoskeleton [88][87]) to control a hybrid orthosis/exoskeleton. These strategies allow generating the desired joint torque or position to compensate for a reduction in muscle performance, by increasing stimulation parameters (i.e. pulse width, amplitude, frequency). Therefore, muscular fatigue recognition and management are usually required. In [99], the authors propose an approach combining open and closed-loop approaches. Joint positions and velocities are measured during one iteration and weighted to calculate the stimulation current intensity to apply in the next iteration. In [87], the authors describe a hybrid orthosis consisting of the orthosis called Walk Trainer and a 20 channels FES system. The developed hybrid control strategy, intended to assist the hip, knee, ankle, and pelvis movements, relies on a closed-loop stimulation strategy which consists of modulating the stimulation pulse-width based on the estimated interaction forces between the wearer and the orthosis using a projection-based function; the Walk Trainer orthosis is controlled using an impedance controller. Clinical study performed with 2 complete and 4 incomplete paraplegia subjects showed a reduction in spasticity according to the ashworth spasticity scale. However, the system is bulky to be used in clinical context and does not provide muscular fatigue monitoring.

In [88], Del ama et al. present a new control strategy for a hybrid exoskeleton. The proposed approach combines an impedance controller of the orthosis actuators and an iterative-loop controller of FES. The FES controller modulates the pulse width of the stimulation to apply in the next iteration by evaluating muscular fatigue [100].

The use of a neuromuscular model for hybrid exoskeletons control has been reported in [101, 102, 103, 104, 105]. The use of such models is mainly motivated by the fact that they allow providing an estimation of muscular fatigue and appropriate pulse width

and/or amplitude for a given desired torque.

In [101][103], the control of a hybrid exoskeleton is formulated as a redundant actuation problem. In [101], a model of the shank-orthosis system, including the quadriceps and hamstring muscles dynamics, is considered in the development of the control strategy. The proposed approach based on a Model Predictive Control (MPC) is designed in a manner that both actuators (motor and muscles) are employed cooperatively and their contributions to the assisted movements vary with respect to their inherent capabilities. (see Figure 2.4).

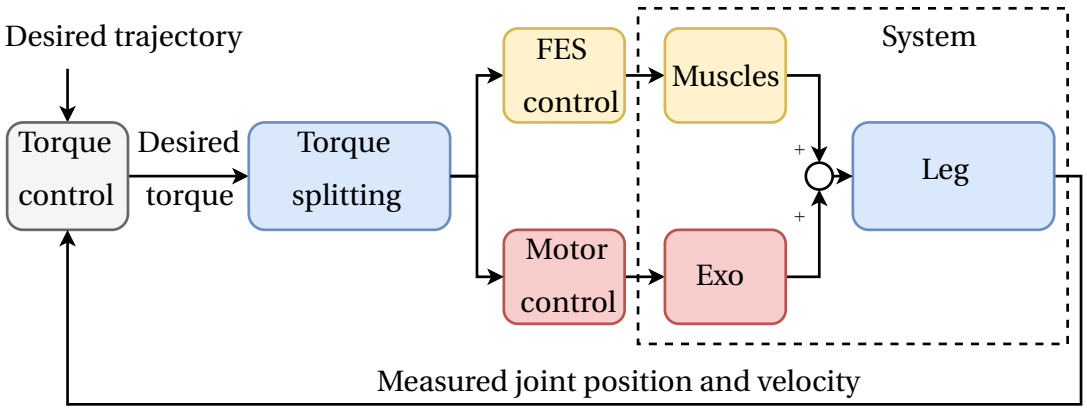

Figure 2.4: Hybrid orthosis/exoskeleton control framework[101]

In [102], simple models, consisting of a double pendulum model of the orthosis/human leg system and Hill type muscle models for the extensor/flexor muscles of the hip and knee, are developed to model walking using FES in combination with an orthosis. Using these models, simulations were performed to find optimal step length, optimal walking speed, and identify crucial differences between able-bodied walking and walking generated via a hybrid orthosis. Outcomes of this simulation study are mainly focused towards providing a knowledge base or preprogrammed stimulation profiles or trajectory tracking closed-loop control. In [104], a hybrid orthosis in which a controller inspired from the muscle synergy principle is implemented to track a gait trajectory. The high dimension of the control input, due to the redundancy of the hybrid orthosis, is lowered by using a Principal Component Analysis (PCA) algorithm. Semi-global uniformly ultimately boundedness is proved using a Lyapunov stability analysis. Simulations were conducted on a 2-DOF fixed hip model. An optimization algorithm was implemented to minimize the amount of stimulation current intensities and motor torques. In [103], to ensure the

dynamic distribution of the control effort among the actuators (muscles via FES and electric actuator), a dynamic control allocation based on a MPC is used for the control of a hybrid orthosis. To estimate the muscle fatigue, Hill model-based muscle dynamics of the knee joint flexor/extensor muscles is used [83]. Simulation results showed how the MPC allocates the control to the orthosis actuator and muscle stimulator simultaneously while minimizing the tracking error and energy expenditure, on the one hand, and differing muscular fatigue, on the other hand. The hybridization approaches, presented in [101, 103, 105], are still showing challenging issues due to the nonlinear behavior of stimulated muscles and the short spectrum development in that field.

As a summary, closed-loop control strategies allow providing the flexibility required to implement "assistance-as-needed" control strategies and improving rehabilitation in incomplete SCI subjects by exploiting subject involvement [106] [107]. Such approaches are interesting since they improve on the long-term functional abilities of subjects.

The metrics used for evaluating hybrid exoskeletons vary considerably from one study to another. The metrics used in a clinical context to quantify gait functions are more suitable for evaluating the performance of such systems within the scope of the pathology for example: walking speed in case of the 10 m walking test, walking distance in case of the 6 min walking test, and walking index for spinal cord injury. These metrics, used to quantify muscle weakness due to paralysis, have proved their reliability in clinical trials. The combination of these three metrics (walking speed in case of the 10 m walking test, walking distance in case of the 6 min walking test, and walking index for spinal cord injury) may constitute a credible measure of improvements in gait and ambulation. The evaluation of hybrid orthoses/exoskeletons may also include a combination of joint kinematics evaluation, kinetics measurements, and physiological costs such as oxygen consumption and muscular fatigue [79].

2.7 Conclusion

In this chapter, a review of wearable robotic systems with a focus on lower limb exoskeletons is first presented. These systems are analyzed from the mechanical design, actuation mode, control strategies and performance assessment points of view. The most relevant

prototypes of these robots, reported in the literature, are intended to be used either for power augmentation, rehabilitation or daily assistance purposes.

Variability in impairment levels, subject ability or the task specificity for which the exoskeleton is designed requires different levels of assistance that must be tuned accordingly. For this purpose, the wearable robot researchers community proposed various control strategies that can be classified into three levels: perception layer, transitional layer, and execution layer. The main requirements for a successful control strategy for lower limb exoskeletons are: good performance in terms of tracking accuracy, robustness with respect to parametric uncertainties, variability between subjects and external disturbances, as well as, the consideration of the wearer's motor ability and/or intention while ensuring his/her safety. To address these challenges, the following objectives were considered in this thesis:

- Development of force/torque control for SEA actuators of lower limb wearable exoskeletons that ensures the wearer's safety, transparency, robustness with respect to modeling uncertainties and external disturbances, and tracking accuracy.

- Developement of an intention-based control strategy to assist the wearer in performing STS movements with minimum sensing measurements from the wearer and which prevent from main failure causes of this task.

An important part of the chapter was also dedicated to the study of hybrid orthoses/exoskeletons, combining FES technology and wearable robots. The usefullness of such orthoses/exoskeletons, and their main control strategies were emphasized. The corresponding hybrid control strategies are of two types: open-loop hybrid approaches and closed-loop hybrid approaches. One of the major challenges behind the development of control strategies for hybrid wearable robotic systems is the estimation of the torque induced by stimulation for which model-based and sensor-based techniques can be used. The latter show limitations since they are either complicated to implement or bulky for their portability. To address these challenges, it is fundamental to develop an estimation method that relies neither on a complex musculo-skeletal modeling nor on using extra sensors, but rather on nonlinear disturbance observer.

Chapter 3

Experimental setups and modeling

If knowledge can create problems,

ignorance will not solve them.

Isaac Asimov

Contents

3.1 Introduction

In this chapter, the different sensors, actuators and wearable robot prototypes (EICOSI, EROWA and ANGELES) used to evaluate the performance of the proposed assistive control strategies, are first described. The dynamic models of the Series Elastic Actuator (SEA) used as actuation mode of the EROWA exoskeleton, and of the the different robot prototypes, along with the identification of their parameters are then developed. For the modeling of the three werables robot, two types of movements are considered: knee joint flexion/extension movements and Sit-To-Stand movements.

3.2 Sensors and actuators

3.2.1 Inertial Measurement Units (IMUs) for motion tracking

An inertial measurement unit (IMU) measures acceleration, angular velocity and the magnetic field vector using a 3D accelerometer, a 3D gyroscope and a 3D magnetometer in one package. In this thesis, MTW IMUs from Xsens (Netherland) are used as wearable motion capture devices (see Figure 3.1). The latter incorporate an embedded Bayesian filter that estimates the absolute orientation of the device with respect to a global fixed coordinate system. This orientation can be expressed using a quaternion, a rotation matrix or Euler angles representation.

3.2.2 Electromyography (EMG) for muscle activity measurement

An EMG sensor is usually used to measure the electrical activity of a muscle and more precisely muscle contraction. EMG sensors are available in two main types; surface EMG (sEMG) sensors and subcutaneous ones [109]. sEMG sensors have advantages since they are non-invasive, and allow gathering the signal at the surface of the skin. However, they can only provide a limited assessment of the muscle activity. This limitation is due to: i) the restriction of sEMG to superficial muscles only, ii) the depth of the subcutaneous tissue at the site of the recording which may depend on the weight of a patient, and iii) the difficulty of distinguishing between the discharges of adjacent muscles [110].

Figure 3.1: Xsens wireless MTW IMUs attached at thigh, shank and foot.

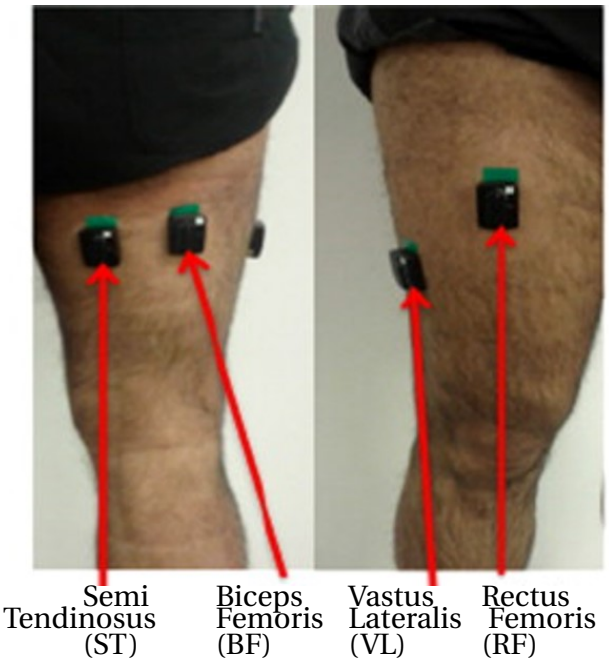

Figure 3.2: Delsys EMG wireless sensors placement at some lower limb muscles (ST, BF, VL, RF) [108].

In the context of exoskeletons control for assistance and rehabilitation, EMG measurements are of great importance to have a quantitative assessment of the provided assis-

tance and rehabilitation outcomes. In this thesis, Trigno surface EMG sensors developed by Delsys (USA) are used (see Figure 3.2).

3.2.3 Functional Electrical Stimulation (FES)

Figure 3.3: RehaStim 2 stimulator and electrodes placement at lower limb muscles according to the SENIAM recommendations [111].

Functional electrical stimulation (FES) is used to support functional movement through the use of controlled electrical pulses that produce muscular contraction. In the last decades, FES has been widely used, mainly to assist walking in stroke patients. In this study, FES is used jointly with the exoskeleton actuation within a hybrid actuation strategy for lower limb movements assistance and rehabilitation. The Rehastim 2 stimulator from Hasomed (Germany) (see Figure 3.3) is used in the experiments. It delivers biphasic current rectangular pulses and the stimulation patterns can be controlled by tuning either the pulse width, the current amplitude and/or the stimulation frequency. The technical specifications of the stimulator are given in the following (Table 3.1).

Table 3.1: RehaStim 2 stimulator technical data

Parameter	Value
Pulse width	20-500 (s)
Impulse intervals	1 (s)
Pulse current amplitude	0-130 (mA)
Stimulation frequency	1-140 (Hz)

3.3 Experimental prototypes

3.3.1 EICOSI orthosis

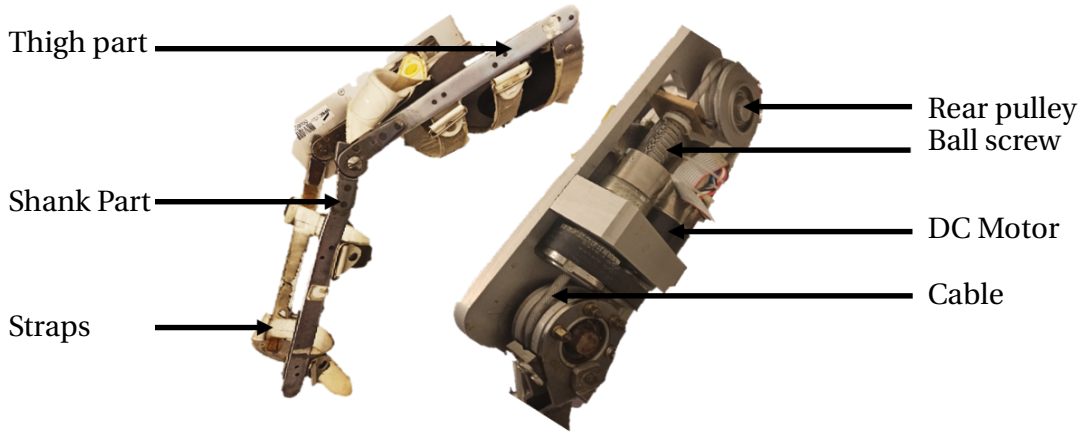

Figure 3.4: EICOSI knee joint orthosis

EICOSI (Exoskeleton Intelligently COmmunicating and Sensitive to Intention) is a 1-DoF orthosis designed to provide power assistance at the wearer's knee joint level (Figure 3.4). This prototype consists of two segments attached separately to the thigh and shank and fixed to the wearer's leg using appropriate braces and its total mass is about 3 Kg. It is actuated using a high-power brushless DC motor (Maxon, Switzerland). To ensure a compact and portable structure and a relatively high output torque, the prototype includes a compact transmission system including a gear motor, a ball screw, a belt transmission and a cable drive. The reduction ratio from the motor side to the joint side is 264:1 and the whole actuator can deliver up to 18 Nm. The motor is equipped with an incremental encoder that measures the motor rotation angle with a resolution of 1000 pulses per revolution. The angular velocity is obtained using a numerical derivation of the joint position. To solve the oversampling problem, a fourth order Butterworth filter is used to filter the raw joint position measurements. The maximal rotation angle and angular velocity are 2.1 rad and ±2.1 rad/s, respectively. The motor is driven using a motion controller EPOS 70/10 from Maxon (Switzerland), and is controlled using a host PC using the Labview software (see Figure 3.5).

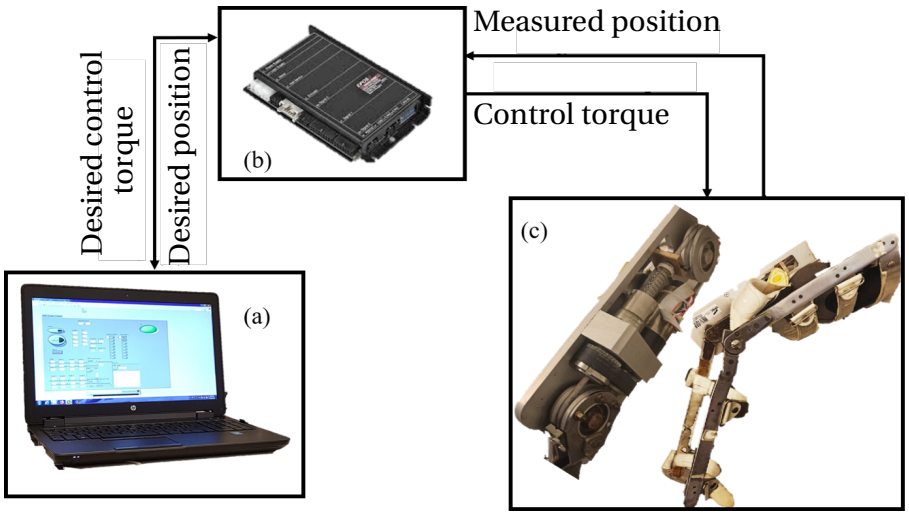

Figure 3.5: Overview of EICOSI control structure. (a) Personal Computer running Labview program, (b) Epos 2 70/10 control card, (c) EICOSI orthosis.

3.3.2 EROWA exoskeleton

Figure 3.6: A subject wearing the EROWA exoskeleton

EROWA (Exoskeletal Robotic Orthotics for Walking Assistance) is a full lower limb wearable robot that has been designed to assist and help elderly people and post-stroke patients to recover their locomotion functions (see Figure 3.6). The weight of the whole

exoskeleton is about 17 Kg.

The main parts of EROWA are the exoskeletal frames, hardware control system, sensor system, and a power unit. The exoskeletal frames consists of 10 DoF and are attached to the wearer's waist and legs by means of straps. Each limb has three DoF, one at the hip joint, one at the knee joint and one at the ankle joint. Shank and thigh lengths are adjustable for different wearer profiles (height: 165-190 cm). The hip and knee joints of each limb are actuated in the sagittal plane (flexion/extension movements) using two compact Rotary Series Elastic Actuators (cRSEAs) while the remaining DoF are passive. cRSEAs have several advantages over traditional actuation modes, in particular, in terms of precision, large torque generation, low output impedance, and hardware compactness.

The use of cRSEA actuators compensates considerably the mechanical impedance of the robot and enables transparent physical assistance with minimal discomfort. The torsional spring included in each cRSEA ensures the measurement of the interaction torque between the wearer and the robot. The maximum torque delivered by each cRSEA is about 25 Nm.

EROWA is equipped with various sensors to estimate the wearer's movement intention in real-time. The inclination angle of the wearer's torso is measured using an Inertial Measurement Unit (IMU) placed in a backpack (Figure 3.6). Two incremental encoders (Maxon, Switzerland), mounted on each cRSEA, are used to measure the motor and joint positions. Four FSR sensors (Tekscan, USA) sensors, placed at different locations of foot soles (i.e., toes, Meta12, Meta45, heel), are used to measure the ground reaction force (GRF) and ensure an accurate detection of gait phases (Appendix B).

3.3.3 ANGELEGS exoskeleton

ANGELEGS is a lighter version of the EROWA exoskeleton (Figure 3.7). The weight of the whole exoskeleton is about 12 Kg.

ANGELEGS is equipped with the same sensors as EROWA except the fact that two air pressure based ground reaction force sensors, placed at two locations of foot soles (heel and toe of each foot), are used to ensure an accurate gait phases detection level.

Figure 3.7: A subject wearing the ANGELEGS Exoskeleton

3.4 Modeling

3.4.1 SEA modeling

A standard SEA consists of an elastic element (normally a spring) in series with a motor, as depicted in Figure 3.8. The motor-side dynamics and the load-side dynamics are coupled by the elastic element (i.e., spring) within a two-mass dynamics model [112]. For a SEA-actuated exoskeleton, the load, i.e., the exoskeletal frame interacts with the wearer and the environment (interaction with the ground during walking). In this chapter, a two-mass nonlinear dynamic model of the SEA-actuated knee joint of the EROWA exoskeleton will be built to estimate the relationship between the SEA input (control torque of the motor) and the resulting output torques: the torque acting on the joint and the spring torque; the latter represents the interaction torque between the wearer and the exoskeleton at the knee joint.

Figure 3.9 shows the actuation mechanism of the SEA-actuated knee joint of the

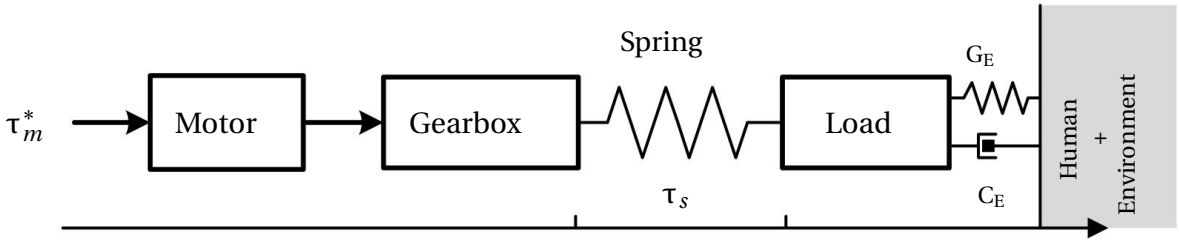

Figure 3.8: Principle of Series Elastic Actuators (SEA) used as actuation mode of the EROWA exoskeleton. Load represents the exoskeletal frame. C_E and G_E denote the wearer/environment damping and stiffness coefficients, respectively.

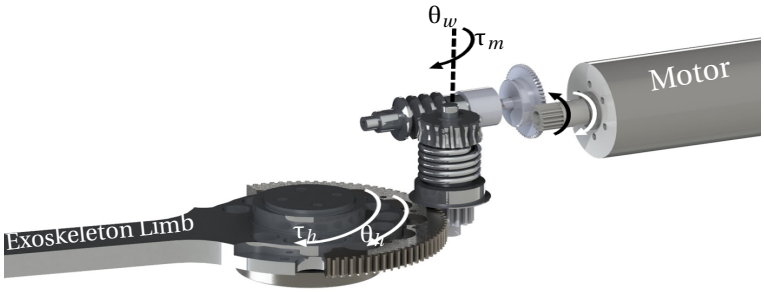

Figure 3.9: Actuation mechanism of the SEA-actuated exoskeleton joint.

EROWA exoskeleton. The presented mechanism consists of: 1) a DC motor, 2) two spur gear sets, 3) a worm gear set, 4) a torsional spring, and 5) the exoskeleton limb, which directly interacts with the wearer's limb; more details can be found in [37]. In the following, we mainly focus on the modeling of the SEA.

3.4.1.1 Modeling of the worm Gear Set

The torque exerted by the torsional spring on the worm wheel (see Figure 3.9) is calculated as follows:

$$\tau_s = K_s(\theta_w - N_j\theta_h). \tag{3.1}$$

where τ_s is the spring torque (i.e. SEA output torque); K_s is the Hooker coefficient of the spring; N_j is the gear ratio of the spur gear set used in joint side; θ_w and θ_h represent the angular positions of the worm gear and knee joint, respectively.

The relationship between the motor torque before and after (i.e. τ_m^*, τ_m) the spur gear set is as follows:

$$\tau_m = N_m\tau_m^*. \tag{3.2}$$

where N_m denotes the gear ratio of the spur gear set used in motor side.

Investigation on the characteristics of the worm gear/worm wheel mechanisms has led to distinguishing between the static and dynamic models of that systems [113]. The static analysis reveals not only the non-back drivability of such mechanisms but also the dependency of break-in torques on the loading torque, direction of motion as well as crucial system parameters such as static friction. The dynamic analysis allows generating conditions on the motion of a worm gear/worm wheel mechanism that depends on the direction of motion and the relative magnitude between the input torque and the loading torque.

- Static model: For the worm gear set, self-locking (i.e., static state) occurs when the following conditions are met [113]

$$\begin{cases} \tau_m > \mathrm{H}\tau_s \text{ and } -\mathrm{A}_1\tau_s \le \tau_m \le -\mathrm{A}_2\tau_s \\ \tau_m < \mathrm{H}\tau_s \text{ and } -\mathrm{A}_2\tau_s \le \tau_m \le -\mathrm{A}_1\tau_s \end{cases} \tag{3.3}$$

  where H, A_1 and A_2 are three parameters expressed as follows:

$$\begin{aligned} \mathrm{H} &= \frac{r_g}{r_w}\cot\lambda > 0 \\ \mathrm{A}_1 &= \frac{r_g(\cos(\phi)\sin(\lambda) - \mu_s\cos(\lambda))}{r_w(\cos(\phi)\cos(\lambda) + \mu_s\sin(\lambda))} < 0. \\ \mathrm{A}_2 &= \frac{r_g(\cos(\phi)\sin(\lambda) + \mu_s\cos(\lambda))}{r_w(\cos(\phi)\cos(\lambda) - \mu_s\sin(\lambda))} > 0 \end{aligned} \tag{3.4}$$

  where, r_g, r_w are the radii of the worm gear and worm wheel, respectively, λ is the lead angle of the worm gear, ϕ denotes the normal pressure angle of the worm gear, and μ_s is the static friction coefficients of the worm gear set.

- Dynamic model: The dynamic model of the worm gear/worm wheel mechanism can be expressed as follows:

$$\tau_m - \mathrm{A}\tau_s = (\mathrm{I}_m\mathrm{N}_w + \mathrm{AI}_w)\ddot{\theta}_w + \mathrm{B}\dot{\theta}_w \tag{3.5}$$

  where θ_w, θ_h are the angular velocity and angular acceleration of the worm gear, respectively. I_m and I_w are the inertia of the motor and worm gear, and the inertia of the worm wheel, respectively; N_w denotes the gear ratio between the worm gear

and the worm wheel, and A is a parameter defined as follows:

$$A = \frac{r_g(\cos(\phi)\sin(\lambda) + \mu\cos(\lambda))}{r_w(\cos(\phi)\cos(\lambda) - \mu\sin(\lambda))} \tag{3.6}$$

where μ represents the dynamic friction coefficient which varies depending on the engagement (i.e., left/right engagement) of the worm gear and worm wheel [113]. Note that the engagement may frequently change when the wearer plays an active role during a movement. Moreover, the friction coefficient may vary based on the lubricant and/or temperature conditions of the worm gear set [37].

3.4.1.2 Modeling of the SEA-actuated knee joint of the EROWA exoskeleton

As shown in Figure 3.8, the exoskeleton physically interacts with the wearer's shank-foot segment and the environment. At the knee joint level, when the exoskeleton is not interacting with the ground, the load of the SEA consists of the spur gear set and the shank-foot segment of the exoskeleton.

Based on the dynamic model of the worm gear set (3.5), the dynamics of the SEA-actuated knee joint of the EROWA exoskeleton can be expressed as follows:

$$\tau_h + N_j\tau_s = M\ddot{\theta}_h + C\dot{\theta}_h + G(\theta_h) \tag{3.7a}$$

$$\tau_m - A\tau_s = (I_m N_w + A I_w)\ddot{\theta}_w + B\dot{\theta}_w \tag{3.7b}$$

where B represents the damping coefficient of the motor and worm gear; M and C are the inertia and damping coefficients, respectively; G is the gravity torque of the spur gear and the shank-foot segment of the exoskeleton. τ_h and τ_m represent the torque generated by the wearer and the motor torque, respectively.

By substituting (3.1) and (3.7a) in (3.7b), the dynamic model of the SEA-actuated knee joint of the EROWA exoskeleton can be expressed using a two-mass system representation, as follows:

$$\tau_m = J_s\ddot{\tau}_s + B_s\dot{\tau}_s + F_s\tau_s + F_h\tau_h + F_0 \tag{3.8}$$

where:

$$
\begin{aligned}
J_s &= \frac{I_m N_w + A I_w}{K_s}, \qquad & B_s &= \frac{B}{K_s}, \\
F_s &= \frac{(I_m N_w + A I_w) N_j^2}{M} + A, & F_h &= \frac{(I_m N_w + A I_w) N_j}{M}, \\
F_0 &= -\frac{(I_m N_w + A I_w) N_j}{M} (C\dot{\theta}_h + G(\theta_h)) + B N_j \dot{\theta}_h.
\end{aligned}
\tag{3.9}
$$

The two-mass dynamic model (3.8) includes the dynamics of both the SEA and the shank-foot segment of the exoskeleton.

From (3.3) and (3.7), we can observe that the characteristics of the SEA-actuated knee joint of the EROWA exoskeleton directly impact the controller design:

1) The model of the SEA-actuated knee joint of the EROWA exoskeleton is highly non-linear, and the spring torque τ_s is determined not only from the motor torque τ_m but also from the wearer's torque τ_h and the varying friction between the worm gear and the worm wheel (see Figure 3.8).

2) When the wearer is active i.e. the wearer produces a torque ($\tau_h \neq 0$), a rapid motor torque response is needed to avoid any resistance force or even a blockage caused by the non-backdrivability of the SEA or friction in its gears due to the worm gear/worm wheel mechanism (Eq 3.3). Moreover, when the motor is powered off ($\tau_m = 0$), the worm gear/worm wheel mechanism will be in the case of gear self-locking [113]. Thus, the interaction torque from the wearer side is fully stored in the spring.

3.4.2 Modeling of the wearer/EICOSI orthosis system

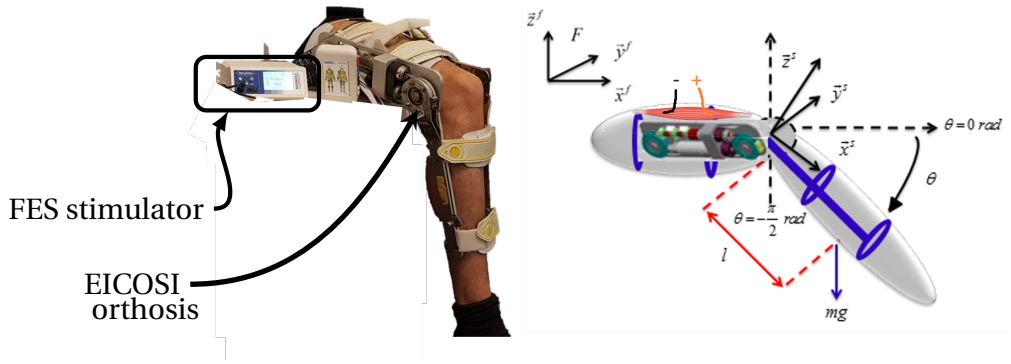

Figure 3.10: Knee joint hybrid orthosis.

The system studied here consists of the wearer's shank-foot segment and the EICOSI

orthosis; the wearer is in a sitting position with the shank freely moving around the knee joint (see Figure 3.10). The subject lower limb movement is generated from both the torque generated by muscle contraction, the torque induced by muscle stimulation through FES, and the assistive torque produced by the orthosis actuator. The muscle stimulation using FES is used to assist the knee joint movements only during the extension phase. Thus, electrodes are placed at the quadriceps muscles according to the recommendations given in [111]. During the flexion phase, the gravitational torque provides the needed assistance torque to guide the orthosis movements to the resting position. Flexion/extension amplitude of the knee joint is in the range between 0° and -120°.

Using the Lagrange formulation, the dynamics of the wearer's shank-foot/orthosis system can be expressed as follows:

$$J\ddot{\theta} = -\tau_g \cos(\theta) - A\,\text{sign}(\dot{\theta}) - B\dot{\theta} + \tau_m + \tau_{stim} + \tau_h \tag{3.10}$$

where θ, $\dot{\theta}$, $\ddot{\theta}$ represent the joint position, velocity, and acceleration of the wearer's shank-foot segment, respectively. J is the inertia of the wearer's shank-foot/orthosis system; A, B are respectively the viscous and solid friction coefficients and τ_g represents the system gravitational torque at the full extension of the shank. τ_m, τ_{stim} and τ_h represent respectively the motor torque, the stimulation torque and the volitional wearer's torque. Note that, as stated before, $\tau_{stim} = 0$ during the flexion phase.

3.4.3 Modeling of the wearer/ANGELEGS exoskeleton system

A schematic view of a subject wearing the ANGELEGS exoskeleton and performing Sit-To-Stand (STS) transfer task is shown in Figure 3.11. During this task, the wearer-exoskeleton system, including the shank-foot segment, thigh and HAT (Head-Arm-Torso) in the sagital plane, can be modeled as a triple inverted pendulum. In this study, we assume that the movements of ankle, knee and hip joints of the wearer-exoskeleton system for the STS transfer task are achieved in the sagital plane. During this task, movements of both legs and exoskeleton are assumed to be synchronous and simultaneous (i.e., the link between the exoskeleton and the subject is assumed to be rigid). Hence, a three DoF model of the wearer/exoskeleton system is used as shown in Figure 3.11. The exoskeleton, worn

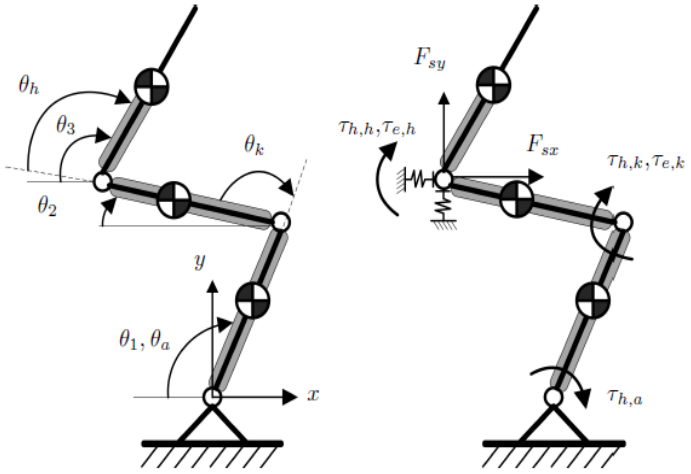

Figure 3.11: Schematic view of a subject performing a STS movement.

by the wearer, is represented by gray rounded rectangles. STS movements during which the subject stands up from a chair without hand assistance are considered in this study. Using the Euler-Lagrange formalism [114], the dynamic model of the wearer/exoskeleton system is described as follows:

$$\mathrm{M}(q)\ddot{q} + \mathrm{C}(q,\dot{q})\dot{q} + \mathrm{G}(q) = \mathrm{U} + \mathrm{J}_{\mathrm{F}}^{\mathrm{T}}\mathrm{F} \tag{3.11}$$

where $q = \left[q_1, q_2, q_3\right]^{\mathrm{T}} = [\theta_1, \theta_2, \theta_3]^{\mathrm{T}}$, the exoskeleton joint coordinates vector, represents the state vector (Figure 3.11). The seat force is modeled as an external force F that acts on the hip joint of the wearer/exoskeleton system. $\mathrm{J_F}$ is the Jacobian matrix. The torque vector U is given as follows:

$$\mathrm{U} = \mathrm{U}_h + \mathrm{U}_e = \mathrm{R}\begin{Bmatrix} \tau_{h,a} \\ \tau_{h,k} \\ \tau_{h,h} \end{Bmatrix} + \mathrm{R}\begin{Bmatrix} \tau_{e,a} \\ \tau_{e,k} \\ \tau_{e,h} \end{Bmatrix} \tag{3.12}$$

U_h and U_e denotes the vector of torques generated by the wearer and the vector of torques provided by the exoskeleton at the different joints, respectively. Note that both ankle joints of the exoskeleton are passive. The transformation matrix R is given as follows:

$$\mathrm{R} = \mathrm{J}_{\Theta}^{-\mathrm{T}} \tag{3.13}$$

where J_θ represents the transformation matrix from the joint space $(\theta_a, \theta_k, \theta_h)$ to the defined state space (q_1, q_2, q_3), as shown in Figure 3.11. The matrices $M(q), C(q,\dot{q}), G(q)$ are defined as follows:

$$M(q) = [M_{ij}]_{3\times 3}, \quad C(q,\dot{q}) = [C_{ij}]_{3\times 3}, \quad G(q) = [G_{ij}]_{1\times 3}. \tag{3.14}$$

with:

$$\begin{aligned}
M_{11} &= I_{e1} + I_{h1} + l_1^2 m_{e2} + l_1^2 m_{e3} + l_1^2 m_{h2} + l_1^2 m_{h3} \\
&\quad + k_{e1}^2 l_1^2 m_{e1} + k_{h1}^2 l_1^2 m_{h1} \\
M_{22} &= I_{e2} + I_{h2} + l_2^2 m_{e3} + l_2^2 m_{h3} + k_{e2}^2 l_2^2 m_{e2} + k_{h2}^2 l_2^2 m_{h2} \\
M_{33} &= m_{e3} k_{e3}^2 l_3^2 + m_{h3} k_{h3}^2 l_3^2 + I_{e3} + I_{h3} \\
M_{12} &= l_1 l_2 (m_{e3} + m_{h3} + k_{e2} m_{e2} + k_{h2} m_{h2}) c_{12} \\
M_{13} &= l_1 l_3 (k_{e3} m_{e3} + k_{h3} m_{h3}) c_{13} \\
M_{23} &= l_2 l_3 (k_{e3} m_{e3} + k_{h3} m_{h3}) c_{23} \\
M_{21} &= M_{12} \\
M_{31} &= M_{13} \\
M_{32} &= M_{23}.
\end{aligned}$$

$$\begin{aligned}
C_{11} &= C_{22} = C_{33} = 0 \\
C_{12} &= l_1 l_2 s_{12} (m_{e3} + m_{h3} + k_{e2} m_{e2} + k_{h2} m_{h2}) \dot{\theta}_2 \\
C_{13} &= l_1 l_3 s_{13} (k_{e3} m_{e3} + k_{h3} m_{h3}) \dot{\theta}_3 \\
C_{21} &= -l_1 l_2 s_{12} (m_{e3} + m_{h3} + k_{e2} m_{e2} + k_{h2} m_{h2}) \dot{\theta}_1 \\
C_{23} &= l_2 l_3 s_{23} (k_{e3} m_{e3} + k_{h3} m_{h3}) \dot{\theta}_3 \\
C_{31} &= -l_1 l_3 s_{13} (k_{e3} m_{e3} + k_{h3} m_{h3}) \dot{\theta}_1 \\
C_{32} &= -l_2 l_3 s_{23} (k_{e3} m_{e3} + k_{h3} m_{h3}) \dot{\theta}_2
\end{aligned}$$

$$
\begin{aligned}
\mathrm{G}_{11} &= (m_{e2} + m_{e3} + m_{h2} + m_{h3} + k_{e1} m_{e1} + k_{h1} m_{h1}) g l_1 c_1 \\
\mathrm{G}_{12} &= (m_{e3} + m_{h3} + k_{e2} m_{e2} + k_{h2} m_{h2}) g l_2 c_2 \\
\mathrm{G}_{13} &= (k_{e3} m_{e3} + k_{h3} m_{h3}) g l_3 c_3 \, .
\end{aligned}
$$

where s_i, c_i, s_{ij} and c_{ij} are the abbreviations of $\sin(\theta_i)$, $\cos(\theta_i)$, $\sin(\theta_i - \theta_j)$ and $\cos(\theta_i - \theta_j)$ respectively, with $i, j = 1, 2, 3$. m_{hi} m_{ei}, k_{hi}, k_{ei}, I_{hi}, I_{ei} with $i = 1, 2, 3$, are the masses, coefficients of distribution of gravity, and inertia corresponding to the shank-thigh-HAT segments of the wearer and the exoskeleton, respectively. l_i $(i = 1, 2, 3)$ represent the lengths of the wearer's shank-thigh-HAT segments. The matrices J_Θ and J_F are given as follows:

$$
\mathrm{J}_\Theta = \begin{bmatrix} 1 & 0 & 0 \\ 1 & 1 & 0 \\ 1 & 1 & 1 \end{bmatrix}, \quad \mathrm{J}_\mathrm{F} = \begin{bmatrix} l_1 s_1 & l_2 s_2 & 0 \\ l_1 c_1 & l_2 c_2 & 0 \end{bmatrix}. \tag{3.15}
$$

The seat force F takes an important role for compensating the wearer's body segments gravity when he/she is in a sitting position. Here, it is supposed to totally compensate the torques acting at the knee and ankle joints induced by the gravity related to the masses of the three wearer's body segments (i.e., the wearer's knee and ankle joints are free (ie. $\tau_{h,a} = \tau_{h,k} = 0$) at the sitting position). The seat force must have a zero value when the position of the hip joint is higher than a certain threshold value (i.e., "Seat-Off" point). However, the seat-off point is difficult to detect using only joint position information since the chair height may change. On the other hand, it is shown that the time required to reach the maximum value of the GRF represents a good approximation of the "Seat-Off" time [115]. Hence, the model of the seat force can be expressed as follows:

$$
\mathrm{F} = \left[\mathrm{F}_{sx} \mathrm{F}_{sy}\right] = \beta_f \mathrm{F}_s \tag{3.16}
$$

where F_{sx}, F_{sy} denote the x and y components of the the seat force F, and:

$$
\beta_f = 1 - \frac{\mathrm{F}_{\mathrm{GRF}}}{\mathrm{F}_{\mathrm{GRF},max}} \tag{3.17}
$$

where β_f denotes a positive ratio ($\beta_f \in [01]$). F_{GRF} represents the measured ground reaction force and $F_{GRF,max}$ its maximum value. The force F_s is the force that can fully compensate for the torques at ankle and knee joint levels by the three wearer's body segments. It is calculated as follows:

$$F_s = (HR^{-1}J_F^T)^{-1}HR^{-1}G(q) \tag{3.18}$$

where H is a constant matrix used to extract the ankle and knee joint torques from the torque vector.

The matrix H is defined as follows:

$$H = \begin{bmatrix} 1 & 0 & 0 \\ 0 & 1 & 0 \end{bmatrix}. \tag{3.19}$$

3.5 Identification

3.5.1 Identification of the SEA-actuated knee joint dynamic model

Figure 3.12: Identification of the SEA-actuated knee joint dynamic model

The parameters of the SEA-actuated knee joint dynamic model (3.7) are estimated

using the least squares optimization method [116]. For this purpose, a sinusoidal input torque τ_m with ten different frequencies ranging from 0.2 to 2 Hz is applied to the SEA-actuated knee joint of the EROWA exoskeleton in open-loop (3.8). The joint position θ_h and the spring torque τ_s are measured simultaneously. The identified parameter values are given in table 3.2.

Table 3.2: Identified parameter values of SEA-actuated knee joint dynamic model

Parameter	Value
$J_s(Kg.m^2)$	0.000376
$B_s(Nm{\cdot}s{\cdot}rad^{-1})$	0.000803
$F_s(N.m)$	0.8864
$F_h)(N.m)$	0.1114
$F_0(N.m)$	$0.01234\dot{\theta}_h$-0.322184-sin(θ_h))

Note that the ankle joint was fixed and no external load was used (see Figure 3.12) during identification.

3.5.2 Identification of dynamic model of the wearer/EICOSI orthosis system

The main parameters to identify are: A, B, J and τ_g. J and τ_g represent respectively the inertia and the gravity torque of the wearer's shank-foot segment/orthosis system. J corresponds to the sum of the inertia of the wearer's shank-foot segment J_s, and the orthosis inertia J_o. τ_g corresponds to the sum of the gravity torque of the wearer's shank-foot segment τ_{gs}, and the orthosis gravity torque τ_{go}. J_s and τ_{gs} are identified using the anthropometric parameters (weight and height) of the wearer and the regression equations of Winter [117], while J_o, τ_{go}, A, and B are identified using the nonlinear least square optimization of Equation 3.10 considering a multi-frequency sinusoidal torque applied at the knee joint. The knee joint velocity and acceleration are estimated by derivation of the knee joint position. The identified wearer's shank-foot segment/orthosis system parameters are shown in Table 3.3.

Table 3.3: Identified dynamic model parameters of the wearer/orthosis system

Parameter	Value
$J(J_o+J_s)(Kg.m^2)$	0.01(0.0117+0.2522)
$\tau_g(\tau_{go}+\tau_{gs})(N.m)$	9.5724(0.2424+9.33)
$A(N.m)$	0.3668
$B(N.m.s.rad^{-1})$	0.7053

3.5.3 Identification of dynamic model of the wearer/ANGELEGS exoskeleton system

A healthy male subject (age: 27 years old; height: 1.80 m; weight: 65 Kg) participated in the experiments. The subject was informed of the experimental protocol approved by Henri-Mondor Hospital, France, and gave his consent before participating in the experiments.

Kinematics and dynamometrics data were measured using a stereophotogrammetric system (Optitrack, Flex 13) and a Wii Balance Board (WIIBB, Nintendo), respectively. A set of six retro-reflective markers, placed on the subject's body, are used to estimate the corresponding joint positions. Joint velocities and accelerations were obtained using centred differences. The WIIBB allows measuring the external force F_Y and the moment M_Z along the vertical and lateral axes, respectively. Note that the WIIBB has been proven accurate enough to perform dynamics identification of a planar model of human [118]. All measured data were low-pass filtered at 5 Hz using a zero-phase 5th-order Butterworth filter.

The identification process was carried out in two steps. The subject was asked first to perform exciting motions without wearing the exoskeleton and then to perform the same motions while wearing the exoskeleton. The retained exciting motions were shown to the subject and consisted of a long continuous motion of two minutes approximately. This motion was composed of 10 squats performed at different velocities, 10 oscillations of the hip/trunk and 10 oscillations of the ankle. These motions were considered as exciting since the condition number of the base parameter regressor matrix was relatively low ($cond(\mathbf{W}_b) = 36$).

The identified inertial parameters of the subject's segments and exoskeleton are given in Table 3.4. Figure 3.14 shows an excellent fitting between both the external vertical force and the moment measured by the WIIBB, and the estimated ones using the identified

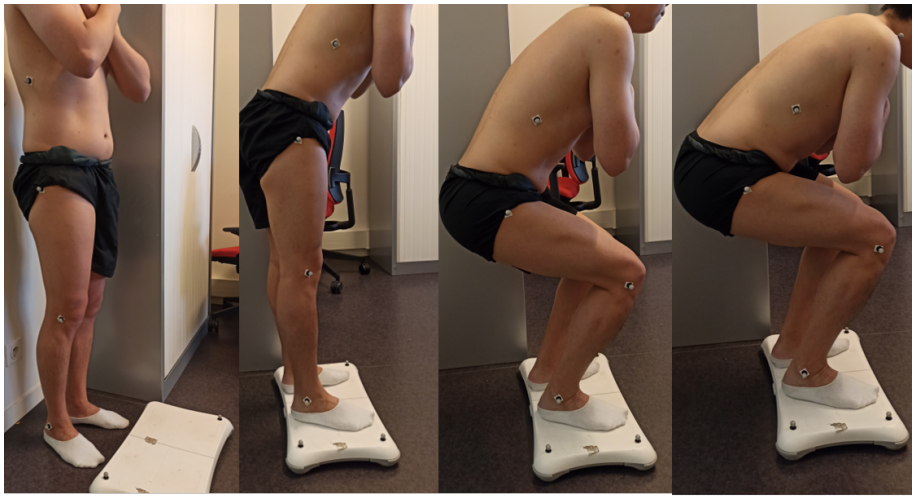

Figure 3.13: Experimental setup: a stereophotogrammetric system and a Wii balance board used to collect kinematic and dynamometric data, respectively. The subject performs typical exciting motions while wearing the exoskeleton.

dynamic model parameters, respectively. RMS estimation errors of the external vertical force and moment are 10.6 N and 6.8 Nm, respectively. Such differences are within the accuracy of the WIIBB and show that the inertial parameters are well identified.

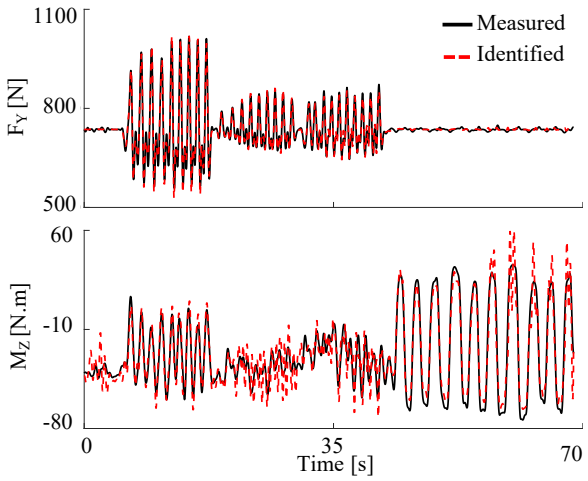

Figure 3.14: Comparison of the external vertical force (F_y) and its corresponding moment M_z measured by the WIIBB and the ones estimated using the identified dynamic model.

Table 3.4: Identified dynamic model parameters of the wearer/ANGELEGS exoskeleton system

Exoskeleton		
Parameters	Values	Units
m_{e1}, m_{e2}, m_{e3}	1, 3.472, 4.9	(kg)
k_{e1}, k_{e2}, k_{e3}	0.5685, 0.50 , 0.1556	$(kg \cdot m)$
I_{e1}, I_{e2}, I_{e3}	0.0796, 0.0097, 0.1614	$(kg \cdot m^2)$
Subject		
Parameters	Values	Units
m_{h1}, m_{h2}, m_{h3}	7.30, 15.5, 40.2	(kg)
k_{h1}, k_{h2}, k_{h3}	0.5256, 0.5646, 0.2515	$(kg \cdot m)$
I_{h1}, I_{h2}, I_{h3}	0.0724, 0.3732, 8.34	$(kg \cdot m^2)$

3.6 Conclusion

In this chapter, we described the different sensors, actuators and wearable robot prototypes (EICOSI orthosis, EROWA exoskeleton, and ANGELEGS exoskeleton) used for the purpose of evaluating the performance of the assistive control strategies proposed in this thesis. Moreover, dynamic modeling and identification of the SEA, EICOSI and ANGELEGS prototypes were carried out.

For the SEA-actuated knee joint of the EROWA exoskeleton, flexion/extension movements were considered. Based on the dynamic model of the worm gear set, a two-mass dynamic model of the SEA-actuated knee joint was developed. The dynamic model parameters were identified using the least square optimization method. The developed model is highly non-linear, and the spring torque, which corresponds to the interaction torque between the wearer and the exoskeleton, depends both on the motor torque, the torque developed by the wearer and also on the varying friction between the worm wheel and the worm gear.

Concerning the EICOSI orthosis, flexion/extension movements of the knee joint have been considered. The parameters of the orthosis were identified using the least square optimization method while those of the wearer's shank-foot segment were determined using the Winter's anthropometric tables.

The ANGELEGS exoskeleton was considered for the study of STS movements. The wearer/ANGELEGS system is modeled as a triple inverted pendulum in the sagital plane.

An identification framework exploiting a wii-board and optical motion tracking device, has been implemented to identify the segments parameters of the wearer/ANGELEGS exoskeleton system.

Chapter 4

Proxy-NDO-based control (PNC) of a SEA-actuated exoskeleton for multimode human-robot interactions

To succeed, it is not enough to plan. You also have to know how to improvise.

Isaac Asimov

Contents

4.1 Introduction

In this chapter, we propose in the first part a Proxy-NDO-based Control (PNC) strategy for three human-robot interaction modes: zero-impedance mode, force tracking mode and high torque mode. The Proxy-based Sliding Mode Control (PSMC) strategy, presented in [119], is exploited and further extended by proposing a Nonlinear Disturbance Observer (NDO) based PD force control of the Series Elastic Actuator (SEA) to ensure an accurate force tracking and robustness with respect to modeling uncertainties and external disturbances, as well as wearer's safety. Furthermore, a human-exoskeleton interaction torque based function is introduced to achieve smooth and stable transitions between the three interaction modes. Moreover, the stability of the proxy-based force controller is theoretically analyzed. In the last part of the chapter, the performance of the proposed controller is evaluated in simulation and through experiments to control the knee joint movements of the EROWA exoskeleton.

4.2 Mathematical preleminaries

In this section we will derivate a relation between sign "sgn" and unit saturation "sat" functions that will be used in the controller design in the following sections.

Let "$sign$" and "sat" be the sign and unit saturation functions defined as follows:

$$sgn(z) = \begin{cases} \frac{z}{|z|} & \text{if} \quad z \neq 0 \\ z & if \quad z = 0 \end{cases} \tag{4.1}$$

$$sat(z) \triangleq \frac{z}{max(1,|z|)} \tag{4.2}$$

The equation expression $y = sign(z)$ can be expressed in the following logic-like expression:

$$(y = \frac{z}{|z|} \wedge z \neq 0) \vee (|y| \leq 1 \wedge z = 0) \tag{4.3}$$

In the following section, we will use the analytical relation between "sign" and "sat":

$$y = sgn(z - y) \quad \Longleftrightarrow \; y = sat(z) \quad \forall y, z \in \mathbb{R} \tag{4.4}$$

proof:

$$
\begin{aligned}
& y = sgn(z-y) \\
& \quad \Longleftrightarrow (y=1 \wedge z-y>0) \vee (y=-1 \wedge z-y<0) \vee (y \in [-1,1] \wedge z-y=0) \\
& \quad \Longleftrightarrow (y=1 \wedge z>1) \vee (y=-1 \wedge z<-1) \vee (y=z \wedge z \in [-1,1]) \\
& y = sat(z)
\end{aligned}
$$

4.3 Proxy-NDO-based control

Figure 4.1 illustrates the entire proposed PNC structure of the SEA-actuated knee joint of the EROWA exoskeleton. The motor control torque τ_m is expressed as follows:

$$\tau_m = \tau_f + F_s \tau_s + F_0 \tag{4.5}$$

where τ_f is the proxy-NDO-based control torque. According to the two-mass model of the SEA-actuated knee joint of the EROWA exoskeleton (Eq. 3.8, chapter 3), $F_s \tau_s$ represents the torque acting on the motor side, related to the spring torque; F_0 represents the shank-foot segment gravity torque.

In the proposed PNC structure (see Figure 4.1), an NDO-based PD controller (i.e., inner-layer controller) is used in replacement of the PID controller part of the standard PSMC [119] to meet the requirements in terms of force tracking accuracy and robustness with respect to modeling uncertainties and external disturbances. Moreover, the SMC is still used as outer-layer controller to ensure effective force compliance and consequently wearer's safety. Since the inertia of the proxy is set to zero (i.e., $j = 0$) [119], the output torques of the outer-layer (τ_{fo}) and inner-layer (τ_{fi}) controllers are equal (see Figure 4.1):

$$\tau_f = \tau_{fi} = \tau_{fo} \tag{4.6}$$

The terms inner and outer refer to the virtual position of the controller (SMC and/or NDO-based PD controller) with respect to the desired torque (τ_d) (see Figure 4.1). The outer-layer, corresponds to the SMC controller as depicted in Figure 4.1, while the inner-

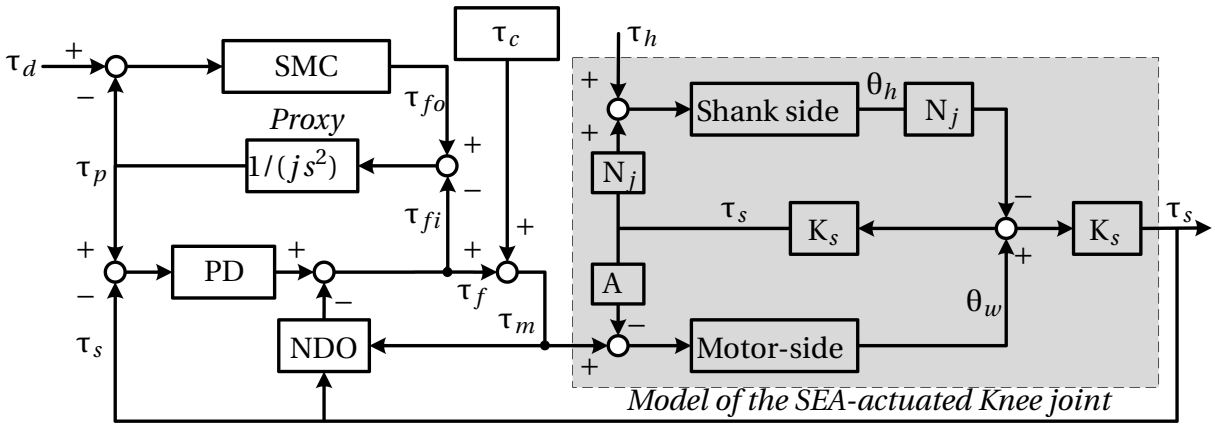

Figure 4.1: Complete control structure of the SEA-actuated knee joint ($\tau_c = F_s\tau_s + F_0$). j denotes the proxy inertia ($j = 0$).

layer is related to the PD-NDO controller which ensures the tracking of the proxy virtual position by the knee joint. In the following, the design of the controllers are detailed.

4.3.1 Inner-Layer controller: NDO-based PD control

As part of the design of the inner-layer control algorithm, an NDO is first introduced (Figure 4.1).

4.3.1.1 Nonlinear Disturbance Observer (NDO)

Let us define the state $x = [x_1\ x_2]^T \in R^2$ with $x_1 = \tau_s$ and $x_2 = \dot{\tau}_s$, where τ_s represents the spring torque. The dynamic model of the SEA-actuated knee joint of the EROWA exoskeleton (3.8) can then be formulated as follows:

$$\begin{cases} \dot{x}_1 = x_2 \\ \dot{x}_2 = \frac{1}{J_s}(-B_s x_2 - F_s x_1 - F_0 + \tau_m) + \frac{1}{J_s} d \end{cases} \tag{4.7}$$

where d represents the lumped disturbance torque on the motor input, including the one caused by the wearer's torque τ_h and the one induced by the modeling errors. J_s, B_s, F_s, and F_0 are the parameters of the two-mass dynamic model (3.8) defined in Chapter 3.

The NDO is designed based on [57, 120]:

$$\begin{cases} \hat{d} = z + p(x) \\ \dot{z} = -K_1 x_2 + \frac{K_2}{J_s}(B_s x_2 + F_s x_1 + F_0 - \tau_m - (z + p(x))) \end{cases} \tag{4.8}$$

where $\hat{d}$ represents the estimated disturbance torque and z an auxiliary variable. $p(x)$ is chosen as $p(x) = K_1 x_1 + K_2 x_2$, and K_1 and K_2 are two positive constants, $K_1, K_2 > 0$.

The estimation error of the disturbance torque is given as $\tilde{d} = (d - \hat{d})$. From (4.7) and (4.8), we obtain:

$$\dot{\tilde{d}} = \frac{K_2}{J_s}(d - \hat{d}) = \frac{K_2}{J_s}\tilde{d}. \tag{4.9}$$

Assuming that the velocity of the disturbance is bounded, $\|\dot{d}\|_\infty < \varepsilon_2$, the following lemma addresses the stability of the NDO.

Lemma 4.3.1 *We assume that the SEA-actuated knee joint of the EROWA exoskeleton system (3.8) is subject to a disturbance, d, described by (4.7) and that the rate of change of the disturbance is bounded, i.e., $\|\dot{d}\| < \varepsilon_2$. The NDO is given in (4.8). The estimation error $\tilde{d}$ is globally, uniformly and ultimately bounded, i.e., $\tilde{d}$ globally exponentially converges into the ball of radius $\frac{J_s \varepsilon_2}{K_2}$.*

Proof: Let's choose the Lyapunov function V_{ndo} as:

$$V_{ndo} = \frac{1}{2}\tilde{d}^2. \tag{4.10}$$

By the derivation of the Lyapunov function V_{ndo} and using (4.8) and (4.9), we obtain:

$$\dot{V}_{ndo} = \tilde{d}\dot{\tilde{d}} = \tilde{d}(\dot{d} - \dot{\hat{d}}) = \tilde{d}\Big(\dot{d} - \frac{K_2}{J_s}\tilde{d}\Big) \leq \|\tilde{d}\|\Big(\varepsilon_2 - \frac{K_2}{J_s}\|\tilde{d}\|\Big). \tag{4.11}$$

Hence, $\dot{V}_{ndo} \leq 0$, $\forall \|\tilde{d}\| \geq \frac{J_s \varepsilon_2}{K_2}$. One can observe that the tracking error $\tilde{d}$ is globally, uniformly and ultimately bounded. If the change in the velocity of the disturbance is zero, i.e., $\dot{d} = 0$, the estimation error $\tilde{d}$ will converge asymptotically to zero. ■

From Lemma 4.3.1, it can be noted that the estimation accuracy of the disturbance observer (4.8) can be further increased by selecting a high value of K_2. However, in practice, the parameter K_2 should be selected as a trade-off between the accuracy requirement, the dynamics of closed-loop system, the measurement noise, and the dynamics of the disturbance, etc. More systematic and optimal selection approaches can be found in [57, 121].

4.3.1.2 NDO-based PD Control

Following the design of the NDO (4.8), the inner-layer NDO-based PD controller is given by:

$$\tau_{fi} = K_p e_p + K_d \dot{e}_p - \hat{d} \tag{4.12}$$

where K_p and K_d are two positive constants that represent the proportional and derivative gains, respectively. e_p is the virtual error, which is defined as follows:

$$e_p = \tau_p - \tau_s \tag{4.13}$$

where τ_p is the virtual torque of the proxy (see Figure 4.1).

4.3.2 Outer-layer controller: SMC

The outer-layer controller (see Figure 4.1) is designed as follows :

$$\tau_{fo} = \Gamma(e_\alpha + H\dot{e}_\alpha) \tag{4.14}$$

where τ_{fo} is the torque generated by the outer-layer controller, and

$$e_\alpha = \tau_d - \tau_p \tag{4.15}$$

Γ and $H > 0$ are the control gains and τ_d the desired torque of the spring. $\mathrm{sgn}(\cdot)$ is defined as: $\mathrm{sgn}(z) = z/|z|$ if $z \neq 0$; $\mathrm{sgn}(z) \in [-1,1]$ if $z = 0$ [119].

We define:

$$\sigma = e + H\dot{e} \tag{4.16}$$

where e represents the tracking error of the spring torque. Specifically, e is given by:

$$e = \tau_d - \tau_s. \tag{4.17}$$

Combined with (4.13) and (4.16), (4.14) can be rewritten as follows:

$$\tau_{fo} = \Gamma(\sigma - e_p - H\dot{e}_p) \tag{4.18}$$

Based on the designed inner-layer NDO-based PD control (4.12) and the outer-layer SMC (4.18), the equation (4.6) can be further expressed as follows:

$$\Gamma(\sigma - e_p - \mathrm{H}\dot{e}_p) = \mathrm{K}_p e_p + \mathrm{K}_d \dot{e}_p - \hat{d} \tag{4.19}$$

By exploiting the relation between the signum function " sgn " and the saturation function " sat " [119], we obtain:

$$y + \mathrm{X}w = \mathrm{Y}\mathrm{sgn}(z - \mathrm{Z}y) \Leftrightarrow y = -\mathrm{X}w + \mathrm{Y}\mathrm{sat}\left(\frac{\frac{z}{\mathrm{Z}} + \mathrm{X}w}{\mathrm{Y}}\right) \tag{4.20}$$

where $y, z, w \in \mathbb{R}$ and X, Y, Z > 0. By using (4.20), the equation (4.19) can be rewritten as follows:

$$\dot{e}_p = \frac{1}{\mathrm{K}_d}\left(-\mathrm{K}_p e_p + \hat{d}\right) + \frac{\Gamma}{\mathrm{K}_d}\mathrm{sat}\left(\frac{\mathrm{K}_d}{\Gamma}\left(\frac{\sigma - e_p}{\mathrm{H}} + \frac{\mathrm{K}_p e_p - \hat{d}}{\mathrm{K}_d}\right)\right) \tag{4.21}$$

Such transformation allows to calculate efficiently $\dot{e}_p$ from (4.19). Furthermore, from (4.21) and (4.19), the control torque τ_f can be written as follows:

$$\tau_f = \tau_{fo} = \tau_{fi} = \Gamma\mathrm{sat}\left(\frac{\mathrm{K}_d}{\Gamma}\left(\frac{\sigma - e_p}{\mathrm{H}} + \frac{\mathrm{K}_p e_p - \hat{d}}{\mathrm{K}_d}\right)\right). \tag{4.22}$$

Note that the PNC controller can be considered as a SMC controller (see equation (4.14)), and the proxy torque τ_p exponentially approaches the desired torque τ_d with a time constant of H as long as $|\tau_f| < \Gamma$ (i.e., $e_\alpha + \mathrm{H}\dot{e}_\alpha = 0$; the proxy lies on the sliding surface), regardless of disturbances [119]. Furthermore, the proxy torque τ_p is used as the desired torque of the NDO-based PD controller. Therefore, the force compliance from a large tracking error can be efficiently adjusted by selecting appropriate value of H. A high value of H reflects satisfactory force compliance, and vice versa. On the other hand, when $e_\alpha = 0$, the PNC controller is equivalent to the NDO-based PD controller (4.12).

4.3.3 Performance analysis

To evaluate the performance of the proposed PNC strategy (4.5) in force tracking and zero-impedance modes, a simulation study was conducted by comparing the proposed control strategy to the standard PD and PSMC (using only the PD) controllers. A compensation

torque $\tau_c = F_s\tau_s + F_0$ was also introduced in the PD and PSMC controllers to compensate for the friction, and the break-in torque at zero velocity in the worm gear set (section 3.4.1.1). The parameters of the PD controller were finely tuned using a trial-and-error method and are given as $K_p = 600$, and $K_d = 6.5$. The same values were also used for the PD parameters of the PSMC controller and the proposed PNC controller, in which a small H value (H = 0.01) was used to evaluate the tracking precision and ensure a relatively fast response. The parameter values of the SEA model (3.5) were set based on the identified parameters shown in section 3.12 and the known coefficients, such as $N_w = 10, N_j = 6.33$, and $K_s = 3.2$ Nm/rad. The nominal dynamics parameters of the exoskeleton shank-foot segment were set as follows: M = 0.2 Kg·m^2, C = 0.05 Nm·s·rad^{-1}, $G = 3.6\sin(\theta_h)$ Nm. A square-wave force reference τ_d (see Figure 4.2) was applied and an actuator saturation ($|\tau_m| \leq 15$ Nm) was imposed for all controllers.

First, the SEA-actuated knee joint of the EROWA exoskeleton was assumed to not interact with human and environment (i.e., absence of external disturbances which means a null environment impedance). Figure 4.2(a) shows that all the control strategies (PD, PSMC, and PNC) can ensure an accurate tracking. The root mean square tracking errors (RMSE) obtained with the three controllers during the steady state of the torque control response (i.e., the period starting 0.1s after each change of the reference) are respectively given as [6.5, 6.4, 5.5]$\times 10^{-5}$ Nm. Then, the SEA-actuated knee joint of the EROWA exoskeleton was assumed to interact with the environment according to an impedance model with the following parameters: inertia $M_E = 0$ Kg·m^2, damping $C_E = 0.5C$, stiffness $G_E = 0.5G$. Figure 4.2(b) shows the obtained simulation results. Notably, the tracking accuracy of the PSMC and PD controllers are similar, and both decrease in the presence of an interaction with the environment (non-null environment impedance) (Figure 4.2(a) and 4.2(b)) (RMSE: 5.8$\times 10^{-3}$ Nm, 5.8$\times 10^{-3}$ Nm, respectively). Conversely, the proposed PNC strategy is more robust with respect to the environment uncertainties (RMSE: 9.7$\times 10^{-5}$ Nm). Figure 4.3 shows the control torque, τ_m, and the compensation torque, $F_s\tau_s + F_0$, using the three controllers (PD, PSMC, and PNC).

Furthermore, to evaluate the zero-impedance tracking performance, we set the desired torque to zero and used a 1-Hz sinusoidal torque with an amplitude of 2 Nm to simulate the wearer's joint torque τ_h. The simulation results show that the tracking error

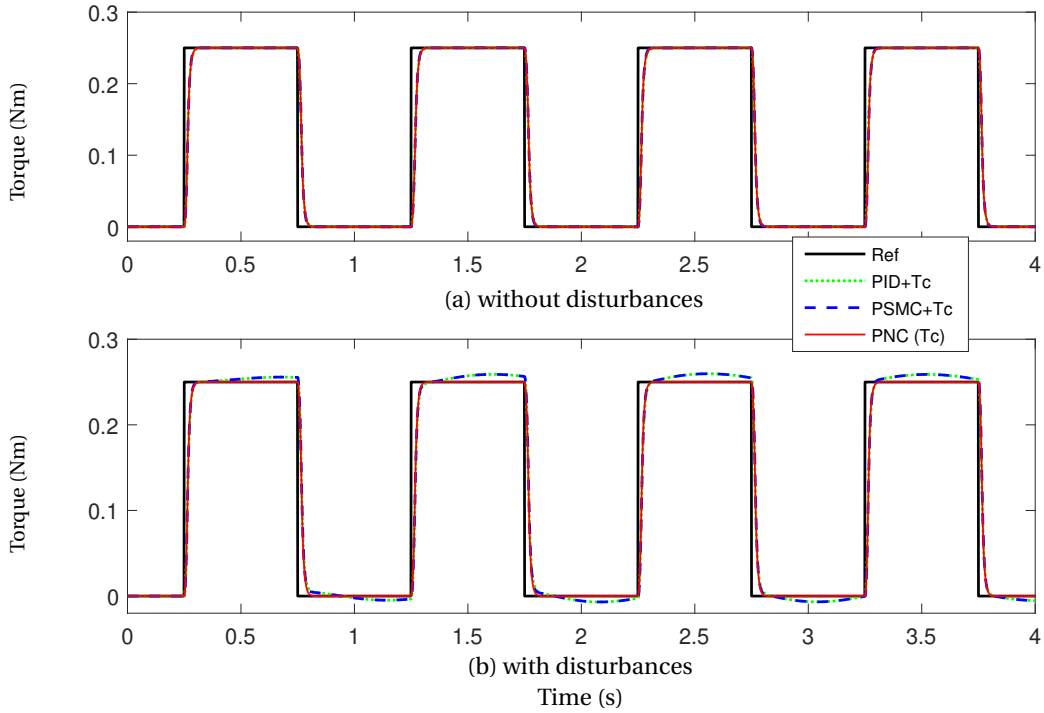

Figure 4.2: Tracking performance with different environmental impedance levels. (Tc= $\tau_c = F_s\tau_s + F_0$).

achieved by the proposed control strategy (RMSE: 0.001 Nm) is much lower than those obtained with the PD (RMSE: 0.0309 Nm) and PSMC (RMSE: 0.0309 Nm) controllers (see Figure 4.4). Figure 4.4(b) shows that the wearer's joint torque τ_h can be accurately estimated using the proposed NDO (RMSE ($\hat{\tau}_h - \tau_h$): 0.003 Nm; $\hat{\tau}_h = -\hat{d}/F_h$).

Remark 1: The two-mass model-based NDO (4.8) improves the robustness of the proxy-NDO-based controller with respect to uncertainties due to system modeling and environment (i.e., wearer's torque and environmental uncertainties). Although the NDO can be directly used in the conventional PSMC controller, it may significantly reduce the safety benefit provided by this controller. Therefore, in the proposed control strategy, the NDO is added to the inner-layer of the proxy-based control structure (see Figure 4.1).

4.3.4 Multi-mode human-robot interaction

In this chapter, three human-robot interaction modes are considered: force tracking mode, zero-impedance mode and high torque mode. In the force tracking mode, a desired reference torque τ_d is imposed for the interaction torque τ_s. In the zero-impedance

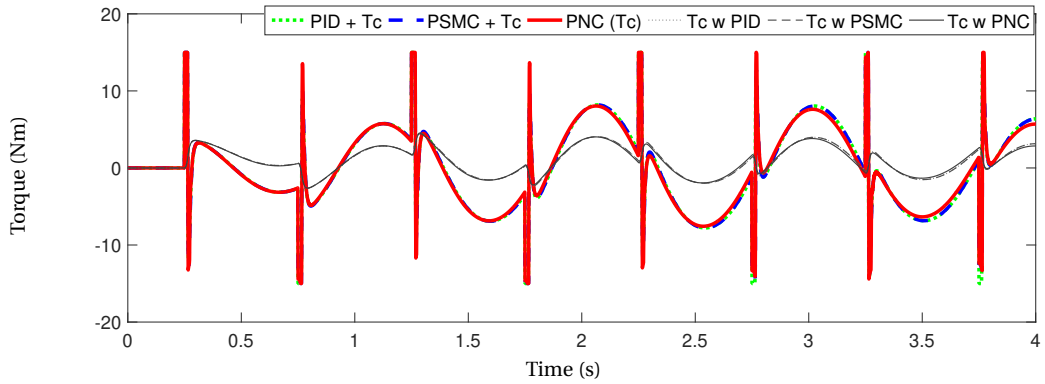

Figure 4.3: Control torques. (Tc=$\tau_c = F_s\tau_s + F_0$). Tc w PD, Tc w PSMC and Tc w PNC denote the compensation forces when using the PD, PSMC and the proposed PNC controllers, respectively.

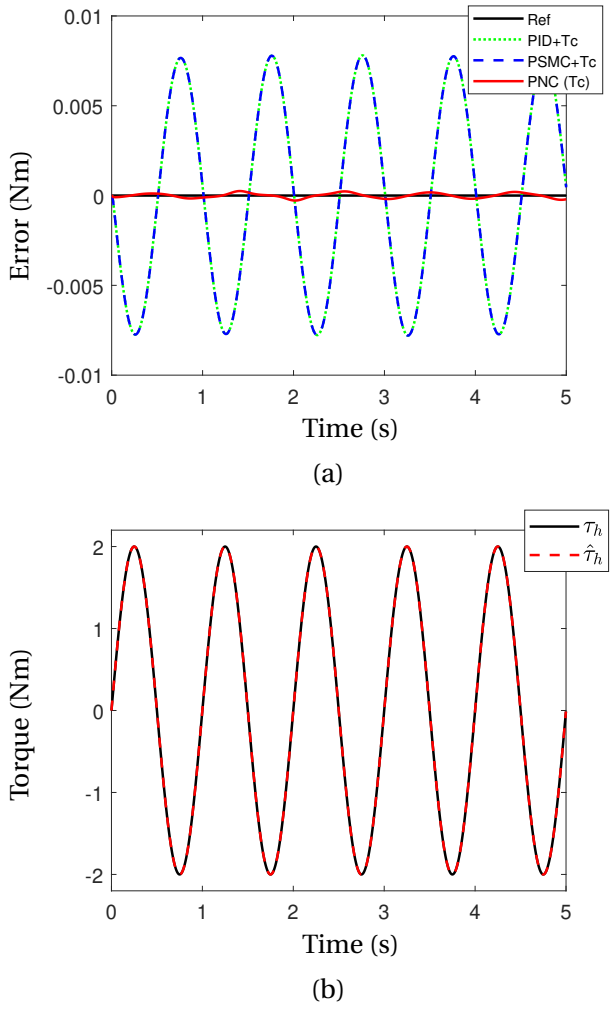

Figure 4.4: zero-impedance control of human initiated movement. (a) tracking error, (b) wearer's torque and the estimated one using the proposed NDO.

mode, the desired torque τ_d is set to zero, therefore, the SEA motor must follow the wearer's joint movements. In the high torque mode, high interaction torque τ_s is im-

posed and the desired torque τ_d is set to zero. In this mode, we are interested in how the interaction torque converges to the desired torque.

According to the analysis in section 4.3.2, the force compliance of the exoskeleton system increases with the increase of the H value. Figure 4.5(a) shows the responses of the wearer/exoskeleton system in terms of interaction torque for different values of the parameter H. To ensure significant force compliance, a high value of H is needed. However, high H values may affect the force tracking performance. Figure 4.6 shows the tracking errors, caused by the wearer's torque τ_h, of the proposed PNC controller during the zero-impedance mode (i.e., $\tau_d = 0$) with different H values. A significant pseudo-resistive behaviour of the system can be observed when a large H value (e.g., H = 0.4) is used. Therefore, setting H with constant value cannot simultaneously satisfy the requirements of significant force compliance and accurate torque control in the presence of modeling uncertainties and external disturbances. In this study, a new formulation of H parameter is proposed for multi-mode human-robot interaction. Since compliance is mainly emphasized in high torque mode to ensure wearer's safety and that an accurate torque control is needed in force tracking and zero-impedance modes, the formulation of H parameter as a function of interaction torque, is proposed as follows:

$$H = \frac{1}{2} H_r [\tanh(\rho(|\tau_s| - \gamma)) + 1] + H_{min} \tag{4.23}$$

where ρ is the sensitivity factor and γ a threshold torque; H_{min} and H_r denote the minimum value and the magnitude of H parameter, respectively. An example profile of H is shown in Figure 4.5(b).

Remark 2: Thanks to the proxy-NDO-based force control structure (see Figure 4.1), the force compliance of the closed-loop system can be efficiently adjusted through the new formulation of H parameter without affecting the stability of the system (see detailed stability analysis in section 4.3.5). Compared to existing works, e.g., [122], the fact of adjusting automatically the force compliance only through the H parameter, appears as an efficient solution leading to a unified control satisfying the requirements of the three human-robot interaction modes: zero-impedance mode, force tracking mode and high torque mode.

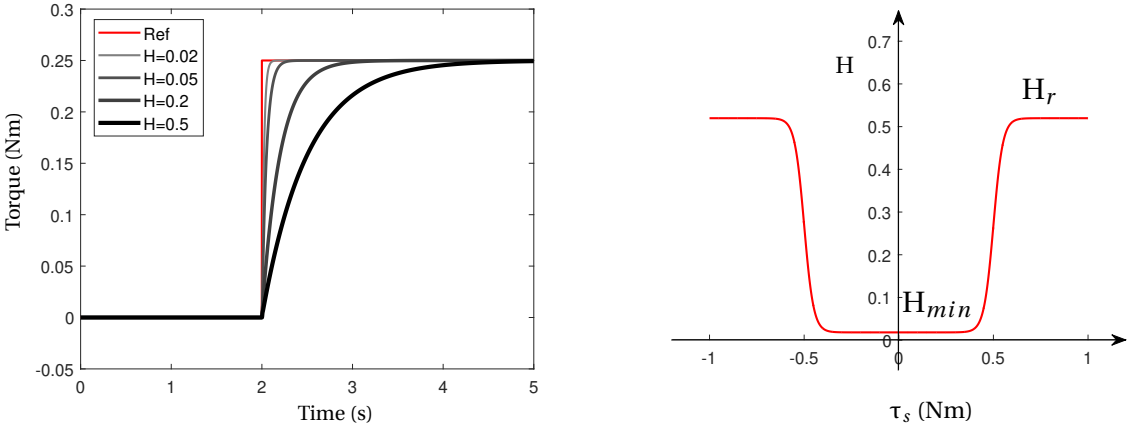

(a) Step response for different H values

(b) Example profile of the H value

Figure 4.5: Step response for different values of H and an example profile of the torque-based H value ($H_{min} = 0.02$, $H_r = 0.5$, $\rho = 10$, and $\gamma = 0.5$).

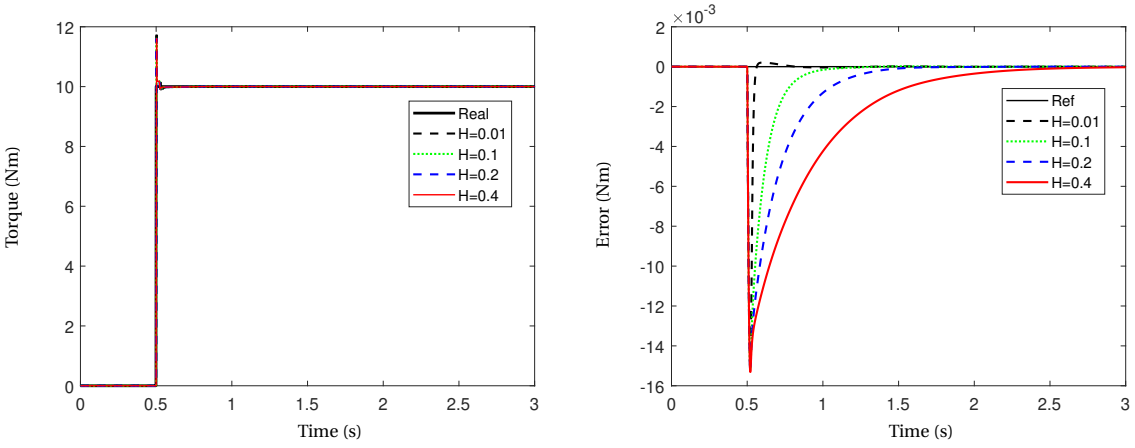

(a) Real/estimtaed wearer's joint torques

(b) Tracking errors

Figure 4.6: Performance of force tracking of the PNC strategy for different values of H in case of zero-impedance mode. The load impedance was set as follows: M = 0.2 Kg·m^2, C = 0.2 Nm·s·rad^{-1}, G = 14.4 sin(θ_h) Nm.

4.3.5 Stability analysis

Define state vectors $\mathrm{E} = [e\ \dot{e}\ \mathrm{E}_p]^{\mathrm{T}} \in \mathrm{R}^4$ and $\mathrm{E}_p = [e_p\ \dot{e}_p]^{\mathrm{T}} \in \mathrm{R}^2$, where e_p is the virtual error. The stability of the proposed PNC strategy (4.5) can be proved using the following lemma:

Lemma 4.3.2 *Consider the system (4.7) in which the disturbance torque d, including the torque provided by the wearer and the torque due to modeling errors, and the disturbance changing rate are bounded, i.e., $\|d\| < \varepsilon_1$ and $\|\dot{d}\| < \varepsilon_2$. The considered system is controlled using the proposed PNC strategy (4.5). Assume that the parameter Γ is set sufficiently high. Thus, there exists a close set Ω including the origin with which $\mathrm{E} \to \Omega$ is achieved as $t \to \infty$ and the closed-loop system under the PNC is input-to-state stable.*

Proof: Let us consider set-point control, i.e., $\dot{\tau}_d = \ddot{\tau}_d = 0$, and choose the following Lyapunov function candidate:

$$\mathrm{V} = \mathrm{E}_p^{\mathrm{T}} \mathrm{P} \mathrm{E}_p + \Gamma \|e - e_p\|_1 \tag{4.24}$$

where $\mathrm{P} \in \mathbb{R}^2$ is a positive definite matrix that satisfies:

$$\mathrm{PA} + \mathrm{A}^{\mathrm{T}}\mathrm{P} = -\mathrm{I}, \quad \mathrm{A} = \begin{bmatrix} 0 & 1 \\ -\mathrm{K}_p/\mathrm{J}_s & -(\mathrm{K}_d + \mathrm{B}_s)/\mathrm{J}_s \end{bmatrix} \tag{4.25}$$

where A is a Hurwitz matrix by selecting appropriate K_p and K_d values; I is the identity matrix. In this relation, V is positive definite, i.e., $\mathrm{V} \geq 0$. From (4.5)-(4.7), (4.12) and $\dot{\tau}_s = -\dot{e} = -\dot{e}_\alpha - \dot{e}_p$, we obtain:

$$\dot{\mathrm{E}}_p = \mathrm{A}\mathrm{E}_p + \left[0\ \ -\frac{1}{\mathrm{J}_s}\tilde{d}\right]^{\mathrm{T}} + \left[0\ \ -\left(\frac{\mathrm{B}_s}{\mathrm{J}_s}\dot{e}_\alpha + \ddot{e}_\alpha\right)\right]^{\mathrm{T}}. \tag{4.26}$$

Based on (4.25) and (4.26), the time derivative of the Lyapunov function candidate yields:

$$\dot{\mathrm{V}} = -\|\mathrm{E}_p\|^2 - 2h(e_p, \dot{e}_p)\left(\frac{1}{\mathrm{J}_s}\tilde{d} + \frac{\mathrm{B}_s}{\mathrm{J}_s}\dot{e}_\alpha + \ddot{e}_\alpha\right) + \dot{e}_\alpha \Gamma(e_\alpha) \tag{4.27}$$

where $h(e_p, \dot{e}_p)$ is given as follows:

$$h(e_p, \dot{e}_p) = [\mathrm{P}_{[1,2]}\ \mathrm{P}_{[2,2]}]\mathrm{E}_p = \frac{\mathrm{J}_s}{2\mathrm{K}_p} e_p + \frac{\mathrm{J}_s(\mathrm{K}_p + \mathrm{J}_s)}{2\mathrm{K}_p(\mathrm{K}_d + \mathrm{B}_s)}\dot{e}_p. \tag{4.28}$$

Thus, we obtain:

$$\dot{V} \leq -\|E_p\|^2 + \frac{\beta_1}{J_s}\|E_p\|\|\tilde{d}\| + \beta_1\|E_p\|\|\frac{B_s}{J_s}\dot{e}_\alpha + \ddot{e}_\alpha\| + \dot{e}_\alpha\Gamma(e_\alpha) \tag{4.29}$$

where $\beta_1 = 2\sqrt{P_{[1,2]}^2 + P_{[2,2]}^2}$. Let Φ a set space defined as follows:

$$\Phi = \left\{ E \in R^4 \left| |\frac{(\sigma - e_p)}{H} + \frac{K_p e_p - \hat{d}}{K_d}| \leq \frac{\Gamma}{K_d} \right.\right\} \cap \left\{ E \in R^4 \left| \beta_1 |\frac{B_s}{J_s} - \frac{1}{H}| \|E_p\| \leq \Gamma \right.\right\} \tag{4.30}$$

Since $\|d\| \leq \varepsilon_1$ and $\|d - \hat{d}\| \leq \frac{J_s \varepsilon_2}{K_2}$, $\hat{d}$ is also bounded. If Γ is set sufficiently high and the tracking error $E \in \Phi$. Therefore, from (4.14) and (4.22), the closed-loop system is always on the sliding surface, i.e., $e_\alpha + H\dot{e}_\alpha = 0$. Thus, we get:

$$\dot{V} \leq 0, \quad \text{if} \quad E \notin \Omega = \{E \in R^4 | \ \|E_p\| \leq \frac{\beta_1}{J_s}\|\tilde{d}\|\} \tag{4.31}$$

Note that the tracking error $e_\alpha = e - e_p$ converges asymptotically to zero regardless of disturbances, as long as $E \in \Phi$ [119]. Therefore, if Γ is set sufficiently high and $E \in \Phi$, there exists a close set $\Omega \subset \Phi$ with which $E \to \Omega$ is achieved as $t \to \infty$. From (4.31) and (4.11); one can conclude that the closed-loop system under the PNC is input-to-state stable. ■

The proof of Lemma 2 can be considered as a specific case of the stability proof (i.e., *Theorem 1*) presented in [119] by further taking into account the NDO and giving a detailed proof of the *Conjecture 1*. In practice, the condition $E \in \Phi$ can be further loosened by taking into account the existence of the sliding mode (see *Theorem 2* [119]). One can note that the stability of the closed-loop exoskeleton system is not affected by the parameter H that depends on the interaction torque (4.23).

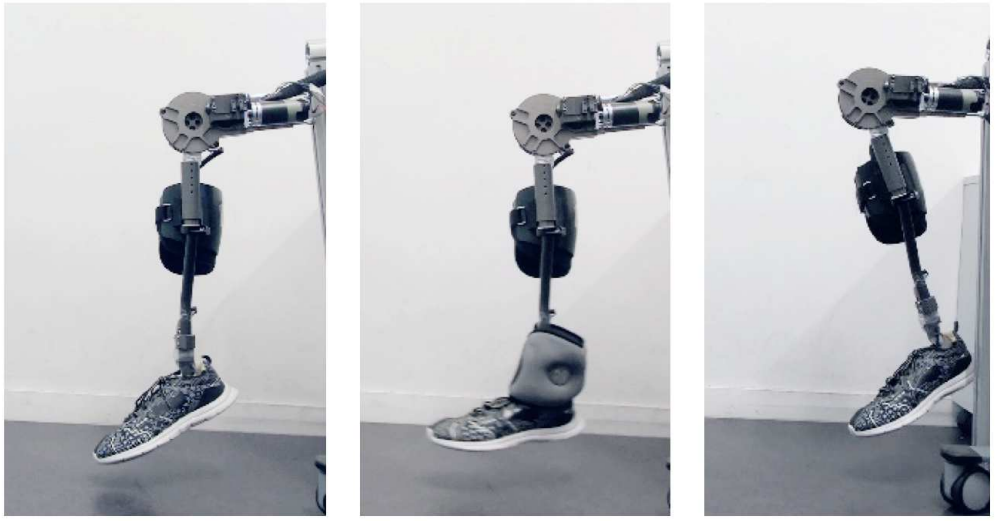

(a) (b) (c)

Figure 4.7: Force control of the SEA-actuated knee joint in force tracking mode. (a) without load, (b) with load, (c) with infinite load (i.e., high environmental stiffness by fixing the knee joint)

Figure 4.8: Force control of the SEA-actuated knee joint in zero-impedance mode.

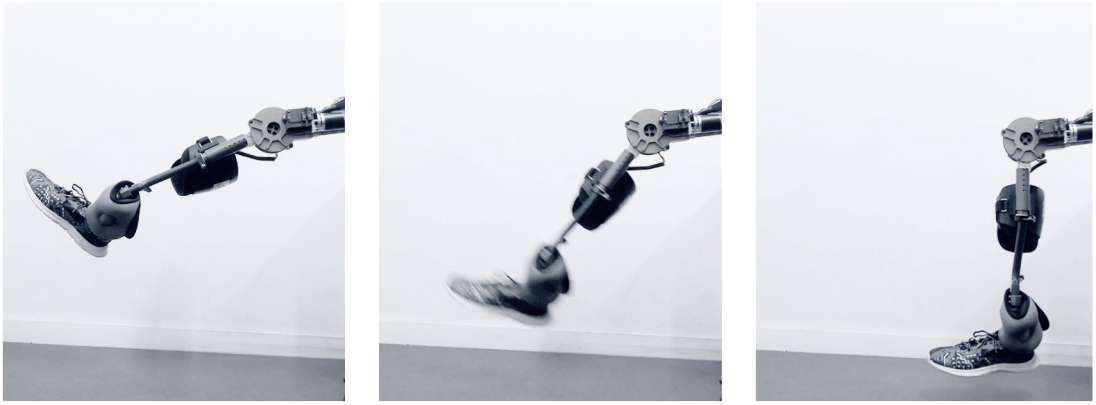

Initial position Intermediate position Final position

Figure 4.9: Force control of the SEA-actuated knee joint in high torque mode.

4.4 Experimental evaluation

4.4.1 Force tracking mode

The performance of the proposed PNC strategy (4.5) in force tracking mode was firstly evaluated experimentally and compared to those obtained with the PID and standard PSMC controllers. The experiments were conducted under three load conditions: without external load, with external load and with infinite external load (i.e., high environmental stiffness by fixing the knee joint) (see Figure 4.7). A 2-kg load was used to simulate the wearer's shank-foot segment. A compensation torque, $\tau_c = F_s\tau_s + F_0$, was also added in the control schemes of the PID and the standard PSMC controllers. The PID controller parameters were first optimally tuned using trial-and-error method, and the same parameter values were used for the remaining controllers (PSMC, and PNC). Note that only PD control is used in the proposed PNC strategy. The value of the parameter Γ was set to the maximum output torque of the motor for both the standard PSMC and PNC controllers. The parameters appearing in the H parameter formulation (4.23) were empirically set as $H_r = 2$, $H_{min} = 0.02$, $\rho = 5$, and $\gamma = 1.5$ to ensure sufficient force compliance for spring torque $\tau_s > 1.5$ Nm. A sinusoidal force with an amplitude of 0.15 Nm and a frequency of 0.5 Hz was used as reference torque, i.e., τ_d. Since the threshold torque γ is equal to 1.5 Nm, the H value is close to H_{min}. Figure 4.10 shows the tracking results. The tracking performance obtained with the PSMC was almost similar to that obtained with the PID controller under the three different load conditions. This is due to the fact that the PSMC

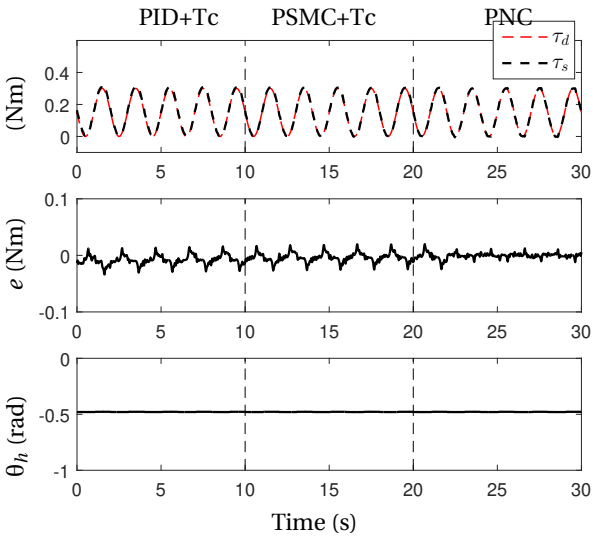

(a)

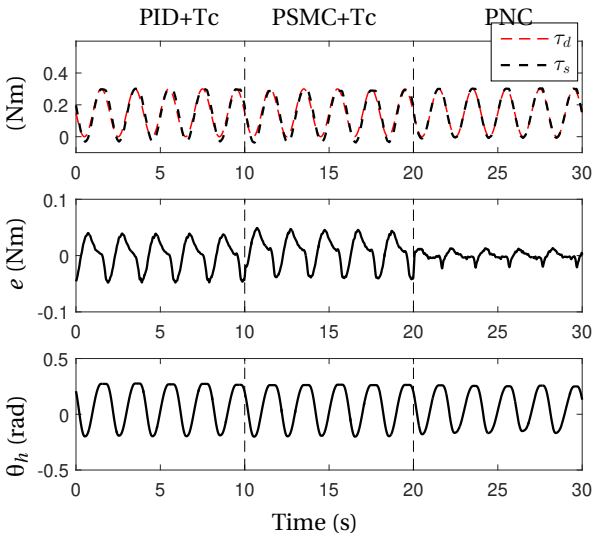

(b)

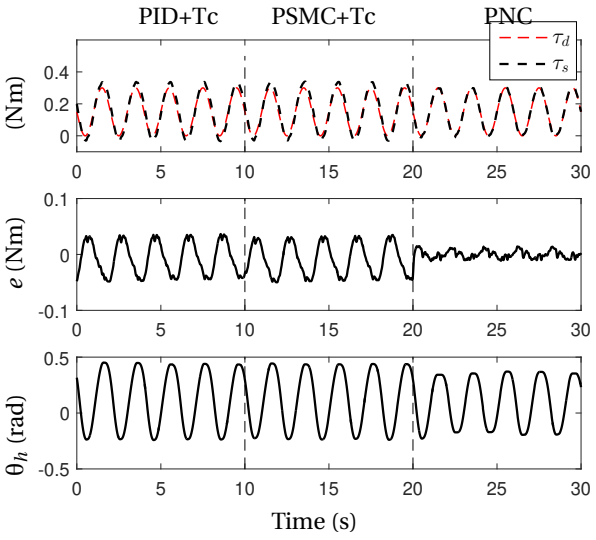

(c)

Figure 4.10: Tracking performance of the three controllers (PID, PSMC, and PNC) under three conditions: (a) Infinite environment stiffness, (b) With an external load, (c) Without external load.

Table 4.1: RMSE achieved by PID, PSMC and PNC controllers for three impedance conditions and four reference frequencies (unit: Nm).

Frequency	Impedance	Controller		
		PID+Tc	PSMC+Tc	PNC (Tc)
0.5-Hz	Stiff	0.0150	0.0160	0.0035
	with	0.0162	0.0172	0.0072
	without	0.0192	0.0188	0.0067
1-Hz	Stiff	0.0172	0.0174	0.0074
	with	0.0187	0.0185	0.0101
	without	0.0201	0.0209	0.0114
2-Hz	Stiff	0.0187	0.0181	0.0090
	with	0.0228	0.0224	0.0109
	without	0.0223	0.0234	0.0120
4-Hz	Stiff	0.0201	0.0180	0.0178
	with	0.0229	0.0212	0.0185
	without	0.0245	0.0283	0.0181

controller is equivalent to a PID controller after convergence of the proxy torque to the reference torque. Additionally, the tracking accuracy of the PID and PSMC controllers decreases under the two following conditions: without/with external load by comparison to the infinite load condition. These results confirm those presented in [123], i.e., the force dynamics of the SEA becomes more sensitive to the environmental inertia for low value of the ratio between the load stiffness and SEA spring stiffness. Moreover, the tracking accuracy obtained with the proposed PNC controller was significantly improved in all load conditions in comparison to the PID and PSMC controllers. Similar phenomenon was observed for the controllers PID, PSMC, and PNC when the frequency of the reference torque τ_d increased to 1, 2 and then to 4 Hz (see Table 4.1). As analyzed in Lemma 1, accuracy improvement due to the use of the NDO is directly related to the setting value of K_2 and to the low value of the external disturbance change rate.

4.4.2 Zero-impedance mode

In this experiment, the three aforementioned control strategies, namely, PID, PSMC and PNC, were evaluated to compare their performance in the zero-impedance mode, in which the interaction torque $|\tau_s|$ should be minimized as much as possible. A healthy subject was asked to walk on a treadmill at self-selected speeds while wearing the EROWA

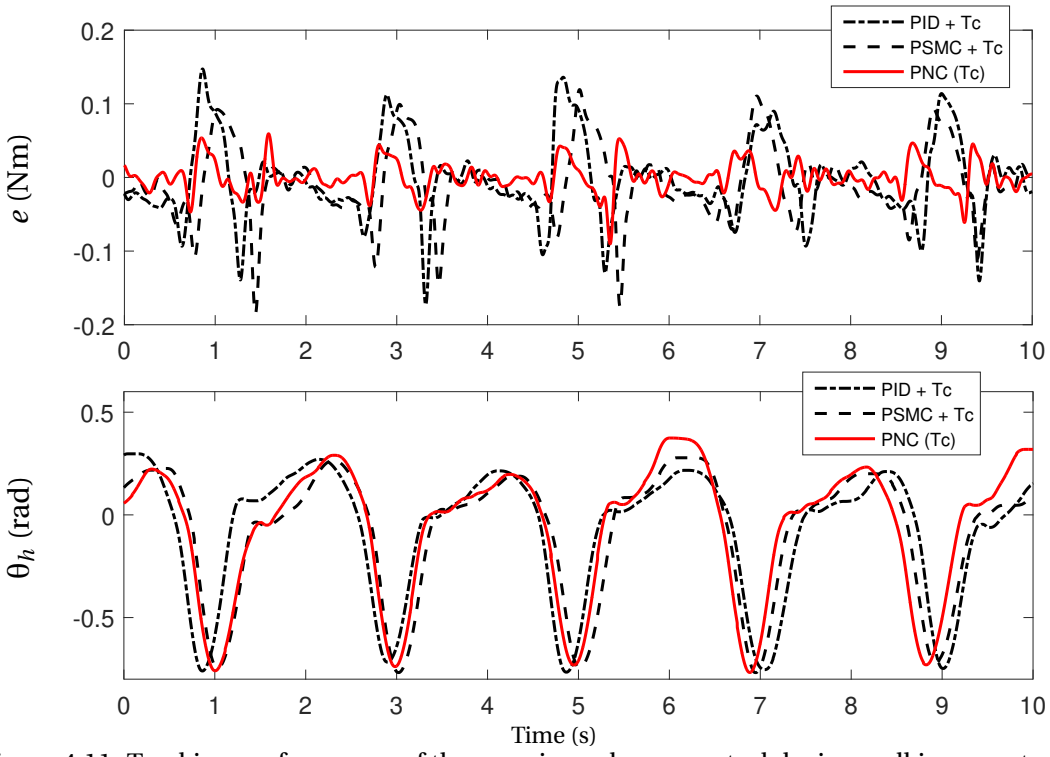

Figure 4.11: Tracking performance of the zero-impedance control during walking on a treadmill

exoskeleton (see Figure 4.8). Figure 4.11 shows the tracking error e along with the knee joint position θ_h for the three control strategies. Note that the subject was asked to keep similar step length during all experiments (see Figure 4.11(b)). The RMSE obtained with the PNC (RMSE = 0.0312 Nm, 20 steps) was lower than those obtained with of the PID controller (RMSE = 0.0626 Nm, 20 steps) and the PSMC controller (RMSE = 0.0542 Nm, 20 steps).

4.4.3 High torque mode

To evaluate the force compliance performance of the proposed PNC strategy in the high torque mode, an experiment was conducted as follows. First, a 2-kg external load is placed at the exoskeleton shank-foot segment without the presence of the wearer and the SEA is powered off (see Figure 4.9). It should be noted that the gravitational torque, induced by the external load and that of the exoskeleton shank-foot segment, acts in this case at the SEA spring since the SEA is in static mode (see section 3.4.1.1). Then, the SEA is powered on, and the desired torque τ_d is set to zero (see Figure 4.9). This experiment is similar to the case where the SEA is not powered on while the wearer shifts his/her limb. Figure 4.12 shows the force tracking trajectories using the proposed PNC for a fixed value

of H (H = H_{min} = 0.02) and for H varying according to (4.23). It can be noted that the torque τ_s suddenly vanishes when H has a fixed value; consequently, the loaded shank-foot segment quickly drops and reaches the knee joint mechanical limit, causing therefore a large reaction force at time t=1.6 seconds (see Figure 4.12(a)). This result shows that if a wearer shifts his/her lower limb when the SEA is powered off, the support from the exoskeleton will suddenly vanish after powering on the SEA when using a fixed value of H and consequently, the safety of the wearer cannot be guaranteed. However, as shown in Figure 4.12(c), the torque τ_s slowly decreases to 1.5 Nm and then to approximately 0 Nm when using H parameter as a function of τ_s (Eq 4.23). Therefore, the support provided by the exoskeleton to the wearer gradually decreases over time to ensure that the latter can adjust the corresponding joint torque. The obtained results also indicate that the use of H parameter as a function of τ_s (Eq 4.5) can efficiently achieve the tracking accuracy (e.g., zero-impedance mode) and safety (e.g., high torque mode) objectives based on the interaction torque between the wearer's shank-foot segment and that of the exoskeleton.

4.5 Conclusion

In this chapter, we presented a proxy-NDO-based force control strategy for the SEA actuator of the EROWA exoskeleton considering three common human-robot interaction modes: zero-impedance mode, force tracking mode and high torque mode. The two-mass dynamic model based NDO, was efficiently integrated into the inner-layer of the conventional PSMC structure to enhance the robustness of the controller with respect to environmental and modeling uncertainties. In addition, enhancement in the wearer's safety is achieved via the improvement of the force compliance exhibited by the exoskeleton using H parameter formulation as function of the spring torque. The stability of the proposed proxy-based control strategy was theoretically proven and the performance of the latter evaluated through simulations and experiments. The experimental results showed a higher tracking accuracy using the proposed control strategy in comparison to PID and PSMC controllers. At the same time, satisfying force compliance is achieved to ensure the wearer's safety under unexpected situations (high change in the interaction torque and/or unexpected assistive torque variation due to an incorrect gait phase detec-

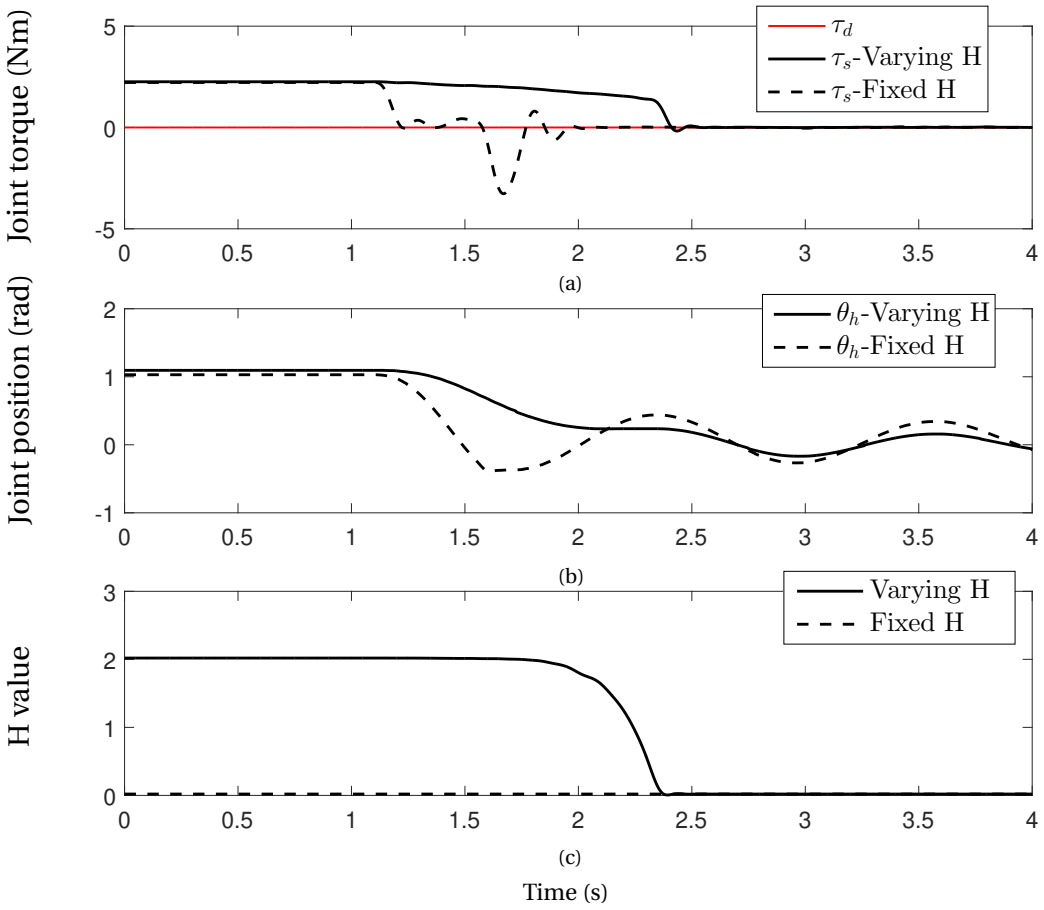

Figure 4.12: Compliance performance of the proposed control strategy with a fixed and varying value of H parameter

tion (Appendix B)).

Chapter 5

Hybrid control for knee joint flexion/extension movements restoration

Alone we can do so little; together we can do so much

Helen Keller

Contents

5.1 Introduction

THIS chapter presents the development of a hybrid control strategy for knee joint flexion/extension movements restoration. Overall description of the hybrid controller is first presented by detailing both parts of the controller i.e. the control of the EICOSI orthosis and the FES controller. The proposed hybrid control strategy increases the involvement of the subject during the knee joint flexion/extension movements. In this study, we explored the use of a non-linear disturbance observer [57] for on-line estimation of the generated stimulation torque. The second part of the chapter describes the used experimental protocol and analyzes the performance of the hybrid controller through simulations and experiments involving a healthy subject.

5.2 Hybrid controller

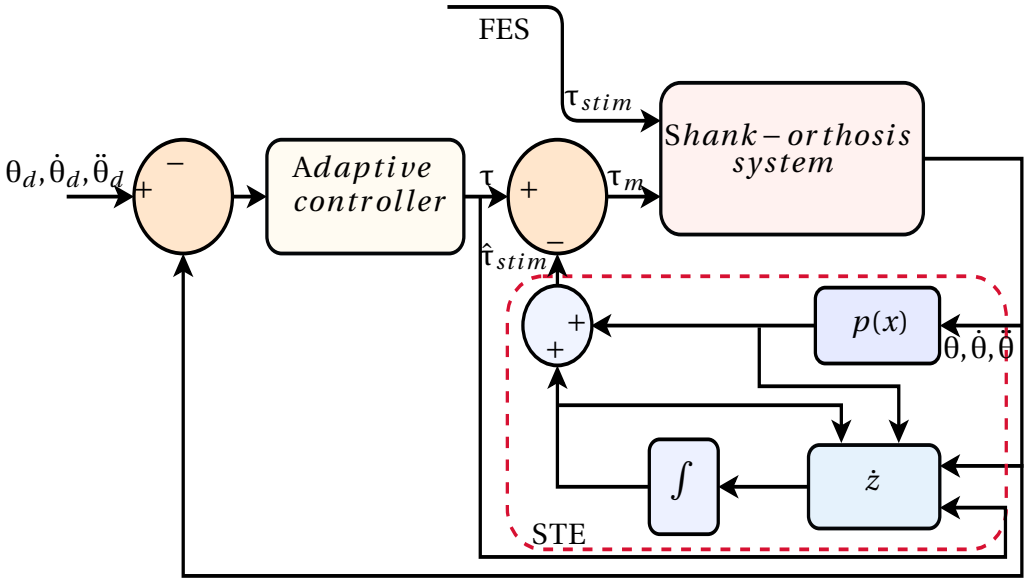

Figure 5.1: Proposed hybrid control strategy scheme

In this study, a hybrid active orthosis combining the use of the EICOSI orthosis as robotic orthosis and FES acting as an electrical stimulation orthosis. The goal of the proposed hybrid controller is to assist the subject when performing repeatable flexion/extension movements. The control architecture (see Figure 5.1) ensures the aforementioned goal by applying both an electrical stimulation at the quadriceps muscles and

a closed-loop adaptive control of the knee joint orthosis, to track a desired knee joint position trajectory. The stimulation torque is estimated using a Stimulation Torque Estimator (STE) which will be detailed in section 5.2.3. An adaptive control of the EICOSI orthosis is used since it does not necessitate any prior identification of the foot-shank segment/orthosis system parameters and guarantees an adaption to changes in the subject parameters due to muscular fatigue.

5.2.1 Adaptive controller

In the proposed hybrid control scheme, an adaptive controller is exploited for the control of the EICOSI orthosis [124, 125]. The desired knee joint position, velocity and acceleration are denoted by θ_d, $\dot{\theta}_d$ and $\ddot{\theta}_d$, respectively. The current position, velocity and acceleration of the joint are respectively denoted by θ, $\dot{\theta}$ and $\ddot{\theta}$. Let $\tilde{\theta} = \theta - \theta_d$, $\dot{\tilde{\theta}} = \dot{\theta} - \dot{\theta}_d$ and $\ddot{\tilde{\theta}} = \ddot{\theta} - \ddot{\theta}_d$ be the position, velocity and acceleration errors, respectively. Define the variable $s = \dot{\tilde{\theta}} + \lambda\tilde{\theta}$ with λ a positive scalar parameter.

Assumption: Assume that the following current and desired states (θ, $\dot{\theta}$, $\ddot{\theta}$, $\dddot{\theta}$, θ_d, $\dot{\theta}_d$, $\ddot{\theta}_d$, $\dddot{\theta}_d$) are bounded.

Exploiting the dynamic model of the wearer's shank-foot segment/orthosis system developed in § 3.4.2, the control torque can be expressed as follows (see Figure 5.1):

$$\tau_m = \tau - \hat{\tau}_{stim} \tag{5.1}$$

where $\hat{\tau}_{stim}$ is the estimated stimulation torque induced by the FES and τ the adaptive control torque defined as follows [124, 125]:

$$\tau = \hat{J}(\ddot{\theta}_d - \lambda\dot{\tilde{\theta}}) + \hat{A}\text{sign}(\dot{\theta}) + \hat{B}\dot{\theta} + \hat{\tau}_g\cos(\theta) - Ks \tag{5.2}$$

where $\hat{J}$, $\hat{A}$, $\hat{B}$, $\hat{\tau}_g$ denote the estimated system inertia, solid and viscous friction coefficients, and gravitational torque, respectively; K is a positive scaling parameter. sign is the

classical signum function. The dynamics of the adaptive law are given by:

$$\begin{aligned}
\dot{\hat{J}} &= -a_1(\ddot{\theta}_d - \lambda\dot{\tilde{\theta}})s, \\
\dot{\hat{B}} &= -a_3\dot{\theta}s, \\
\dot{\hat{A}} &= -a_2\text{sign}(\dot{\theta})s, \\
\dot{\hat{\tau}}_g &= -a_4\cos(\theta)s
\end{aligned} \tag{5.3}$$

where a_1, a_2, a_3 and a_4 are positive scaling parameters.

Substituting (5.1) in the model equation (3.10) defined in § 3.4.2 and considering $\ddot{\theta} = \dot{s} - \lambda\dot{\tilde{\theta}} + \ddot{\theta}_d$, the dynamics of the closed-loop system can be written as follows:

$$J\dot{s} = \tilde{\tau}_{stim} - Ks - \tilde{J}(\ddot{\theta}_d - \lambda\dot{\tilde{\theta}}) - \tilde{A}\text{sign}\dot{\theta} - \tilde{B}\dot{\theta} - \tilde{\tau}_g\cos(\theta) \tag{5.4}$$

where $\tilde{\tau}_{stim} = \tau_{stim} - \hat{\tau}_{stim}$, $\tilde{J} = J - \hat{J}$, $\tilde{A} = A - \hat{A}$, $\tilde{B} = B - \hat{B}$, and $\tilde{\tau}_g = \tau_g - \hat{\tau}_g$.

5.2.2 Stimulation intensity envelope

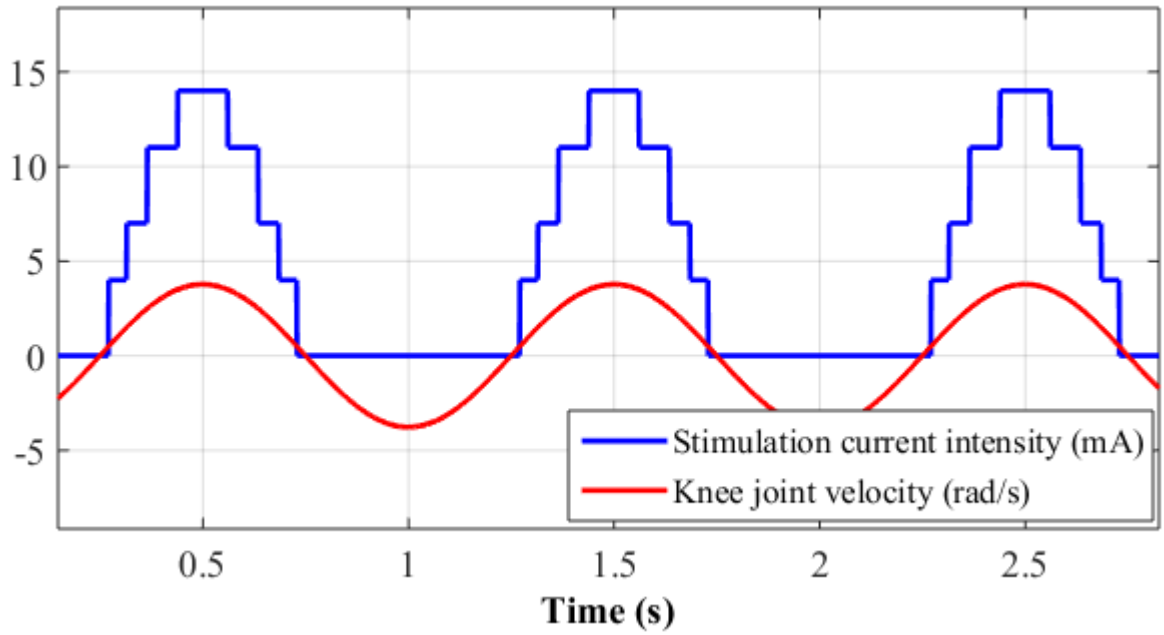

Figure 5.2: Stimulation intensity envelope. (Blue) Stimulation intensity. (Red) Knee joint velocity.

In the proposed hybrid approach, an open-loop FES is applied to the quadriceps muscles to produce the knee joint extension. Since the FES is applied only during the exten-

sion phase of the movement, the latter must be accurately detected. This detection is function of the joint velocity, and the stimulation is enabled when the velocity is positive. As shown in Figure 5.2, the stimulation lasts for the whole duration of the extension phase. To ensure a smooth reaction of the stimulated muscle, the stimulation intensity has been chosen to be gradually increasing/decreasing as shown in Figure 5.2. The stimulation frequency and the pulse-width are set to constant values while only the stimulation amplitude varies during the knee joint extension phase.

The stimulation intensity is defined as follows:

$$i_s(t) = \begin{cases} i_{max}\frac{\dot{\theta}(t)}{\dot{\theta}_{max}} \text{ if } \dot{\theta}(t) > 0 \\ 0 \text{ otherwise} \end{cases} \tag{5.5}$$

where i_{max} and $\dot{\theta}_{max}$ represent respectively the maximum current amplitude, which is a subject specific parameter, and the maximum joint velocity.

Note that, as shown in Figure 5.2, and due to the stimulator device specificity (see section 3.2.3, chapter 3), only the integer part resulting from (5.5) is considered, and the stimulation intensity is updated at a discrete time step.

5.2.3 Estimation of the torque induced by stimulation

In this study, the torque resulting from the muscular stimulation is considered as an external disturbance of the wearer's shank-foot segment/orthosis system (see Figure 5.1). Thus, an estimation of the induced stimulation torque is obtained using a Non-linear Disturbance Observer. Let's define the state variables as $[x_1, x_2]^{\mathrm{T}} = [\theta, \dot{\theta}]^{\mathrm{T}}$. The dynamic model (3.10) can be rewritten as follows:

$$\dot{x} = \mathrm{F}(x) + \mathrm{G}_1(x)u + \mathrm{G}_2(x)d \tag{5.6}$$

with:

$$\mathrm{F}(x)=\begin{bmatrix} x_2 \\ \frac{1}{\mathrm{J}}(-\mathrm{A}sign(x_2)-\mathrm{B}x_2-\tau_g\cos(x_1)) \end{bmatrix}$$

$$\mathrm{G}_1(x)=\mathrm{G}_2(x)=\begin{bmatrix} 0 \\ \frac{1}{\mathrm{J}} \end{bmatrix}$$

$$u=\tau_m$$

$$d=\tau_{stim}$$

Let $\hat{\tau}_{stim}$ be the estimation of τ_{stim}; the stimulation torque observer is designed as follows:

$$\begin{aligned} \hat{\tau}_{stim} &= z+p(x) \\ \dot{z} &= \mathrm{L}\big(-\mathrm{F}(x)-\mathrm{G}_1(x)u-\mathrm{G}_2(x)(z+p(x))\big) \end{aligned} \tag{5.7}$$

where $p(x)$ is chosen as $p(x)=k_1x_1+k_2x_2$; k_1 and k_2 are two positive constants, and L is defined as follows:

$$\mathrm{L}=\frac{\partial p}{\partial x}=[k_1\,k_2]$$

From (5.7) , the derivative of the estimated stimulation torque can be expressed as follows:

$$\dot{\hat{\tau}}_{stim}=\mathrm{L}\mathrm{G}_2(\tau_{stim}-\hat{\tau}_{stim})=\frac{k_2}{\mathrm{J}}(\tau_{stim}-\hat{\tau}_{stim}) \tag{5.8}$$

Considering $\tilde{\tau}_{stim}=\tau_{stim}-\hat{\tau}_{stim}$, and assuming that the torque generated by the stimulation is constant or changing with a very slow rate, then:

$$\dot{\tilde{\tau}}_{stim}=\frac{-k_2}{\mathrm{J}}\tilde{\tau}_{stim} \tag{5.9}$$

Since k_2 is a positive constant, then the stimulation torque estimation error approaches zero as the time increases and (5.9) is exponentially stable. However, in practice, the torque resulting from muscular stimulation is generally highly varying.

Assumption: Assume that the variation rate of the stimulation torque $\hat{\tau}_{stim}$ is bounded i.e, $\dot{\hat{\tau}}_{stim_\infty}<\dot{\tau}_{stim,max}$.

Proposition: Assume that the wearer's shank-foot segment/orthosis system is subject to the torque resulting from stimulation τ_{stim} and that the latter is estimated using the STE $\hat{\tau}_{stim}$ described by (5.7). Assume also that the variation rate of the estimated human joint torque is bounded (as stated in the above assumption). The stimulation torque estimation error given by $\tilde{\tau}_{stim} = \tau_{stim} - \hat{\tau}_{stim}$ is uniformly ultimately bounded.

Proof: Consider the candidate Lyapunov function v defined by:

$$v = \frac{1}{2}\tilde{\tau}_{stim}^2 \tag{5.10}$$

The derivative of the Lyapunov function can be written as follows:

$$\begin{aligned}
\dot{v} &= \tilde{\tau}_{stim}\dot{\tilde{\tau}}_{stim} \\
&= \tilde{\tau}_{stim}(\dot{\tau}_{stim} - \dot{\hat{\tau}}_{stim}) \\
&= \tilde{\tau}_{stim}(\dot{\tau}_{stim} - \frac{k_2}{J}\tilde{\tau}_{stim}) \\
&\leq |\tilde{\tau}_{stim}||\dot{\tau}_{stim,max}| - \frac{k_2}{J}\tilde{\tau}_{stim}^2 \\
&\leq |\tilde{\tau}_{stim}||\dot{\tau}_{stim,max}| - \frac{k_2}{J}(1-\beta)\tilde{\tau}_{stim}^2 - \beta\frac{k_2}{J}\tilde{\tau}_{stim}^2
\end{aligned}$$

where $0 < \beta < 1$. Thus,

$$\dot{v} \leq -\frac{k_2}{J}(1-\beta)\tilde{\tau}_{stim}^2, \quad \forall |\tilde{\tau}_{stim}| \geq \frac{J}{\beta k_2}|\dot{\tau}_{stim,max}| \tag{5.11}$$

As a result, the solutions $\tilde{\tau}_{stim}$ are uniformly ultimately bounded and the ultimate bound is equal to $\frac{J}{\beta k_2}|\dot{\tau}_{stim,max}|$.

5.2.4 Stability analysis

Consider first the system with $\tau_{stim} = 0$.

Proposition: Consider the wearer's shank-foot segment/orthosis system defined by (3.10) with the electrical stimulation $\tau_{stim} = 0$. Assume that the derivatives of the desired position θ_d, $\dot{\theta}_d$, $\ddot{\theta}_d$, $\dddot{\theta}_d$ are bounded. Applying the control torque (5.1- 5.3) to the orthosis ensures the asymptotic stability of the equilibrium point $[\tilde{\theta},\dot{\tilde{\theta}}]^T = [0,0]^T$.

Proof: Consider the Lyapunov function V defined as follows:

$$V = \frac{1}{2}Js^2 + \frac{1}{2a_1}\tilde{J}^2 + \frac{1}{2a_2}\tilde{A}^2 + \frac{1}{2a_3}\tilde{B}^2 + \frac{1}{2a_4}\tilde{\tau}_g^2 + K\lambda\tilde{\theta}^2 \tag{5.12}$$

The derivative of V is given by:

$$\dot{V} = sJ\dot{s} + \frac{1}{a_1}\tilde{J}\dot{\tilde{J}} + \frac{1}{a_2}\tilde{A}\dot{\tilde{A}} + \frac{1}{a_3}\tilde{B}\dot{\tilde{B}} + \frac{1}{a_4}\tilde{\tau}_g\dot{\tilde{\tau}}_g + 2K\lambda\tilde{\theta}\dot{\tilde{\theta}} \tag{5.13}$$

Substituting Eq. 5.1- 5.4 in Eq. 5.13, the derivative of the Lyapunov function becomes:

$$\dot{V} = -Ks^2 + 2K\lambda\tilde{\theta}\dot{\tilde{\theta}} = -K\dot{\tilde{\theta}}^2 - K\lambda^2\tilde{\theta}^2 \leqslant 0$$

Therefore, the Lyapunov function is decreasing. Besides, considering Assumption 1, $\tilde{\theta}$, $\dot{\tilde{\theta}}$ are bounded and the second derivative of the Lyapunov function $\ddot{V}$ is also bounded which implies that $\dot{V}$ is uniformly continuous. Thus, the system is asymptotically stable.

Let's now consider the stimulation torque as non-zero ($\tau_{stim} \neq 0$).

Proposition: Consider the wearer's shank-foot segment/orthosis system defined by (3.10) with $\tau_{stim} \neq 0$. Assume that the derivatives of the desired position θ_d, $\dot{\theta}_d$, $\ddot{\theta}_d$ are bounded. Assume also that the stimulation torque τ_{stim} is bounded, i.e. $\tau_{stim} \leqslant \alpha$. Applying the control torque (5.1- 5.3) to the orthosis ensures the input-to-state stability of the system with respect to the stimulation torque τ_{stim}.

Proof: Consider the candidate Lyapunov function V defined in Eq. 5.12. The derivative of V is given by:

$$\begin{aligned}
\dot{V} &= sJ\dot{s} + \frac{1}{a_1}\tilde{J}\dot{\tilde{J}} + \frac{1}{a_2}\tilde{A}\dot{\tilde{A}} + \frac{1}{a_3}\tilde{B}\dot{\tilde{B}} + \frac{1}{a_4}\tilde{\tau}_g\dot{\tilde{\tau}}_g + 2K\lambda\tilde{\theta}\dot{\tilde{\theta}} \\
&= -Ks^2 + 2K\lambda\tilde{\theta}\dot{\tilde{\theta}} + \tilde{\tau}_{stim}s \\
&= -K\dot{\tilde{\theta}}^2 - K\lambda^2\tilde{\theta}^2 + \tilde{\tau}_{stim}s \\
&\leqslant -K\dot{\tilde{\theta}}^2 - K\lambda^2\tilde{\theta}^2 + \tilde{\tau}_{stim}(\dot{\tilde{\theta}} + \lambda\tilde{\theta})
\end{aligned}$$

It can be verified that:

$$\tilde{\tau}_{stim}(\dot{\tilde{\theta}}) \leqslant \frac{1}{2}K\dot{\tilde{\theta}}^2 + \frac{\tilde{\tau}_{stim}^2}{2K}$$

and

$$\lambda\tilde{\tau}_{stim}\tilde{\theta} \leqslant \frac{1}{2}K\lambda^2\tilde{\theta}^2 + \frac{\tilde{\tau}_{stim}^2}{2K}$$

Thus,

$$\dot{V} \leqslant -\frac{1}{2}K\dot{\tilde{\theta}}^2 - \frac{1}{2}K\lambda^2\tilde{\theta}^2 + \frac{\tilde{\tau}_{stim}^2}{K} \tag{5.14}$$

$\frac{\tilde{\tau}_{stim}^2}{K}$ is bounded and converges to zero if $\tilde{\tau}_{stim}$ converges to zero. Therefore, there exists a scalar σ that tends to zero such that:

$$\dot{V} \leq 0 \quad \forall x \quad \text{such that} \quad x \geqslant \sigma \tag{5.15}$$

Considering (5.12 ,5.14,5.15) and that the asymptotic stability of the system not subject to a stimulation torque ($\tau_{stim} = 0$), the wearer's shank-foot segment/orthosis system is input-to-state stable with respect to the bounded input τ_{stim} .

5.3 Performance evaluation

5.3.1 Experimental protocol

To evaluate the proposed hybrid control strategy, the EICOSI orthosis described in § 3.4 is used. Regarding the Functional Electrical Stimulation (FES), RehaStim 2 from Hasomed (Germany), a 8 channel biphasic stimulator, is used (please refer to section 3.2.3, chapter 3). The stimulator and the orthosis are synchronously controlled using Labview.

By following the recommandations of the rehabilitation staff at CHU Mondor (Créteil, France), each experiment session has lasted 12 seconds. The amplitude and the frequency of the flexion/extension movements were determined to fit the human daily living activities parameters, and to take advantage of the maximum range of motion provided by the orthosis. Prior to each experimental session, a calibration procedure is needed to tune the stimulation parameters fitting the subject (pulse width, frequency and maximal current amplitude). These parameters were determined by observation of the quadriceps muscles contraction. In order to evaluate the proposed approach, two case studies have been considered during the experiments: without / with muscular stimulation. The sub-

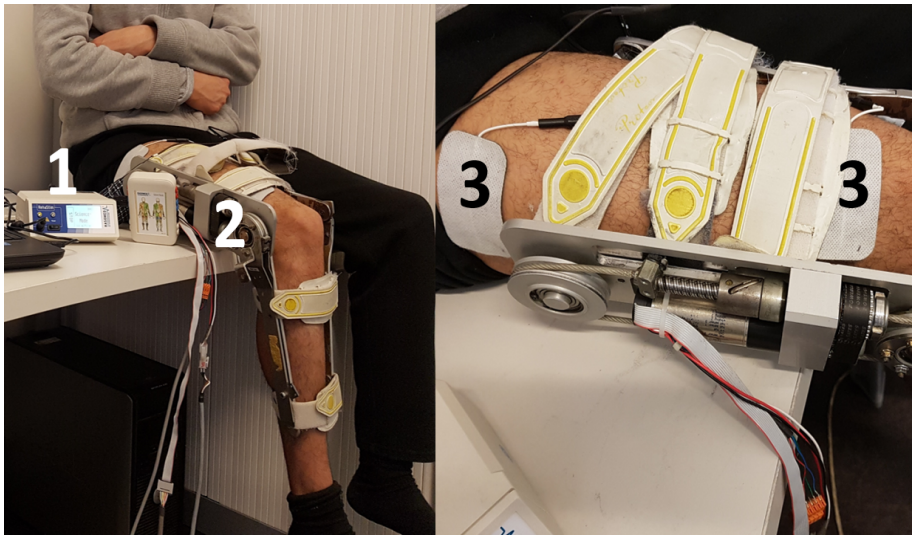

Figure 5.3: Experimental setup. (1) Stimulator. (2) Knee joint orthosis. (3) Stimulation Electrodes

ject involved in the experiments is a healthy subject (age=26 years, body weight=64 kg, height=1.78 m).

5.3.2 Simulation results

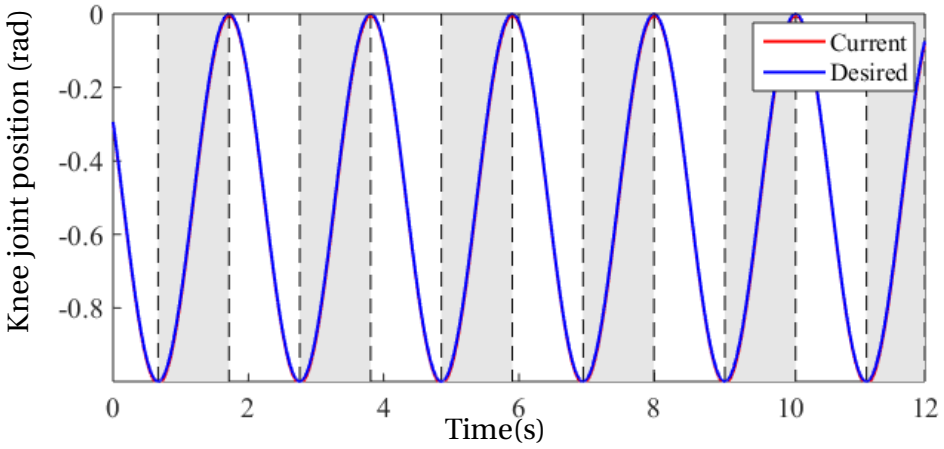

Figure 5.4: Tracking performance when FES is enabled. The grey bars represent the knee joint extension phases. The tracking error between the reference trajectory (plotted in blue) and the actual knee joint position (plotted in red) is about 0.0064 rad.

The proposed control strategy was first evaluated in simulation using the wearer's shank-foot segment/orthosis model (3.10). This model was implemented in Simulink/Matlab under a Windows PC (Intel Core i7 6600U CPU @2.60GHZ 2.81GHZ). The stimulation torque is applied during the knee joint extension phase as an external assistive torque.

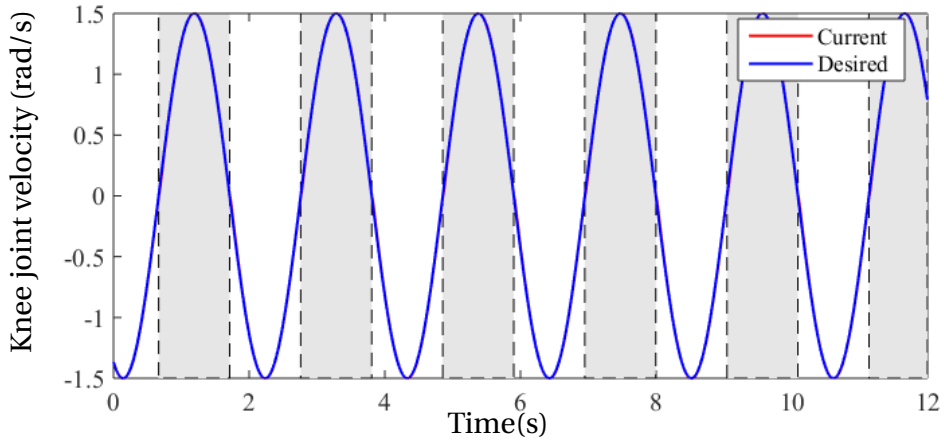

Figure 5.5: Desired and measured joint velocity when FES is enabled. The grey bars represent the knee joint extension phases. The tracking error between the reference (plotted in blue) and the actual joint velocity (plotted in red) is 0.0004 rad/s.

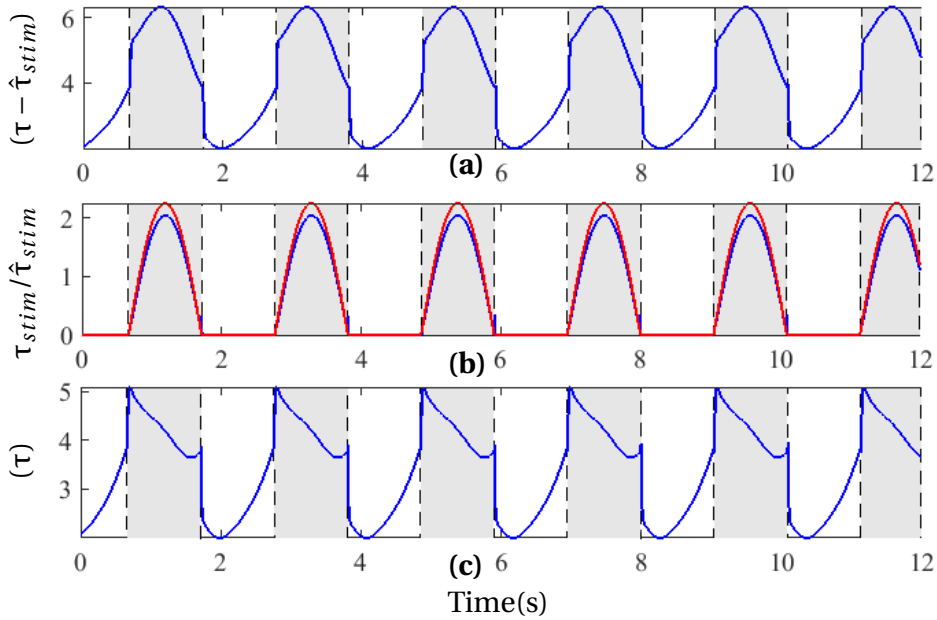

Figure 5.6: The control torque when FES is enabled (simulation results). (a) Motor Torque ($\tau - \hat{\tau}_{stim}$).(b) Dashed red line: actual stimulation torque (τ_{stim}). Blue line: estimated stimulation torque ($\hat{\tau}_{stim}$). (c) Control torque (τ). The grey bars represent the extension phases when the FES is enabled.

Two case studies were analyzed. In the first case, the thigh muscles i.e. the quadriceps are stimulated using the FES, while in the second case, the FES is not applied. The simulation results show an accurate tracking of the position and velocity (Figures 5.4, 5.5, 5.7, 5.8) for the two considered cases; besides, one can note acceptable values of joint velocity and torque guaranteeing the safety of the subject. Note that the average position tracking error is equal to 0.0064 rad (with stimulation) and 0.0057 rad (without stim-

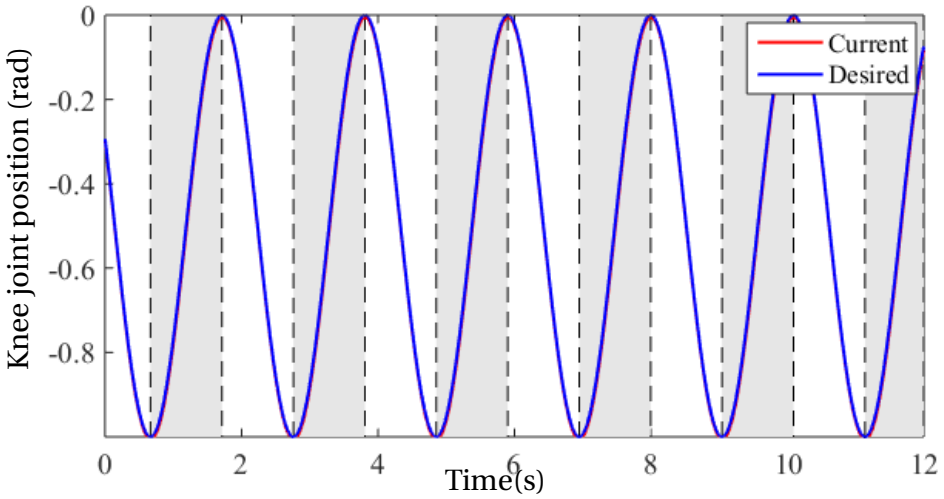

Figure 5.7: Tracking performance when FES is not enabled. The grey bars represent the knee joint extension phases. The tracking error between the reference trajectory (plotted in blue) and the actual joint position (plotted in red) is 0.0057 rad.

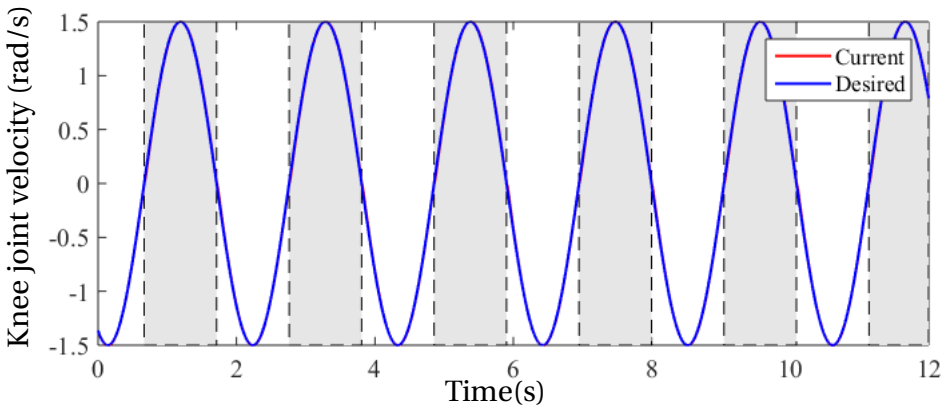

Figure 5.8: Desired and measured joint velocity when FES is not enabled. The grey bars represent the knee joint extension phases. The tracking error between the reference (plotted in blue) and the actual joint velocity (plotted in red) is 0.0336 rad/s.

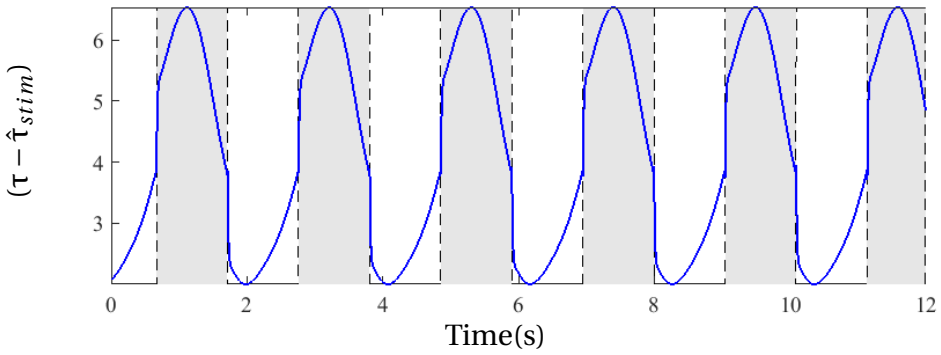

Figure 5.9: Control torque when FES is not enabled. Motor torque $(\tau - \hat{\tau}_{stim})$. The grey bars represent the extension phases.

ulation). Figures 5.6 and 5.9 show the different control torques acting on the wearer's shank-foot segment/orthosis system for these two case studies respectively. Figure 5.6(a), shows the torque developed by the orthosis actuator (τ_m). This torque is computed as: $\tau_m = \tau - \hat{\tau}_{stim}$ as shown in Figure 5.1. The stimulation torque as well as its estimate and the the adaptive control torque are plotted in Figures 5.6(b) and 5.6(c), respectively. Regarding Figure 5.6(b), note that FES is applied only during the extension phases marked by grey bars. Note also the ability of the STE to estimate the torque induced by stimulation with a relatively good precision; the mean estimation error is equal to 0.0721 N.m with a standard deviation of 0.0810. The adaptive control torque formulated in (5.2) is shown in Figure 5.6(c). As expected, the control torque, in the second case study, i.e. without muscular stimulation, is greater than the one developed when stimulation is activated.

5.3.3 Experimental results

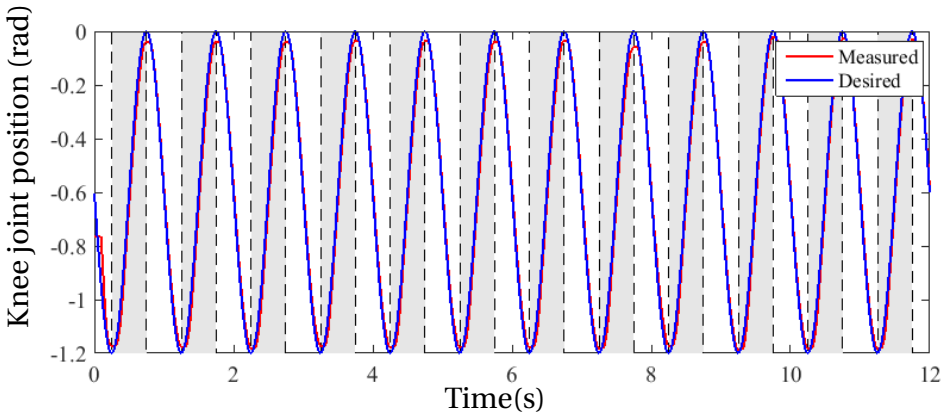

Figure 5.10: Tracking performance when FES is not enabled. The grey bars represent the knee joint extension phases. The tracking error between the reference trajectory (plotted in blue) and the actual knee joint position (plotted in red) is about 0.0108 rad.

To assess experimentally the proposed control strategy, the subject who participated in the experiments has undergone 5 experimental sessions of 12s each and has respected 30s of rest between two consecutive sessions. A sinusoidal trajectory with a frequency of 1Hz has been used as reference trajectory for position tracking. The pulse width and the frequency of the stimulation have been set to 150 µs and 35Hz, respectively. The joint position has been measured using the incremental encoder of the orthosis and the joint velocity has been obtained using a numerical derivation of the joint position. The trajec-

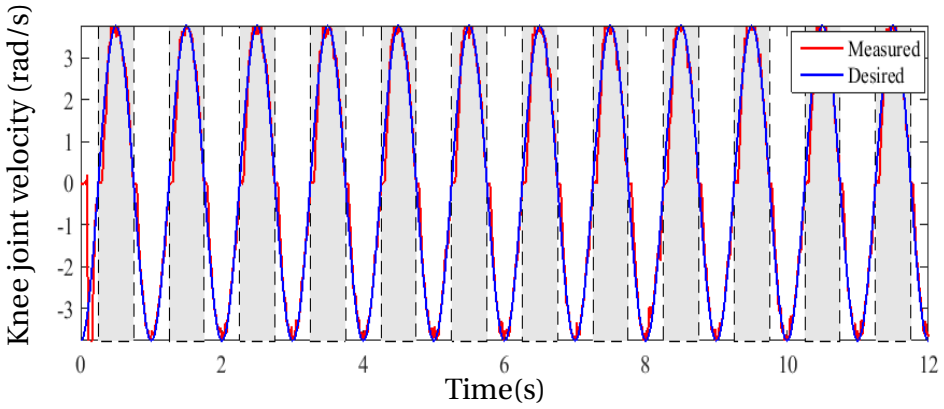

Figure 5.11: Desired and measured joint velocity when FES is not enabled. The grey bars represent the knee joint extension phases. The tracking error between the reference (plotted in blue) and the actual joint velocity (plotted in red) is 0.0153 rad/s.

tory tracking results during the knee joint flexions/extensions are plotted for both cases (without/with stimulation) in Figures 5.10 and 5.13 respectively. These results show a good tracking performance with a mean absolute error of 0.0108 rad and 0.0130 rad when FES is not enabled and when it is enabled, respectively. Besides, as shown in Figures 5.11 and 5.14, for the two cases, the joint velocity reveals a good tracking with a mean absolute error of 0.0153 rad/s and 0.0336 rad/s, respectively. Figures 5.12and 5.15(a) show the control torques provided by the orthosis actuator τ_m when FES is not enabled and when it is enabled, respectively. It can be noted that the joint velocity and the torque have acceptable values, guaranteeing the safety of the subject. Furthermore, it is worthy noting that when FES is enabled, the control torque is lower than the one applied when the stimulation is not enabled. This is due to the contribution of the torque provided by the

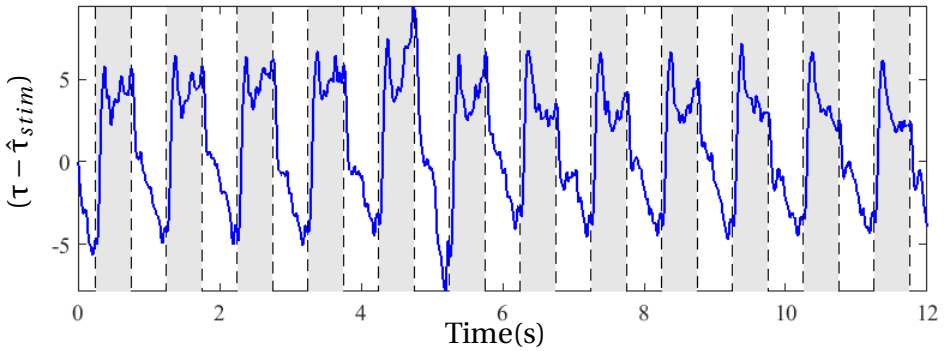

Figure 5.12: Control torque when FES is not enabled. The grey bars represent the knee joint extension phases.

quadriceps muscles to the movement generation when the FES is applied. Figure 5.15(b)

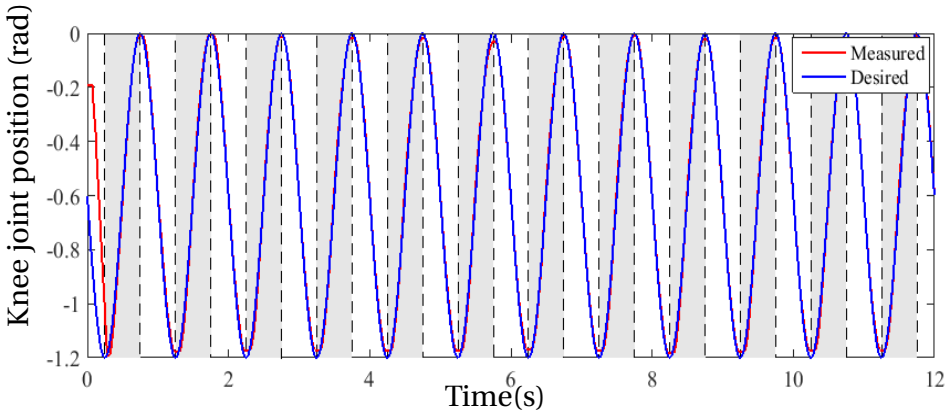

Figure 5.13: Tracking performance when FES is enabled. The grey bars represent the knee joint extension phases when FES is enabled. The tracking error between the reference trajectory (plotted in blue) and the actual joint position (plotted in red) is 0.0130 rad.

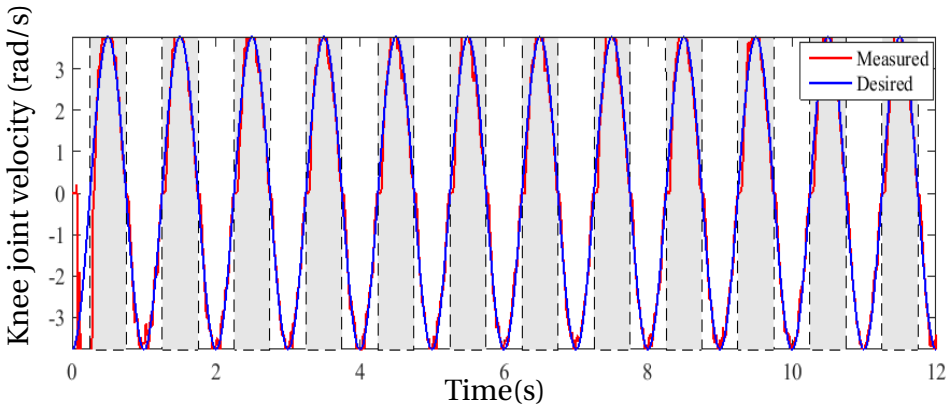

Figure 5.14: Desired and measured joint velocity when FES is enabled. The grey bars represent the knee joint extension phases. The tracking error between the reference (plotted in blue) and the actual joint velocity (plotted in red) is 0.0336 rad/s.

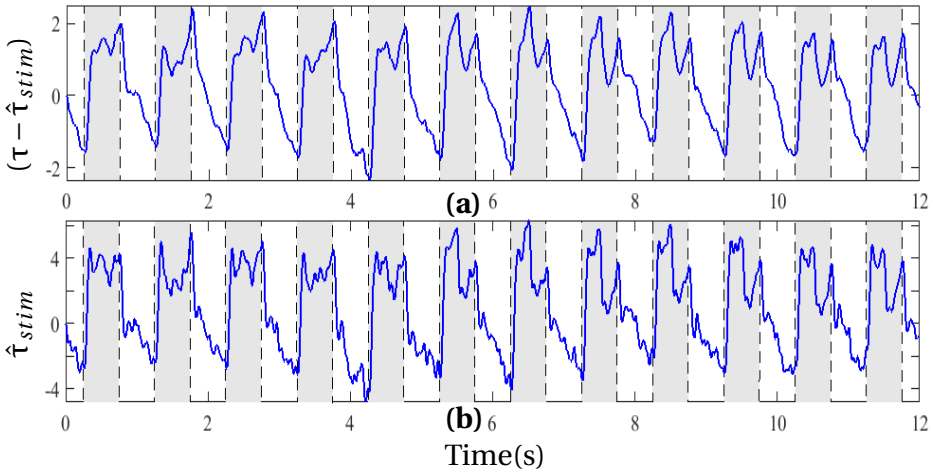

Figure 5.15: Control torque when FES is enabled: (a) Motor torque $(\tau - \hat{\tau}_{stim})$, (b) Estimated stimulation torque (τ_{stim}). The grey bars represent the knee joint extension phases when FES is enabled.

shows the estimated torque $\hat{\tau}_{stim}$ using the STE (5.7). During the extension phase, this torque corresponds to the estimated stimulation torque while during the flexion phase, it corresponds to the gravitational torque. The reduction percentage of the absolute mean torque when using FES is about 19.04% ± 4% . Figure 5.16 shows the temporal evolution of the dynamic model parameters estimates (5.3). Note that the system was able to track the desired trajectory within the first seconds of the experiment and the adaptive parameters have converged to bounded range of values afterwards.

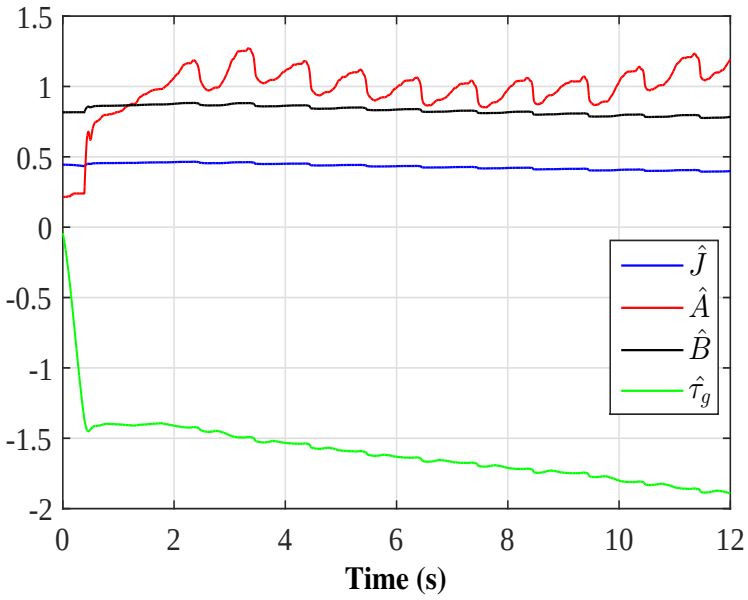

Figure 5.16: Temporal evolution of the dynamic model parameters estimates.

5.4 Conclusion

In this chapter, a hybrid control strategy combining the use of the EICOSI orthosis and quadriceps FES was developed. The purpose of this control strategy is to ensure knee joint flexion-extension movements restoration. The joint torque induced by FES is considered as an external disturbance estimated using a non-linear disturbance observer. The estimated torque is complemented by an adaptive control torque applied to the orthosis in such a way i) to minimize the required motor torque and ii) to guarantee an accurate joint position tracking. The input-to-state stability of the whole system with respect to the estimated stimulation torque was proved using a Lyapunov analysis. The simulation and experimental results show the ability of the STE in estimating the muscle stimulation

torque. They show also the ability of the proposed hybrid controller to ensure an accurate tracking of the desired trajectory. The advantages of the proposed control strategy are its dependency on neither a relatively complex musculo-skeletal modeling nor on the use of extra force/torque sensors, and it ensures effective reduction of the motor torque.

Chapter 6

Impedance modulation-based control of the ANGELEGS exoskeleton for Sit-to-Stand movements assistance

Some people want it to happen, some wish it would happen, and others make it happen

Unknown

Contents

6.1 Introduction

SIT-to-stand (STS) constitutes a key movement of our daily living activities and is a critical prerequisite of upright mobility, such as walking on ground floor, stair descent, etc. From a clinical point of view, standing-up from a sitting position is a difficult task facing elderly and dependent people suffering from musculoskeletal disorders.

In this chapter, an impedance modulation-based control strategy of the ANGELEGS exoskeleton is proposed to provide assistance and balance reinforcement to subjects suffering from limited motor ability during STS movements. A time-varying desired impedance model is developed to provide appropriate assistance according to the wearer's STS speed. The proposed impedance modulation-based control strategy exploits a human joint torque observer (HJTO) aimed to estimate the wearer's motor ability and a sliding mode-based controller (SMC) to ensure an accurate joint position tracking. In addition, a Balance Reinforcement Controller (BRC) module is designed to avoid two typical failed STS movements due to the lack of balance, i.e., "sit-back" and "step-forward". The robustness of the proposed control strategy with respect to modeling uncertainties is theoretically analysed and its effectiveness evaluated in simulations and experiments.

6.2 Impedance modulation-based control strategy

The proposed impedance modulation-based control strategy consists of two modules: impedance compensation-based control and balance reinforcement-based control.

6.2.1 Impedance compensation-based control

The impedance compensation-based controller consists of three parts: a nonlinear human joint torque observer (HJTO), a sliding mode controller (SMC) and a desired impedance model (Figure 6.1). The nonlinear observer is used to estimate the wearer's joint torque (T_h) whereas the sliding mode controller is used to track the reference position trajectory (Θ_d) generated from the desired impedance model. The original wearer/exoskeleton system impedance is adapted to the desired impedance according to the estimated wearer's torque ($\hat{T}_h$) if the following conditions are satisfied: 1) the nonlin-

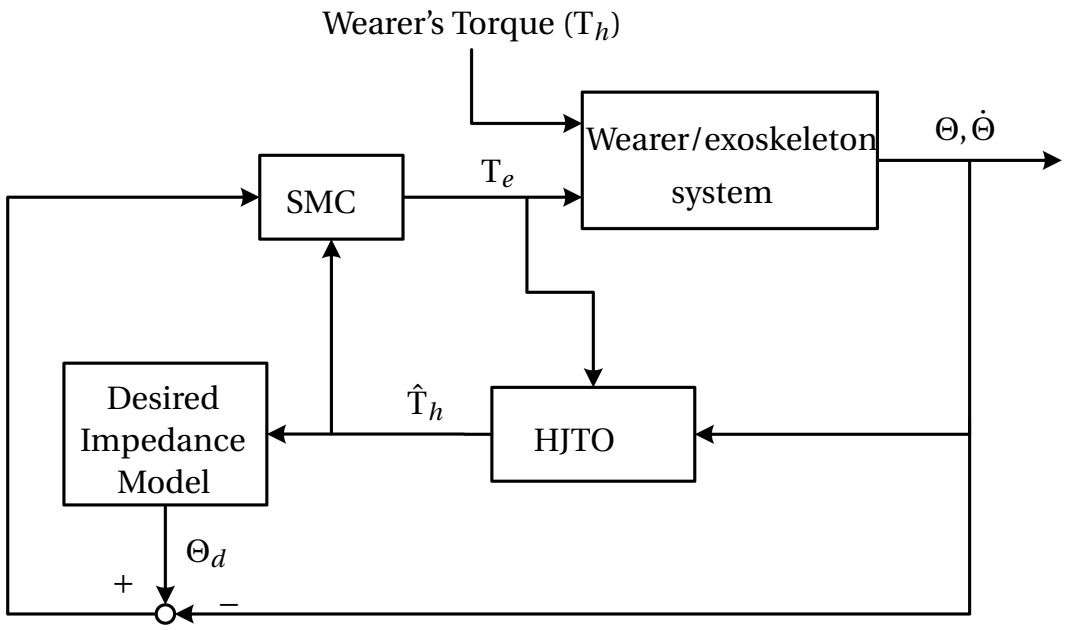

Figure 6.1: Impedance compensation-based control structure. $\hat{T}_h$: estimated wearer's torque; Θ_d: desired joint position.

ear observer accurately estimates the wearer's joint torque (i.e., $\hat{T}_h = T_h$); 2) the SMC controller shows a high tracking accuracy (i.e., $\Theta = \Theta_d$). In the following, we present the design of the impedance compensation-based controller including the Human Joint Torque Observer (HJTO) and the Sliding Mode Controller (SMC) (see Figure 6.1). The robustness of the proposed control strategy with respect to modeling uncertainties is addressed in Appendix A.

6.2.1.1 Human Joint Torque Observer (HJTO)

The HJTO is developed using a non-linear disturbance observer [57] [121] where the wearer's joint torque U_h is considered as an external disturbance of the wearer/exoskeleton system. The dynamic model (see chapter 3, Eq.3.11) can be transformed into a nominal model using an additional disturbance term U_h:

$$M(q)\ddot{q} + C(q,\dot{q})\dot{q} + G(q) = (U_e + J_F^T F) + U_h. \tag{6.1}$$

where $q = [q_1\ q_2\ q_3]^T$ represents the state vector. The seat force is modeled as an external force F that acts on the hip joint of the wearer/exoskeleton system. J_F is the Jacobian matrix and U_e is the input torque vector.

The HJTO is defined as follows:

$$\begin{cases} \dot{z} & = -\mathrm{L}(q,\dot{q})z + \mathrm{L}(q,\dot{q})(\mathrm{C}(q,\dot{q})\dot{q} + \mathrm{G}(q) \\ & \quad -\mathrm{U}_e - \mathrm{J}_{\mathrm{F}}^{\mathrm{T}}\mathrm{F} - p(q,\dot{q})), \\ \hat{\mathrm{U}}_h & = z + p(q,\dot{q}), \end{cases} \tag{6.2}$$

where $\hat{\mathrm{U}}_h$ denotes the estimated joint torques generated by the wearer. z is an auxiliary variable used to avoid the acceleration measurement. The observer gain matrix $\mathrm{L}(q,\dot{q})$ and the vector $p(q,\dot{q})$ satisfy:

$$\begin{cases} \mathrm{L}(q,\dot{q}) = \mathrm{X}^{-1}\mathrm{M}^{-1}(q) \\ p(q,\dot{q}) = \mathrm{X}^{-1}\dot{q} \end{cases} \tag{6.3}$$

Let us define the disturbance tracking error as $\tilde{\mathrm{U}}_h = \mathrm{U}_h - \hat{\mathrm{U}}_h$. From (6.1) - (6.3), the error dynamics of the tracking disturbance can be written as follows:

$$\dot{\tilde{\mathrm{U}}}_h = \dot{\mathrm{U}}_h - \mathrm{L}(q,\dot{q})\tilde{\mathrm{U}}_h. \tag{6.4}$$

The following proposition addresses the tracking performance of HJTO (6.2) for the wearer/exoskeleton system (6.1).

Proposition 1.Consider the wearer/exoskeleton system subject to the disturbance U_h *(i.e., the wearer's joint torque). The HJTO is defined in (6.2) with the observer gain matrix* $\mathrm{L}(q,\dot{q})$ *and auxiliary vector* $p(q,\dot{q})$ *defined in (6.3). The matrix* X *is invertible and there exists a positive definite and symmetric matrix* Γ*, such that [121]:*

$$\mathrm{X} + \mathrm{X}^{\mathrm{T}} - \mathrm{X}^{\mathrm{T}}\dot{\mathrm{M}}(q)\mathrm{X} \geq \Gamma\,, \tag{6.5}$$

1) *If the rate of change of the wearer's torque is negligible (i.e.,* $\dot{\mathrm{U}}_h \approx 0$*), the tracking error of the wearer's joint torque* $\tilde{\mathrm{U}}_h$ *converges exponentially to zero for any* $\tilde{\mathrm{U}}_h \in \mathrm{R}^n$.

2) *If the rate of change of the wearer's torque is bounded (i.e.,* $\|\dot{\mathrm{U}}_h\| < \varepsilon$*), the tracking error of the wearer's joint torque* $\tilde{\mathrm{U}}_h$ *is globally uniformly ultimately bounded.*

For sake of simplicity, in practice, the matrix X can be chosen as a diagonal matrix. A

possible analytical solution of X suggested in [121] is given by:

$$\mathrm{X}^{-1} = \frac{1}{2}(\zeta + 2\beta_o\sigma_1)\mathrm{I}, \tag{6.6}$$

where β_o is the minimum convergence rate of the wearer's joint torque estimation. I represents the identity matrix. ζ and σ_1 are two constants that satisfy the following conditions:

$$\| \mathrm{M}(q) \| \leq \sigma_1, \ \| \dot{\mathrm{M}}(q), \| \leq \zeta \tag{6.7}$$

It should be noted that there is a trade-off between the accuracy of the estimated wearer's joint torques and the noise amplification when using the HJTO. In this study, the convergence rate β_o is set by taking into account the wearer's movements main frequency during STS [121]. During STS movements, the wearer's joint torques variations are bounded (i.e. $\|\dot{\tau}_d\| < \varepsilon$). As pointed out in [121], the tracking error converges with an exponential rate, $\frac{(1-\eta)\Gamma}{2\sigma_2\|\mathrm{X}\|^2}$, to a ball with a radius of $\frac{2\varepsilon\sigma_2\|\mathrm{X}\|^2}{\eta\Gamma}, 0 < \eta < 1$. Γ represents a positive value. More details on the proof are provided in [121]. From a control point of view, the reduction of the noise amplification makes the system more stable. As it regards the estimation of the wearer's movement intention, a relatively high convergence rate is required to rapidly detect the wearer's intention.

6.2.1.2 Sliding Mode Controller (SMC)

In order to accurately track the wearer's movement intention, q_r, computed using the desired impedance (6.13), tracking performance of the SMC is a key factor. Regarding the design of the SMC, a Non-linear Disturbance Observer (NDO)-based SMC is used to ensure an accurate trajectory tracking. Since the wearer's joint torques U_h are considered as external disturbances for the exoskeleton, the HJTO is used as a disturbance observer in the proposed controller.

Let us define:

$$s = c_1 e + \dot{e}, \quad e = q - q_r \tag{6.8}$$

where s represents a virtual error vector. q_r is the trajectory computed using the desired impedance model (6.13). c_1 is a positive constant.

The multi-joint NDO-based SMC controller is designed as follows:

$$\begin{aligned} \mathrm{U}_e = &-c_1(\mathrm{M}(q)\dot{e} + \mathrm{C}(q,\dot{q})e) + (1-\lambda_1)(\mathrm{M}(q)\ddot{q}_r + \\ &\mathrm{C}(q,\dot{q})\dot{q}_r) + (1-\lambda_2)(\mathrm{G}(q) - \mathrm{J}_\mathrm{F}^\mathrm{T}\mathrm{F}) - \sigma_s sat(s) - \lambda_s s, \end{aligned} \tag{6.9}$$

where σ_s denotes a positive constant and $sat(\cdot)$ the saturation function ($sat(\cdot) \in [-1, 1]$). Note that ankle joints are only controlled by the wearer (i.e., $q_{r1} = q_1$, $e_1 = 0$ and $u_{r1} = 0$).

The stability of the proposed controller (6.9) is addressed using the following proposition.

Proposition 2. The multi-joint NDO-based SMC controller is given by (6.9), and $e_1 = 0$, $\sigma_s > \frac{2\varepsilon\sigma_2\|\mathrm{X}\|^2}{\eta\Gamma} + \varepsilon_v$. *The virtual tracking error (s) converges exponentially to zero for all* $s(0) \in \mathrm{R}^3$. *Note that* τ_v *(see Eq.6.19) is close to zero when the horizontal position of the center of mass* $\mathrm{X}_{\mathrm{CoM}}$ *is in the range* $[-x_c, x_c]$.

Proof: Consider the following candidate Lyapunov Function:

$$\mathrm{V} = \frac{1}{2} s^\mathrm{T}\mathrm{M}(q)s. \tag{6.10}$$

By differentiating both sides of (6.10), we obtain:

$$\dot{\mathrm{V}} = s^\mathrm{T}\mathrm{M}(q)\dot{s} + \frac{1}{2} s^\mathrm{T}\dot{\mathrm{M}}(q)s. \tag{6.11}$$

Since $\dot{\mathrm{M}}(q) - 2\mathrm{C}(q,\dot{q})$ is skew-symmetric, we have:

$$s^\mathrm{T}[\dot{\mathrm{M}}(q) - 2\mathrm{C}(q,\dot{q})]s = 0. \tag{6.12}$$

From (3.11), (6.12), (6.18), and (6.9), equation (6.11) can be expressed as follows:

$$\begin{aligned} \dot{\mathrm{V}} &= s^\mathrm{T}\mathrm{M}(q)\dot{s} + s^\mathrm{T}\mathrm{C}(q,\dot{q})s \\ &= s^\mathrm{T}(\mathrm{M}(q)c_1\dot{e} + \mathrm{M}(q)\ddot{e} + \mathrm{C}(q,\dot{q})s) \\ &= s^\mathrm{T}(\mathrm{M}(q)c_1\dot{e} + \mathrm{M}(q)\ddot{q} - \mathrm{M}(q)\ddot{q}_r + \mathrm{C}(q,\dot{q})s) \\ &= s^\mathrm{T}(\mathrm{M}(q)c_1\dot{e} + \mathrm{U}_h + \mathrm{U}_e + \mathrm{J}_\mathrm{F}^\mathrm{T}\mathrm{F} - \mathrm{G}(q) \\ &\quad - \mathrm{C}(q,\dot{q})\dot{q} - \mathrm{M}(q)\ddot{q}_r + \mathrm{C}(q,\dot{q})s) \end{aligned}$$

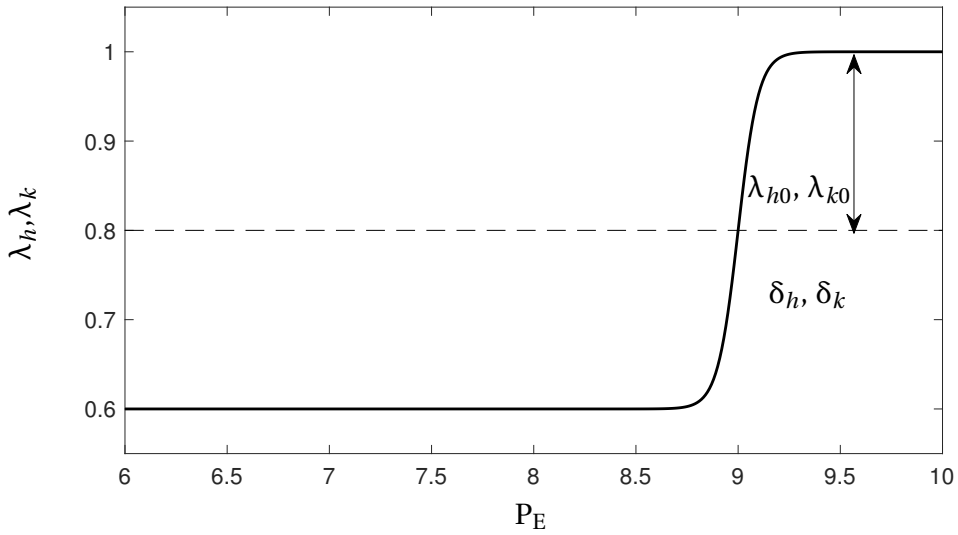

Figure 6.2: Example of function characterizing the assistance rates.

$$= s^{\mathrm{T}}(U_h - \hat{U}_h - R\tau_v - \sigma_s sat(s) - \lambda_s s)$$
$$= s^{\mathrm{T}}(\tilde{U}_h - R\tau_v - \sigma_s sat(s) - \lambda_s s) \leq 0.$$

Therefore, the Lyapunov function is decreasing. This completes the proof. In practice, σ_s can be set to a smaller value, $\varepsilon_v < \sigma_s < \frac{2\varepsilon\sigma_2\|X\|^2}{\eta\Gamma} + \varepsilon_v$, to avoid the chattering effect in control torque. In this case, the tracking error s converges into a range $\|s\| < \frac{\varepsilon_v}{\lambda_s}$, which can be easily proved according to the aforementioned proof [1] .

6.2.1.3 Desired impedance model

To ensure successful STS movements, important lower limb joint torques are required, which makes performing these movements a challenging task for individuals suffering from lower limb muscular weaknesses. With the support of an exoskeleton, an efficient control strategy to reduce the required human joint torques during STS movements is to partially compensate for the gravity and inertia (i.e., impedance) of the human body. In other words, a desired impedance lower than the original one of the human body is expected to reduce the required human effort. A major advantage of such a strategy lies within the fact that STS movements will be controlled by the wearer while the exoskeleton

[1] Huo, W., **Alouane, M. A.**, Vincent Bonnet, Jian Huang, Yacine Amirat, Ravi Vaidyanathan, and Samer Mohammed. (2020). Impedance Modulation Control of a Lower Limb Exoskeleton to Assist Sit-to-Stand Movements. IEEE Transactions on Robotics. (Under-Review)

provides the required assitive torques to the wearer to effectively carry out these movements. The desired impedance model can be designed based on the wearer's lower limb motor ability which can be assessed using the well-known Five-Times-Sit-To-Stand (FTSTS) test [126]. Several studies in the literature showed that an elderly showing a relatively longer standing-up time is usually associated with an increasing factor of disability, morbidity and fall risk [126]. From the wearer/ANGELEGS exoskeleton system model developed in chapter 3 (Eq.3.11), a wearer's motor ability based impedance compensation model is proposed as follows:

$$\lambda_1(\mathrm{M}(q)\ddot{q}_r + \mathrm{C}(q,\dot{q})\dot{q}_r) + \lambda_2\mathrm{G}(q) = \mathrm{R}\hat{\tau}_h + \mathrm{J}_\mathrm{F}^\mathrm{T}\mathrm{F}, \tag{6.13}$$

with:

$$\lambda_1 = \lambda_2 = (1, \lambda_k, \lambda_h), \quad \lambda_k, \lambda_h \in (0, 1), \tag{6.14}$$

where λ_h and λ_k are set to define the assistance rates related to the hip and knee joints, respectively. These rates represent the contribution levels of the exoskeleton in terms of torques to perform STS movements. Note that both ankle joints are controlled only by the wearer, and therefore, the desired position of each ankle joint is always equal to the current one (i.e., $q_{r1} = q_1$). λ_h and λ_k are defined as follows:

$$\lambda_h = \lambda_k = \lambda_{k0}\tanh(s_k(p_\mathrm{E} - h_{th})) + \delta_k \tag{6.15}$$

with p_E, a variable defined as follows:

$$p_\mathrm{E} = \kappa_v v_{torso}^2 + g h_{torso}^2 \tag{6.16}$$

In this study, the assistance ratios related to the hip and knee joints are chosen equal. v_{torso} and h_{torso} denote the vertical linear velocity and position of the centre of mass (CoM) of the torso, respectively; g is the gravitational acceleration; h_{th} is a threshold value and s_k is a sensitivity coefficient related to the function slope. An example of the assistance rate function defined in Eq.(6.15) is shown in Figure 6.2. It can be observed that λ_h and λ_k increase quickly to 1 when p_E is greater than the threshold h_{th}. In other words, when the wearer stands up with a relatively low speed in case of insufficient mo-

tor ability, the desired impedance remains low until the position of the torso CoM will be greater than the threshold h_{th}. Conversely, high standing-up speeds trigger a quick increase in the λ_h and λ_k values. It is assumed that no or limited assistance is needed for individuals who can stand up from a chair with a normal or even fast speed [126].

6.2.2 Balance reinforcement-based control

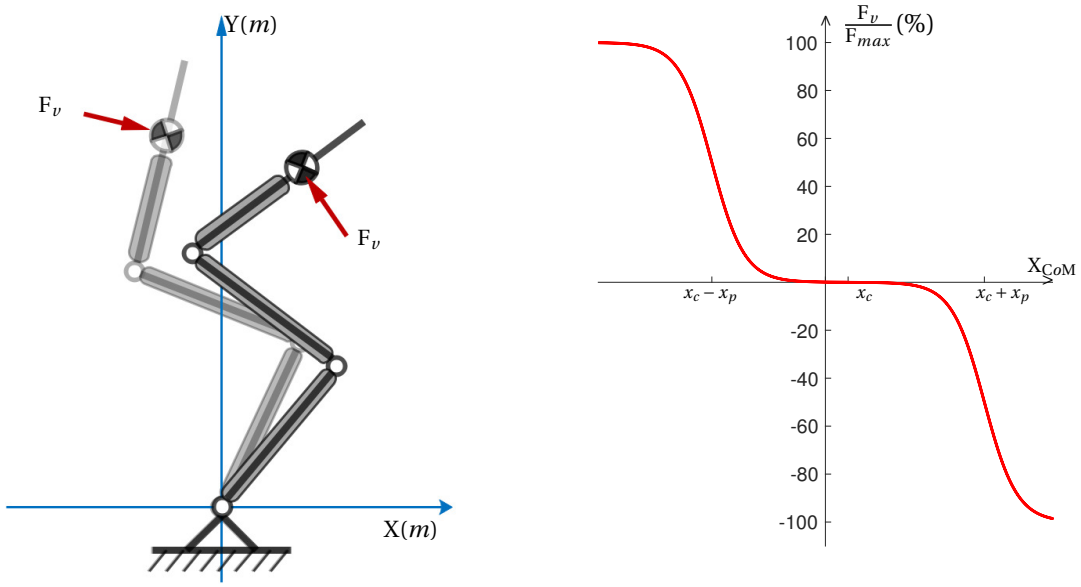

(a) (b)

Figure 6.3: Principle diagram of the Virtual Stiffness Force (VSF). (a) VSF directions, (b) Example of function characterising the VSF.

Balance control is fundamental to ensure successful STS movements. A virtual stiffness force generating an elastic effect, applied to the wearer's torso, is then introduced to reinforce his/her balance control ability (see Figure 6.3). The proposed virtual stiffness force, F_v, is assumed to be always normal to the wearer's torso while acting at his/her CoM:

$$F_v = -F_{max}\text{sign}(X_{CoM} - x_c)(\tanh(K_s(|X_{CoM} - x_c| - x_p)) + 1) \tag{6.17}$$

where F_{max} represents the maximum value of the virtual stiffness force; sign(.) is the signum function and K_s the sensitive gain; X_{CoM} represents the horizontal position of the CoM of the wearer/ANGELEGS exoskeleton system; x_c and x_p denote the virtual centre

and margin of the CoM position X_{CoM}, respectively (see Figure 6.3b).

The virtual stiffness force (6.17) is used to guarantee that the horizontal position of the CoM of the wearer/ANGELEGS exoskeleton system X_{CoM} is at a given distance with respect to the foot position (i.e., the origin) (i.e., within the interval defined as $[x_c - x_p,\ \ x_c + x_p]$) as shown in Figure 6.3. If $|X_{CoM} - x_c| < x_p$, the virtual stiffness force is negligible and the wearer can freely adjust his/her posture. Conversely, if $|X_{CoM} - x_c| > x_p$, a significant stiffness force is applied to the wearer's torso to prevent loss of balance (see Figure 6.3).

By combining the virtual stiffness force and the impedance compensation principles (i.e., (6.13)), the desired impedance model can be expressed as follows:

$$\lambda_1(M(q)\ddot{q}_r + C(q,\dot{q})\dot{q}_r) + \lambda_2 G(q) = R(\hat{\tau}_h + \tau_v) + \lambda_2 J_F^T F \tag{6.18}$$

with:

$$\tau_v = \frac{F_{GRF}}{F_{GRF,max}}[0\ 0\ F_v l_3 k_{h3}]^T \tag{6.19}$$

where τ_v represents the virtual torques vector induced by the virtual stiffness force (6.3), $\|\tau_v\| < \varepsilon_v$. The virtual torque vector τ_v is also defined as a function of the ground reaction force F_{GRF}. Note that the components of the virtual torque vector become zero when the wearer is sitting on a chair, i.e., $F_{GRF} = 0$.

6.3 Performance evaluation

6.3.1 Simulation results

The performance of the proposed impedance modulation-based control strategy, in terms of assistance and robustness with respect to modeling uncertainties, was evaluated in simulation. Since the wearer's capability is taken into account during STS movements, a PD controller was used to simulate the wearer's role [127]. In addition, an alternative simplified method was used to directly detect the "Seat-Off" time rather than using the

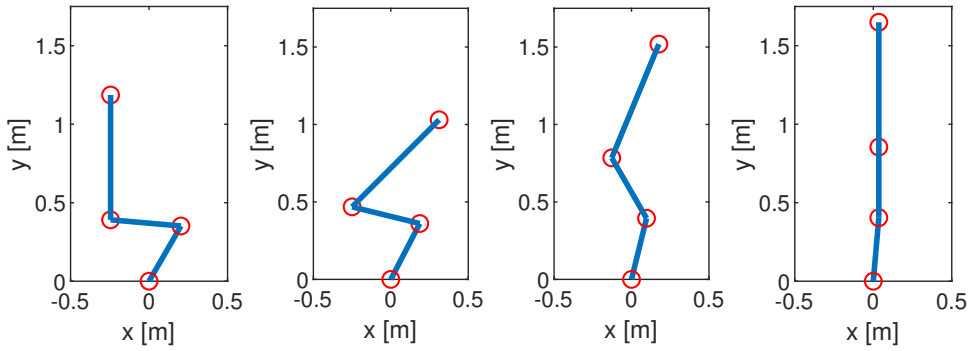

Figure 6.4: Start, intermediate and end postures of the wearer's body performing STS movements.

GRF (see Chapter 3, Eq.(3.17)), as follows:

$$\begin{cases} \beta_F = 1, & \text{if } t > T_{th} \\ \beta_F = \frac{t^2}{T_{th}^2}, & \text{if } t < T_{th} \end{cases} \tag{6.20}$$

where t represents the simulation time and T_{th} a time threshold after which the seat force completely converges to zero.

During the following simulations, the identified subject's parameters as well as those of the ANGELEGS exoskeleton were used to build the wearer/exoskeleton model (Eq.3.11, Table 3.4). The PD parameter values were empirically tuned and set as follows: $K_p = 1000$ and $K_d = 100$. The parameter values related to the sliding mode controller (6.9) and torque observer (6.2) are as follows: $c_1 = 20$, $\sigma_1 = 50$, $\sigma_2 = 100$, $\beta = 6$, $\zeta = 40$. In the simulation, we assumed that the exoskeleton was able to fully support the required torques while performing STS movements.

6.3.1.1 Performance of impedance compensation-based control

Firstly, the wearer/ANGELEGS exoskeleton system was controlled using a PD controller to track a normal STS reference trajectory extracted from STS movements of a healthy subject. Figure 6.4 shows the start and end postures of the wearer's body while performing STS movement. According to the reference trajectory, the horizontal position of the CoM is located at $0 - 0.1m$ in front of the ankle joint during STS movement. In addition, the

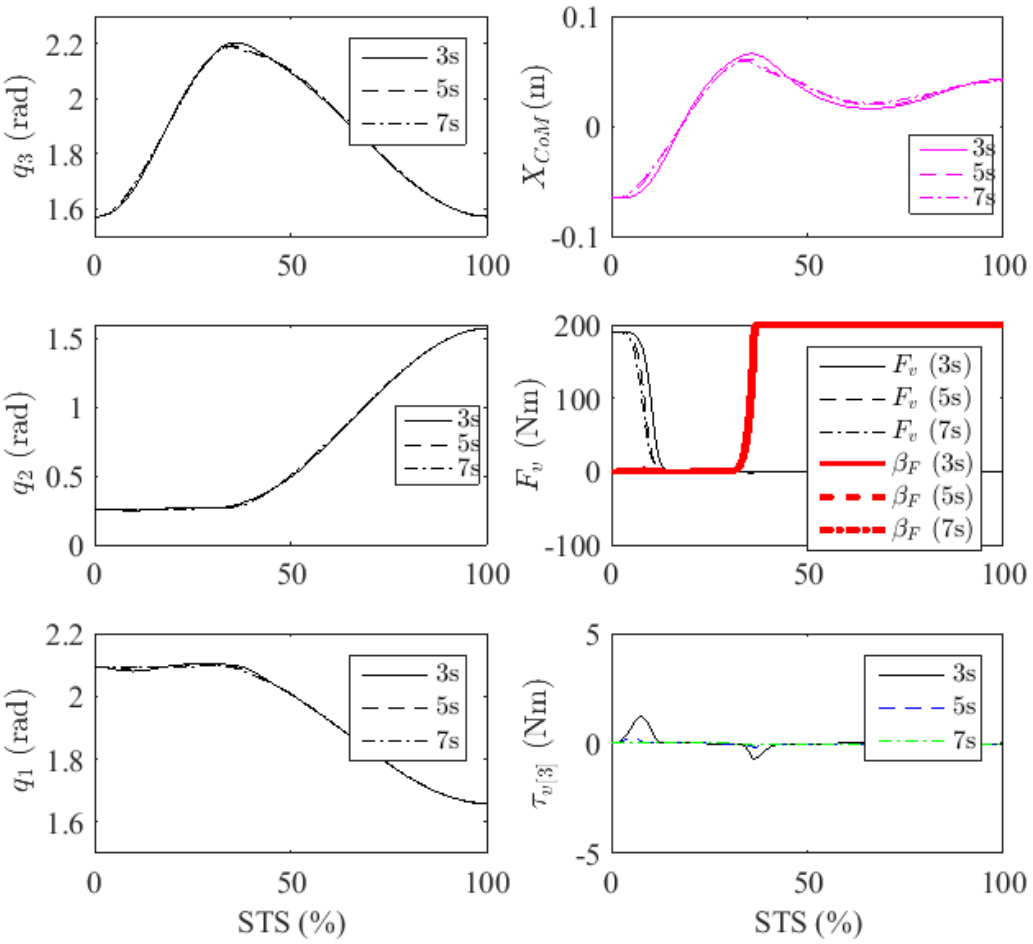

Figure 6.5: STS movements performed at three different speeds. Simulation results: (left) Joint positions, (right) CoM position, virtual force and virtual torque $\tau_{v[3]}$ during the normal STS movement (3s).

virtual centre and margin of the CoM in equation (6.17) are set to $0.05m$ and $0.07m$, respectively. To assess the performance of the impedance compensation provided by the proposed control strategy, three simulations were performed with different STS periods (i.e., 3s, 5s, and 7s). According to the five-time STS test [128] , if the subject is able to perform a successful STS movement in $3s$, this means that no external assistance is needed. Otherwise, longer STS time means insufficient lower limbs muscular ability. The parameter values related to the assistance rates are set to $\lambda_{k0} = 0.25$, $s_k = 10$, $\dot{y}_{3,0} = 0.1$, and $\delta_k = 0.75$. Moreover, the wearer (the PD controller) was assumed to be able to perform successful STS movements with the three different STS speeds.

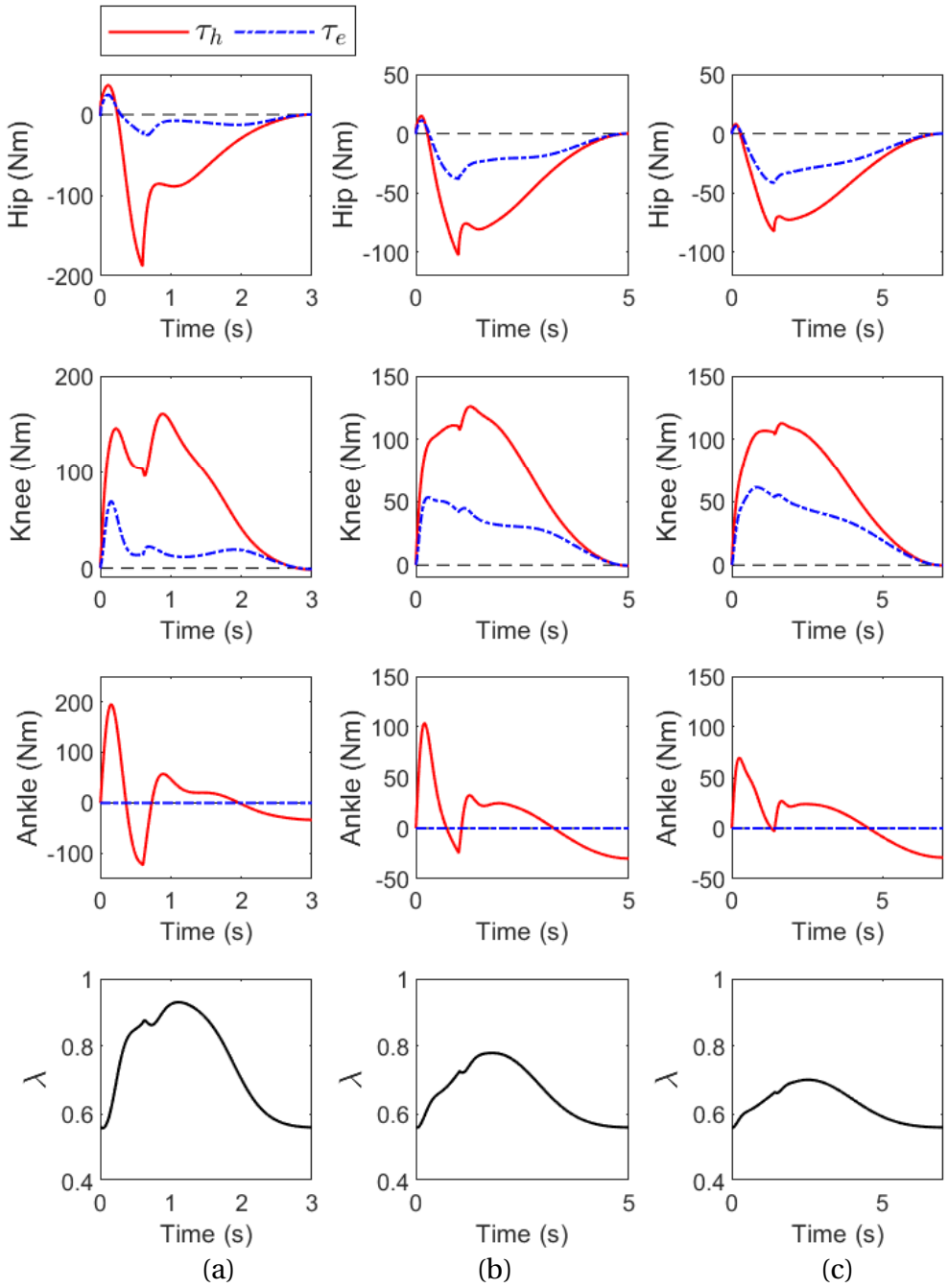

Figure 6.6: Wearer's and exoskeleton torques at hip and knee joints during STS movement performed at three different speeds. (a) High speed; (b) Normal speed; (c) Slow speed. λ is the ratio between the wearer's torques and exoskeleton torques

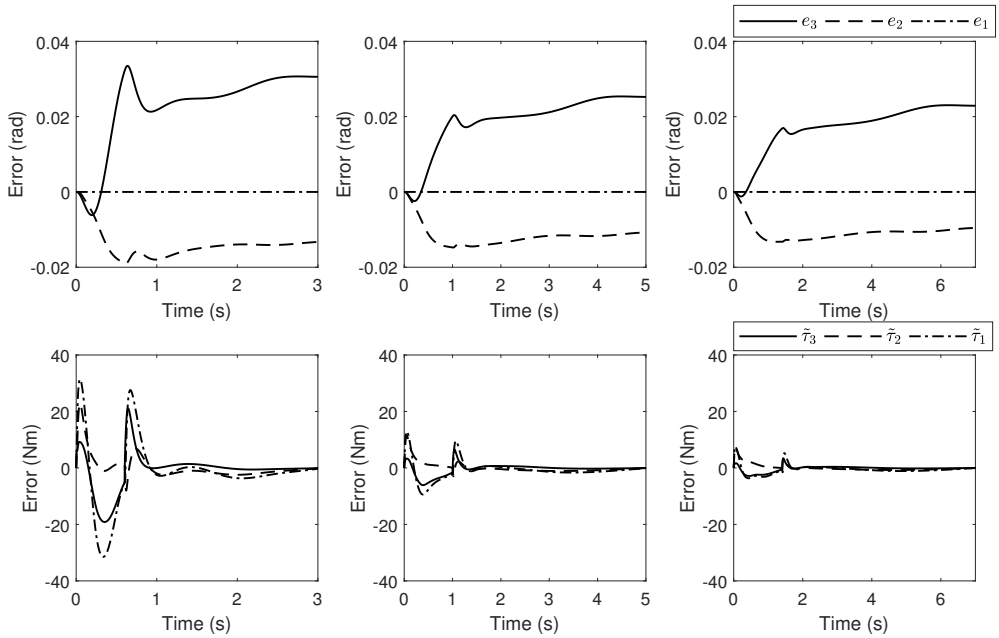

Figure 6.7: STS movements performed at three different speeds. Simulation results: tracking performance of the SMC-based controller and estimation accuracy of the torque observer.

Figure 6.5 shows the normalized measured joint positions. During the three groups of STS movements performed with three different speeds, the wearer's joint positions are almost the same. The seat forces were set to converge to zero in the first 20% of each STS movement (see Figure 6.5). Based on the measured CoM position and the "seat_-off" detection parameter β_F (see Figure 6.5), one can observe that the generated virtual torque $\tau_{v[3]}$ is relatively small (< 15 Nm) and similar for the three groups of STS movements. However, significant differences can be observed in the torques provided by the wearer and the exoskeleton (see Figure 6.6) across the three STS groups. During normal STS movement (in 3s), the exoskeleton provides the wearer a low assistance at the beginning of the movement and a relatively important assistance during the 7s STS movement to reduce the required wearer's effort. For similar STS movements with different speeds, the average ratios between the wearer's torques and the exoskeleton torques at the hip and knee joint levels show clear decrease with the increase of the STS time (see Figure 6.6). In other words, the required wearer's torques for achieving STS movements can be reduced to a desired level (see λ in Figure 6.6) according to the wearer's lower limb muscular ability. Note that the balance reinforcement torque τ_v is always maintained at a low level (F_v < 10 Nm) during normal STS movements.

Furthermore, the simulation results (Figure 6.5) showed that the tracking errors obtained with the SMC-based controller can be limited to a very small range ($\|e\| < 0.04$ rad). The estimation errors of the wearer's joint torques during normal-speed STS movement were relatively high but, at the same time, limited within 15% of the wearer's joint torques. A large decrease in the estimation error of the HJTO can be observed with the increase of the STS time. Note that a trade-off between the estimation accuracy and the noise reduction has been made in the simulations.

6.3.1.2 Performance of the balance reinforcement-based control

In this simulation, two common failed STS movements that are "sit-back" and "step-forward" were analyzed. As explained in [129], these failed movements represent a transient loss of balance control that might lead up to a fall if no external assistance is provided. To simulate the sit-back failed STS, the wearer was assumed to stand up from a posture in which the hip joint position is ninety degrees ($\theta_3 = \pi/2$, see Figure 6.8) while he/she is providing an insufficient upper body momentum at the beginning of the STS movement by limiting his/her hip joint torque for flexing the upper-body (setting $\max(\tau_{h,h}) = 20$ Nm). The reference position trajectory was designed to first flex the upper-body so that the CoM could be shifted to a normal range and then allow the wearer to stand up (see Figure 6.8). Regarding the step-forward failed STS, the horizontal position of the CoM was considered to be too forward relative to the ankle joint and a forward step was caused due to balance loss. In this case, the wearer was assumed to stand up with an excessive upper-body flexion (see Figure 6.8) without being able to provide sufficient hip joint torque to quickly extend the upper-body to shift the CoM to a normal range. Similarly, the reference position trajectory was designed to allow the wearer first extend his/her upper body and then stand up.

During the "sit-back" STS simulation, the wearer's CoM and the hip joint positions are quickly shifted back to their normal ranges thanks to the balance reinforcement-based control compared to the case where no balance reinforcement-based control is provided (see Figure 6.8). It can be observed that relatively high wearer's joint torques at the hip and knee joint levels are required at the beginning of STS movement without balance reinforcement-based control, which significantly increases fall risk for the wearer (see

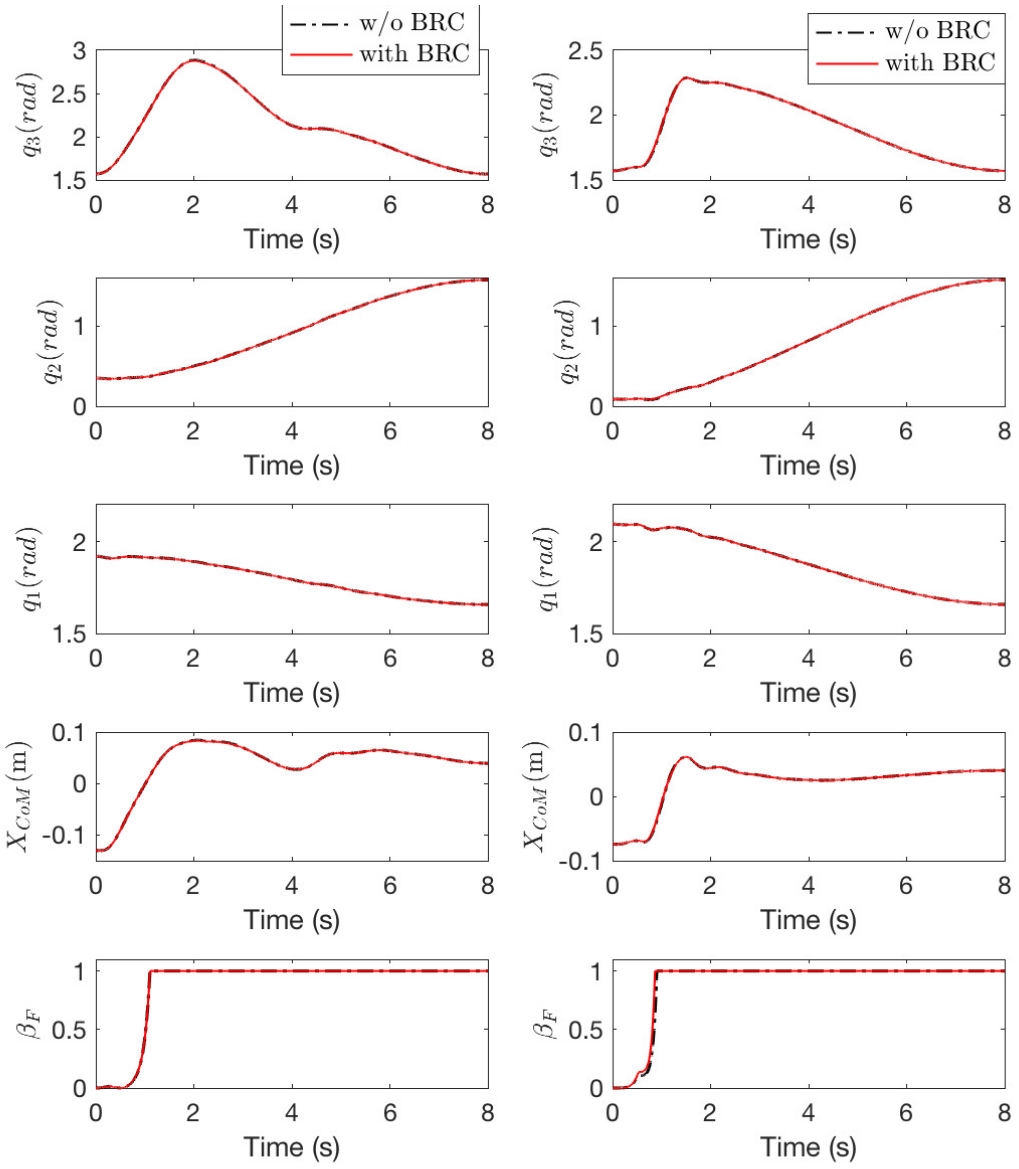

Figure 6.8: Two abnormal STS movements: actual position trajectories of hip, knee and ankle joints, and CoM for the cases: without balance reinforcement control (BRC) and with BRC. (a) "step-forward" case, (b) "sit-back" case.

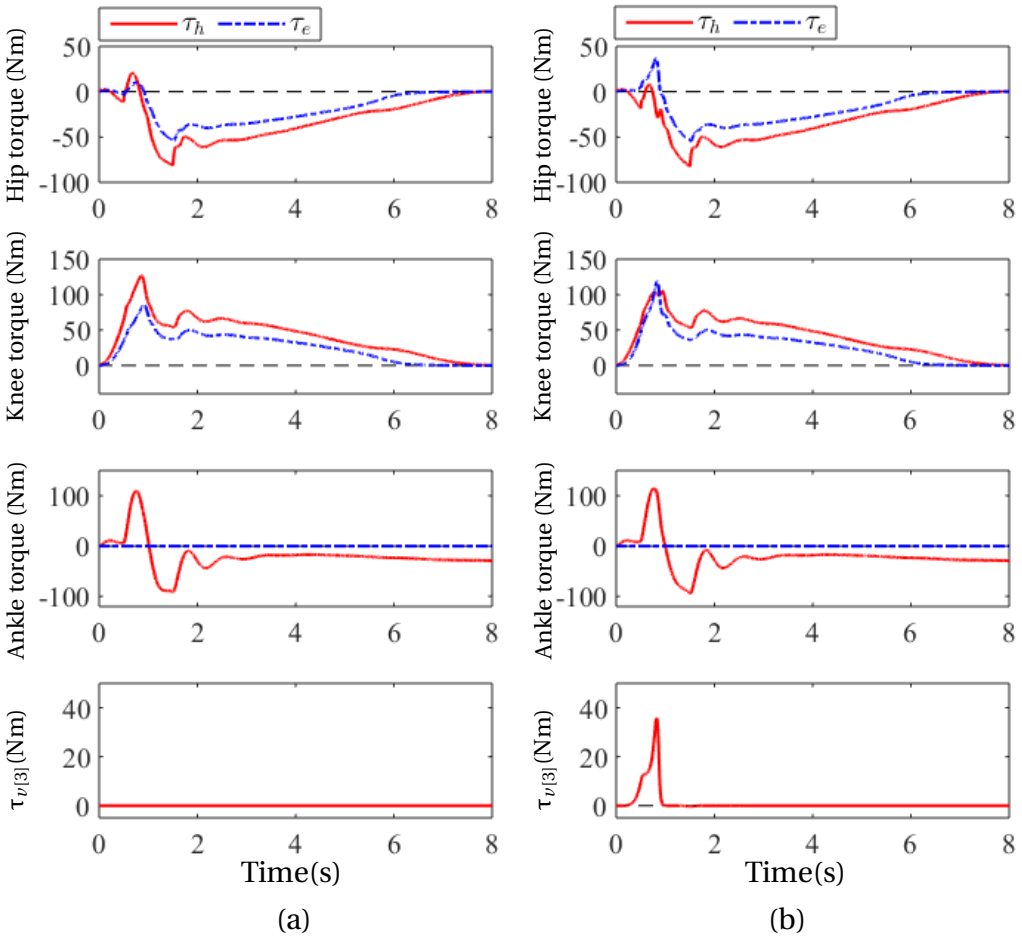

Figure 6.9: "Sit-back" STS movement simulation. $\tau_{v[3]}$ represent the generated virtual torque at hip joint using the balance reinforcement-based control (BRC). τ_h represents the wearer's joint torque for the cases: without BRC (a) and with BRC (b).

Figure 6.9). Note that the wearer's hip and knee joint torques were also limited to 250 and 200 Nm in the simulation by taking into account the maximum real wearer torques.

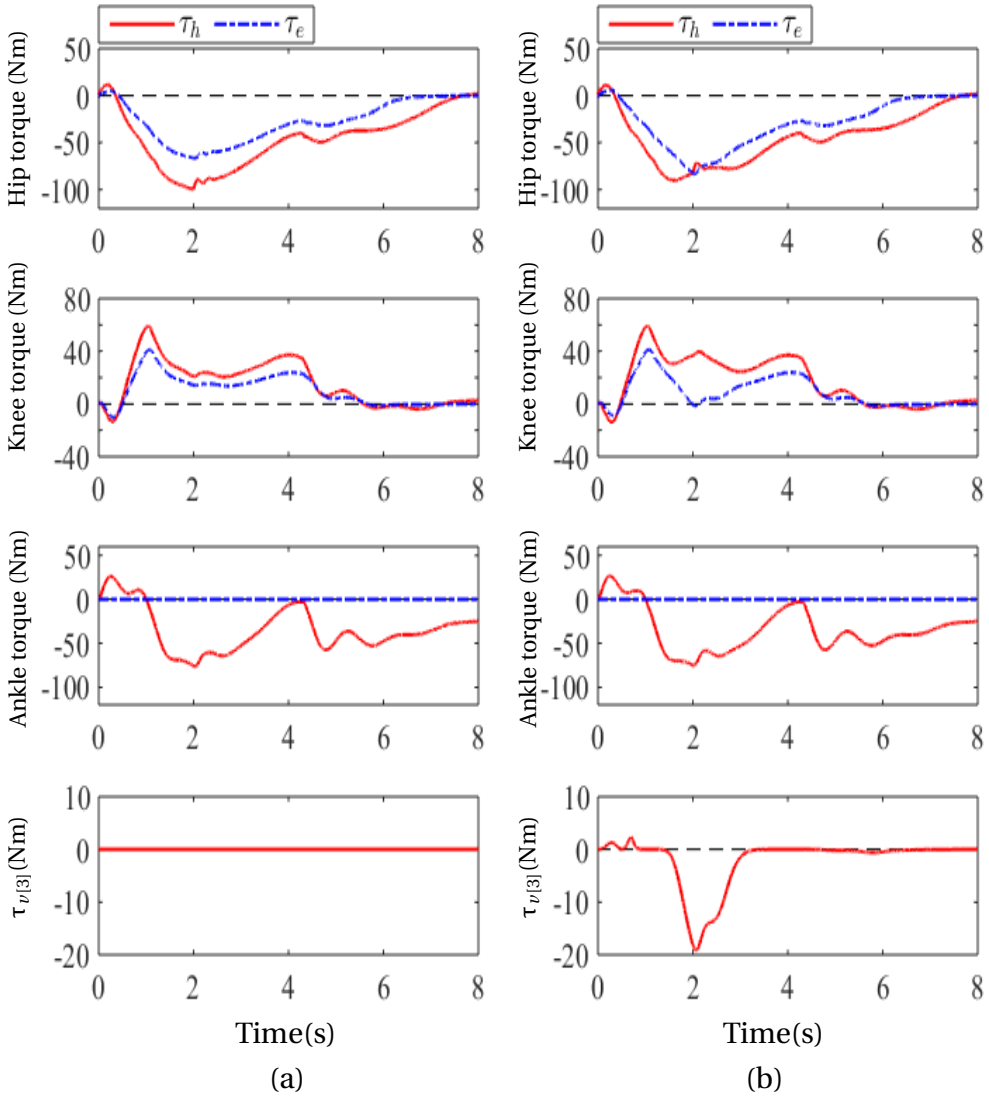

Figure 6.10: "Step-forward" STS movement simulation. $\tau_{v[3]}$ represent the generated virtual torque at hip joint using the balance reinforcement-based control (BRC). τ_h represents the wearer's joint torques for two cases: without BRC (a) and with BRC (b).

In the "step-forward" STS simulation (see Figures. 6.8 and 6.10), the wearer looses directly the balance when the balance reinforcement-based control is not enabled and performs successful STS movements when balance reinforcement-based control is enabled. As shown in Figure 6.10, large virtual torques are generated to assist the wearer to move back the CoM into the normal range.

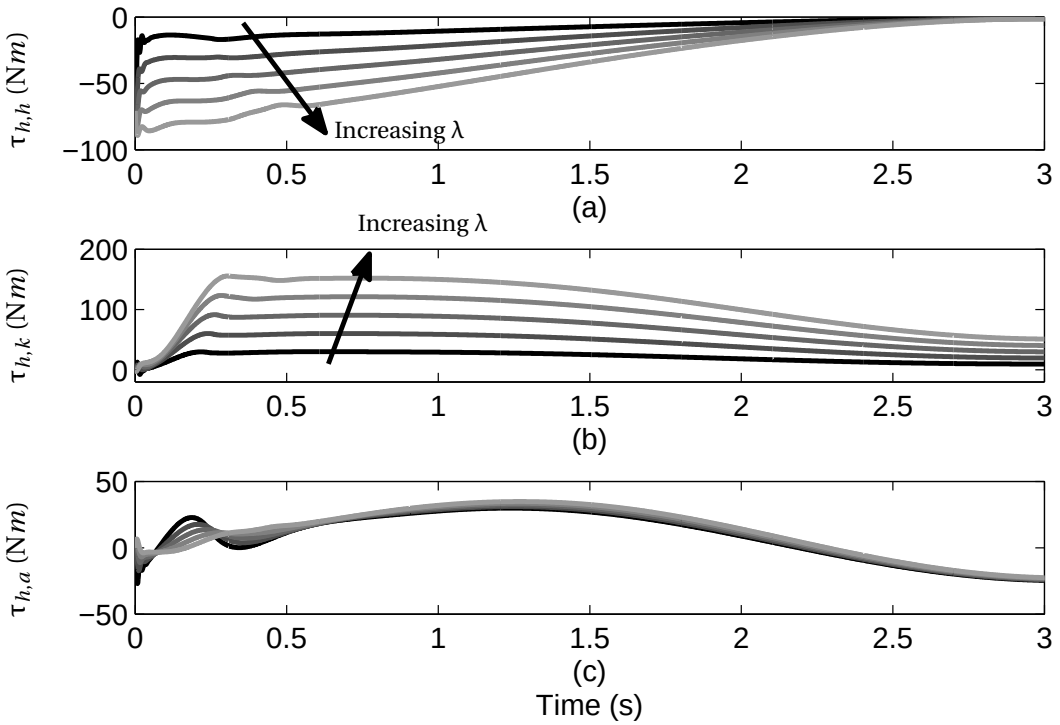

Figure 6.11: Wearer's torques with different λ ($\lambda_h = \lambda_k = \lambda$ = 1, 0.8, 0.6, 0.4, 0.2). (a) Wearer's hip-joint torque. (b) Wearer's knee-joint torque; (c) Wearer's ankle-joint torque.

6.3.1.3 Robustness with respect to modeling uncertainties

To evaluate the robustness with respect to modeling uncertainties shown in Appendix A, a modeling uncertainty ($\alpha = -0.4$) was introduced in the dynamic model of the wearer/ANGELEGS exoskeleton system. Three simulations were performed with different desired impedance parameter values ($\lambda_h = \lambda_k$ = 0.5, 0.4, 0.28). According to the stability condition (8.17), the wearer/exoskeleton system (see Figure 6.1) becomes unstable if λ_h and λ_k are smaller than 0.286. Figure 6.12 shows the assistance torques provided by the exoskeleton, indicating clearly that when λ_h and λ_k are higher than 0.286, the system is stable while instability is reached immediately when λ_h and λ_k become lower than 0.286. As a consequence, the desired impedance model (6.2) should be designed by taking into account the modeling uncertainties.

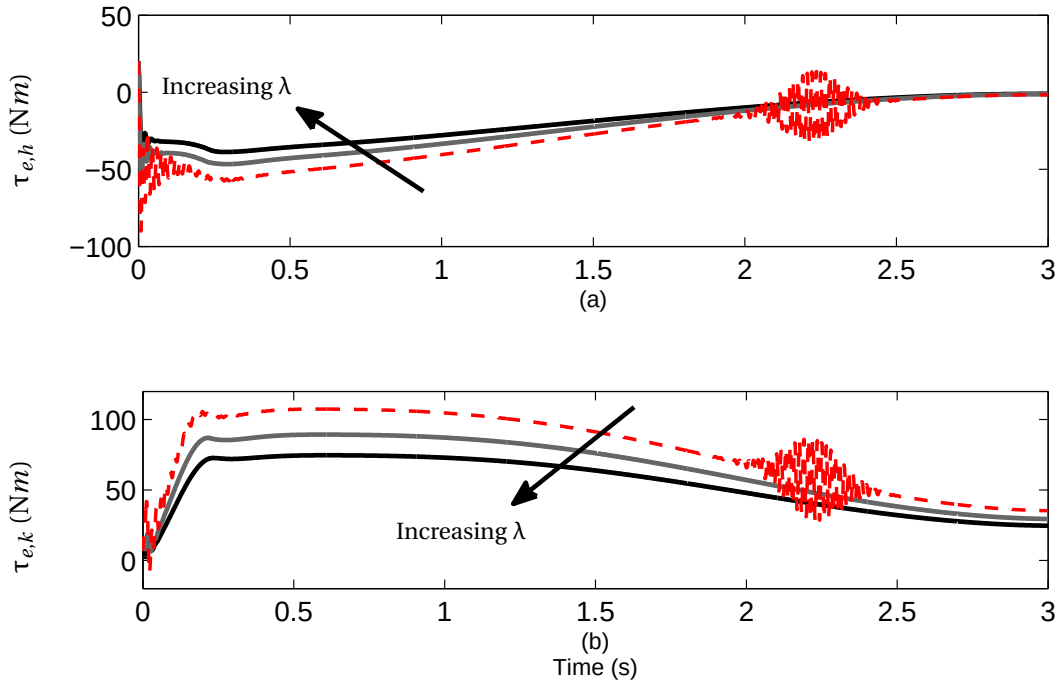

Figure 6.12: Evaluation of the robustness of the proposed control strategy with respect to modeling uncertainties ($\lambda = \lambda_h = \lambda_k = 0.5, 0.4, 0.28$ and $\alpha = -0.4$). (a) assistive torque provided at the hip joint level; (b) assistive torque provided at the knee joint level.

6.3.2 Experimental results

Experiments were conducted using the ANGELEGS exoskeleton to evaluate the performance of the proposed control strategy in case of impedance compensation-based control and balance reinforcement-based control.

6.3.2.1 Five-Time-Sit-to-Stand tests

The main goal of the proposed control strategy is to reduce the required wearer's torque for achieving a successful STS movement. To evaluate the assistance performance of the proposed control strategy, a healthy subject was asked to carry out two trials of FTSTS tests with two different speeds (normal speed (in 5s) and slow speed (in 10s)), respectively. To perform STS movements at each of the above speeds, an animation video shown on a monitor and a sound beeper were used to help the subject controlling his/her speed. The parameter values related to the proposed impedance modulation-based control are given in Table 6.1.

Table 6.1: Experimental parameter settings

Eq.s	Parameters	Values
(6.15), (6.16)	$h_{th}, \delta_k, \lambda_{k0}, \kappa_v$	9.87, 0.8, 0.2 150
(6.17)	x_c, x_p, F_{max}	0.82, 0.84, 150
(6.6)	β_o, ζ, σ_1	60, 40 , 50
(6.9)	c_1, σ_s, λ_s	12.5, 10, 100

Figure 6.13 shows average and standard deviation of experimental results across ten STS movements (i.e., two FTSTSs). The tracking errors, e_{q2} and e_{q3}, obtained with the proposed SMC controller are bounded into a small range for the two different speeds. The root mean square (RMS) of e_{q2} and e_{q3} are respectively 0.018 rad and 0.01 rad during normal STS movements, and 0.003 rad and 0.014 rad during slow STS movements. Such accuracy guarantees the adaption of the mechanical impedance of the wearer/exoskeleton system to the desired one. An increase in the tracking errors can be observed at the beginning of the hip and knee joint movements. Such an increase is mainly due to the HJTO designed to be less sensitive to fast variations of joint torques to reduce the noise effects. The tracking errors increase cause transient changes in the patterns of the assistive torques, $\tau_{e,h}$ and $\tau_{e,k}$, compared to those of the estimated wearer's joint torques $\tau_{h,h}$ and $\tau_{h,k}$.

During the normal-speed STS movement, the X_{CoM} position is in the range $[-0.022, 0.04$ m] after the subject shifts his/her body up (i.e., seat-off), and therefore, no balance assistance is needed (see Figure 6.13). The virtual torques during normal STS are negligible ($\tau_{v[3]} < 0.05$ Nm). Since the X_{CoM} position is calculated based on the dynamic model of the wearer/exoskeleton system, it could be close to -0.1m when the subject is in the sitting position. Considering that the F_{GRF} is almost zero at sitting position, then, according to Eq 6.19, the virtual torque tends to zero at that position.

When the subject stands-up with a normal speed, the assistive torque is provided at the beginning of STS movement, and then, becomes zero when the subject starts extending hip and knee joints (see Figure 6.13(a)). During low-speed STS movements, the impedance ratios $\lambda_h = \lambda_k$ gradually increase to 1 with the increase of the wearer's torso vertical position h_{torso}. Correspondingly, important assistive torques are needed during low-speed STS movements (see Figure 6.13 (b)). Due to the fact that it is dif-

ficult for healthy subjects to perform continuous and smooth STS movements at a low speed, a low-frequency fluctuation occurred in the estimated wearer's joint torques in the middle of STS movements (Figure 6.13(a)). The experimental results (figure 6.13) show the changes of impedance ratios with respect to STS speeds. By tuning the threshold h_{th} and the sensitive ratio s_k in equation (6.15), the assistance duration and assistance rates changes can be further increased or decreased. Compared to the peak values in wearer/exoskeleton system hip and knee joint torques, the wearer's hip and knee joint torques can be reduced up to 48.9% and 30.6 %, on average, respectively.

6.3.2.2 Performance of Balance reinforcement-based control

To evaluate the effectiveness of the balance reinforcement-based control, the subject was asked to perform STS movements while wearing the exoskeleton in two abnormal cases which may cause sit-back and step-forward, respectively. In the first case, the subject was asked to sit on a chair (0.6 m) while keeping the torso in vertical direction, and then, standing-up directly without a prior forward bending of the torso. Significant torques are required from the wearer at the knee and ankle joint levels to shift the CoM of the wearer/exoskeleton system forward. In the second case, the subject was asked to first flex the hip joint to around 60 degrees in sitting position, and then, standing-up without extending the hip joint during the first two seconds. The CoM position of the wearer/exoskeleton system is more than 0.1 m in front of the ankle joint, which may lead the subject to make a step in order to restore balance.

Figure 6.14(a) shows the experimental results obtained in the first case. Although the subject was able to achieve successful STS movements by adjusting his/her posture without assistance of the exoskeleton, significant wearer's torques at both joints were required at the beginning of STS. The balance reinforcement control allows providing a large virtual torque $\tau_{v[3]}$ to assist the wearer moving the CoM into the defined range by flexing hip joint at the beginning of the STS. The wearer's hip and knee joints torques show curve patterns similar to those of normal STS movements (see Figure 6.13). In the second case, conversely, a virtual torque was generated to assist the wearer to extend the hip joint so as to move the CoM back to the defined range (see Figure 6.14(b)).

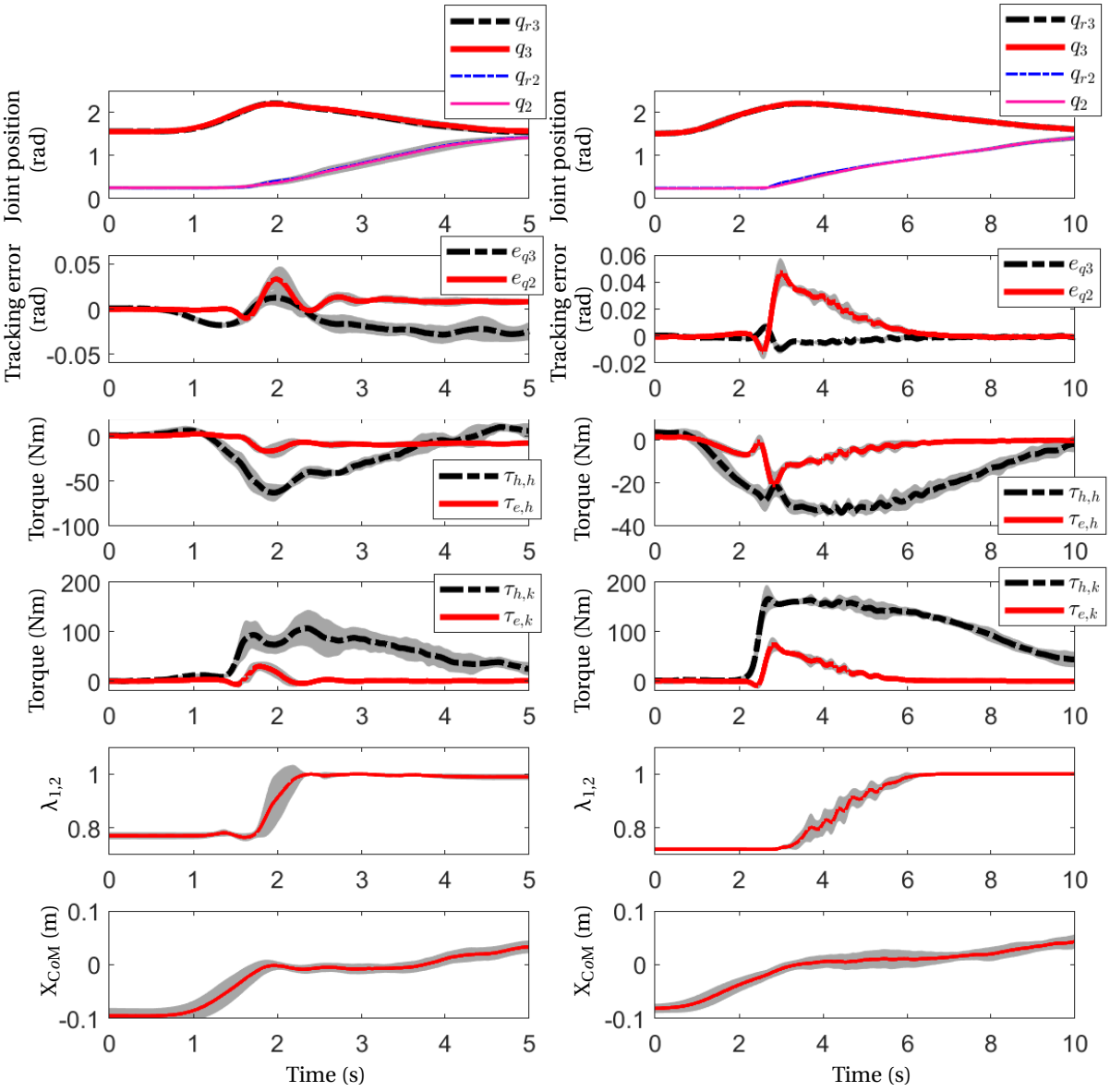

(a) (b)

Figure 6.13: Experimental results with a healthy subject (on average, across 10 STS movements). Gray zones represent standard deviations; q_i and q_{ri} (i=2,3) denote measured and reference joint positions of knee and hip joints, respectively; e_{qi} (i=2,3) denote tracking errors at knee and hip joints, respectively; $\tau_{h,h}$ and $\tau_{e,h}$ are the wearer's and exoskeleton hip joint torques, respectively; $\tau_{h,k}$ and $\tau_{e,k}$ are the wearer's and exoskeleton knee joint torques, respectively. (a) standing-up with normal speed. (b) standing-up with low speed.

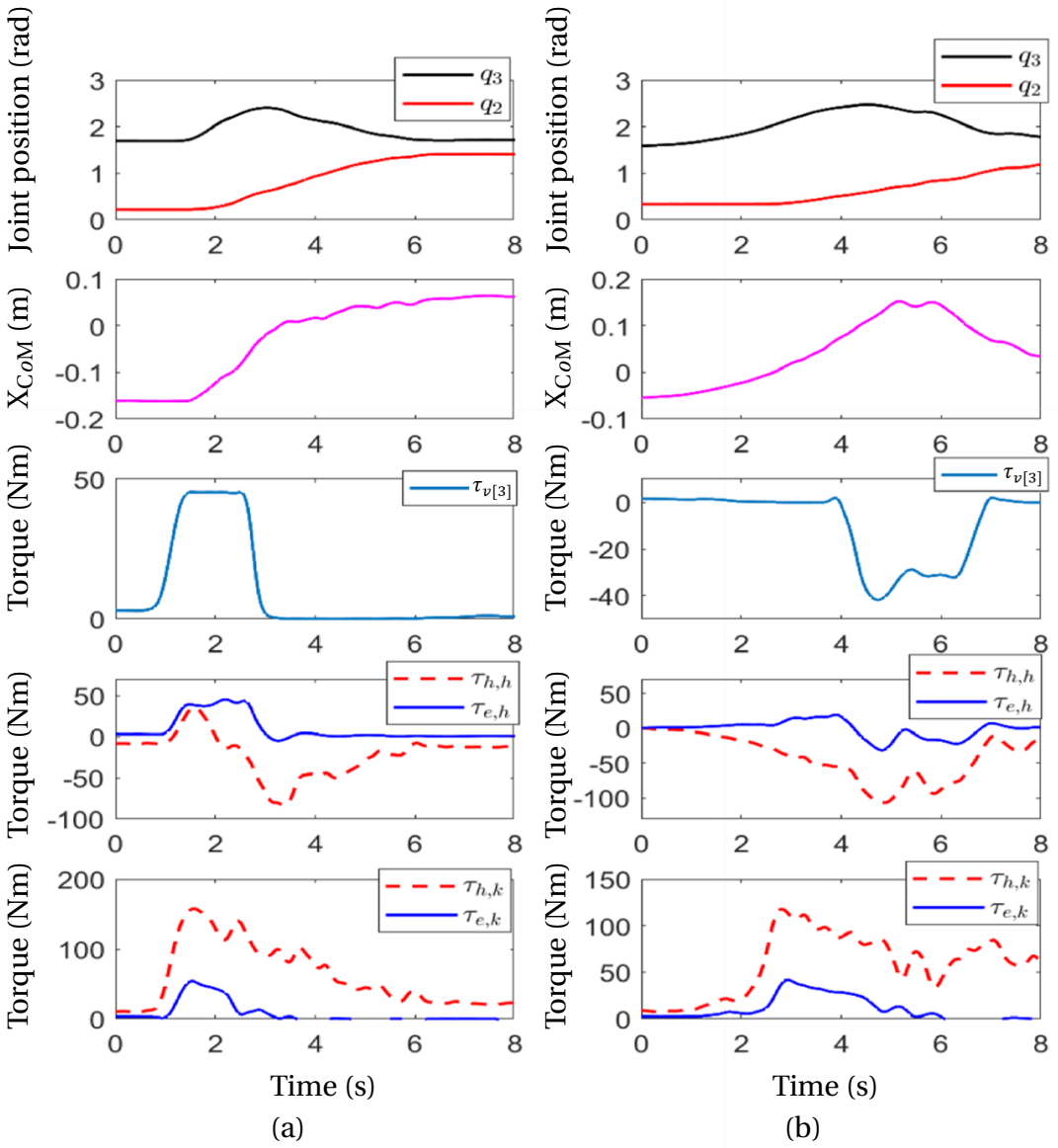

Figure 6.14: Abnormal STS movement; q_i (i=2,3) denote measured and reference joint positions of knee and hip joints, respectively; X_{CoM} represents the CoM position; $\tau_{v[3]}$ represents the virtual torque acting at the hip joint; $\tau_{h,h}$ and $\tau_{e,h}$ are the wearer's and exoskeleton hip joint torques, respectively; $\tau_{h,k}$ and $\tau_{e,k}$ are the wearer's and exoskeleton knee joint torques, respectively. (a) "Sit-back" case, (b) "Step-forward" case.

6.4 Conclusion

In this chapter, an impedance modulation-based control strategy for the ANGELEGS exoskeleton is proposed to assist a subject to achieve successful sit-to-stand movements. The potential users are supposed to have a certain lower limb motion ability, but not sufficient to ensure a successful STS movement. In this case, an impedance compensation-based control is used to reduce the mechanical impedance of the wearer/exoskeleton system and bring it to a level lower than the wearer's one. Moreover, a balance reinforcement-based control was developed for two typical failed STS movements, "seat-back" and "step-forward". To adapt the wearer/exoskeleton system impedance to the desired one, a human joint torque observer is used to estimate the wearer's motor capability, then, a time-varying desired impedance model is proposed to adapt the desired impedance accordingly. Besides, a Sliding Mode Controller (SMC) is used to provide sufficient power support to ensure an efficient assistance. Furthermore, characteristics and robustness with respect to modeling uncertainties of the proposed control strategy, were theoretically analyzed in simulation. As a consequence, conditions on impedance compensation parameters were drawn out to ensure stability of the wearer/exoskeleton system. Finally, the performance of the proposed control strategy is evaluated in simulation and experiments. The obtained results show that the proposed control strategy can efficiently estimate the wearer's joint torques, reduce the wearer/exoskeleton system impedance, and provide appropriate power support to the wearer for both human effort reduction and balance reinforcement.

Chapter 7

Hybrid impedance control

Man, a hybrid of plant and ghost.

Friedrich Nietzsche

Contents

7.1 Introduction

In this chapter, a hybrid Assistance-As-Needed (AAN) control strategy is developed. It combines the use of exoskeleton/orthosis impedance control with quadriceps FES. The hybrid impedance control strategy is applied in two case studies: i) flexion/extension movements of the knee joint, ii) Sit-To-Stand movements. For each case study, the orthosis/exoskeleton impedance and FES controllers are developed; besides, the used experimental protocol is described and performance of the proposed control strategy is presented and analyzed.

7.2 Hybrid impedance control in the case of knee joint flexion/extension movements

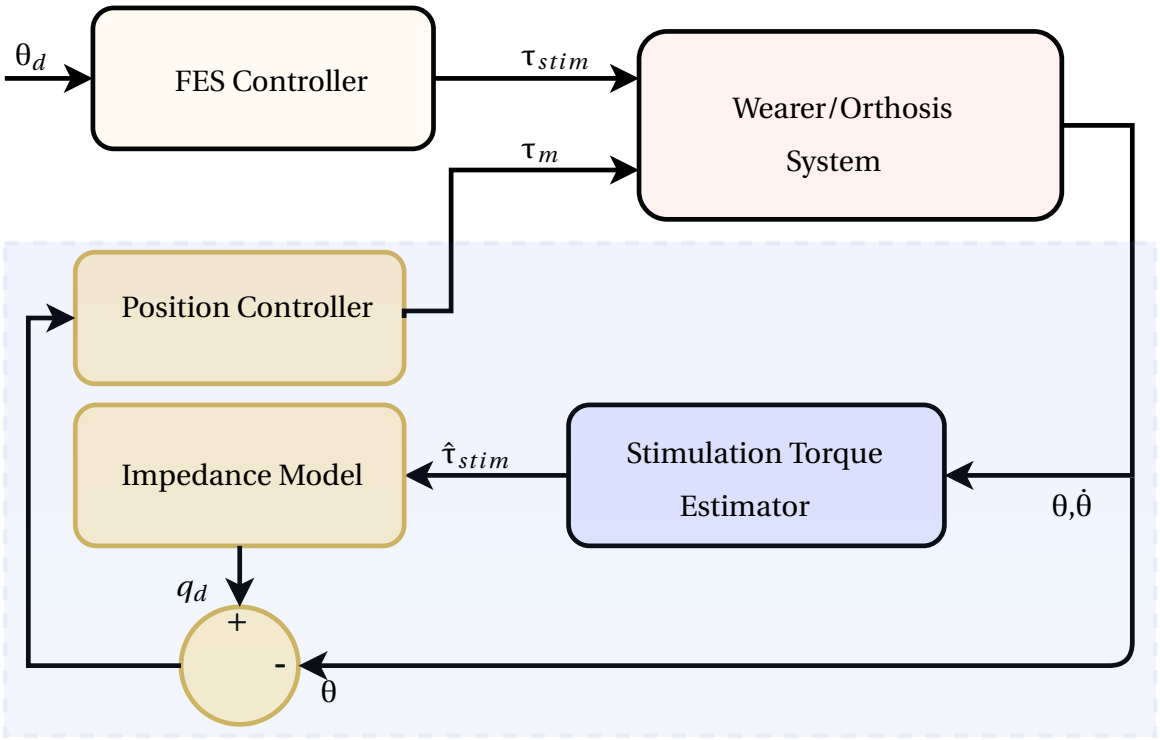

Figure 7.1: Proposed hybrid controller: the blue shaded area represents the impedance controller along with the position controller

In this sub-section, the hybrid impedance control of knee joint flexion/extension

movements of the wearer/orthosis system is studied. In this study, the EICOSI orthosis along with quadriceps FES are exploited jointly to assist these movements. FES is applied in open-loop while the EICOSI orthosis is controlled in closed-loop using an impedance control. The main advantage of this strategy is that it allows reducing and delaying the muscular fatigue as much as possible within the Assistance-As-Needed control paradigm. The proposed approach does not require any muscle modeling process nor extra force/torque sensor; it uses a non-linear disturbance observer for on-line estimation of the generated stimulation torque.

7.2.1 Hybrid controller

7.2.1.1 Orthosis impedance controller

The key aspects of impedance control is to enable the orthosis to provide assistance effort that reduces the impedance of the wearer's shank-foot segment/orthosis system [130]. Impedance control is used to regulate the interaction between the orthosis and the wearer. To illustrate how the orthosis can modify the wearer's shank-foot segment impedance, let's first define the impedance of the wearer's shank-foot segment as follows:

$$Z_h(s) = I_h s + B_h + \frac{K_h}{s} \tag{7.1}$$

where I_h, B_h and K_h are inertia, damping and stiffness coefficients of the wearer's shank-foot segment.

The wearer's shank-foot segment/orthosis system is considered as rigid; thus, the equivalent impedance of the whole system can be expressed as follows:

$$Z_o^h(s) = Z_h(s) + Z_e^d(s) \tag{7.2}$$

where $Z_e^d(s)$ is the desired orthosis impedance, and Z_o^h the equivalent impedance of the wearer's shank-foot segment/orthosis system.

To provide assistance, the wearer's shank-foot segment/orthosis system must show an

equivalent impedance lower than the initial impedance, i.e.:

$$Z_o^h(s) \leq Z_h(s) + Z_e^d(s) \tag{7.3}$$

To achieve the compliance requirements, the impedance of the closed-loop wearer's shank-foot segment/orthosis system is computed using a linear desired impedance model defined as follows [90]:

$$\frac{\theta(s)}{\tau_{stim}} = \frac{1}{I_d s^2 + B_d s + K_d} \tag{7.4}$$

where I_d, B_d and K_d denote the desired inertia, damping and the stiffness parameters, respectively. The impedance control strategy requires to take into account the maximum velocity response of the orthosis and the one of the wearer's shank-foot segment to ensure the stability of the closed-loop wearer's shank-foot segment/orthosis system. A low desired impedance may result in a high velocity of the orthosis, constraining the wearer to develop high efforts to stabilize the wearer/orthosis system. Indeed, this may result also in a wearer/orthosis system instability [90].

7.2.1.2 FES controller

For the knee joint flexion/extension movements assitance, FES is enabled during the extension phase as stated in chapter 5.

Different combinations of stimulation frequencies and pulse-width values were evaluated in [131] during knee joint flexion/extension performed by healthy subjects. It has been shown that setting both frequency and pulse width values while adapting stimulation intensity yielded in better muscular responses and less muscular fatigue. The results of this study showed that using a medium frequency with a medium pulse duration (i.e. pulse width= 150µs, frequency=40 Hz) induces less muscular fatigue [131]. This choice has been also approved by the rehabilitation department staff at CHU Mondor (Créteil, France).

To control the knee joint movements through quadriceps FES, the current amplitude

$i_s(t)$ of the stimulation profile is given as follows:

$$i_s(t) = \begin{cases} i_s^{'}(t) \text{ if } i_s^{'}(t) > 0 \\ 0 \text{ otherwise} \end{cases} \tag{7.5}$$

where:

$$i_s^{'}(t) = \begin{cases} i_{max} \text{ if } \dot{\theta}(t) > 0 \ \ and \ \theta < \frac{\theta_{max}+\theta_{min}}{2} \\ i_{max}\frac{\dot{\theta}(t)}{\dot{\theta}_{max}} \text{ if} \dot{\theta}(t) < 0 \ or \ \theta > \frac{\theta_{max}+\theta_{min}}{2} \end{cases}$$

where i_{max} denotes the maximum stimulation current amplitude; θ and $\dot{\theta}$ represent the knee joint position and velocity, respectively; θ_{max} and θ_{min} are respectively the maximum and minimum knee joint positions.

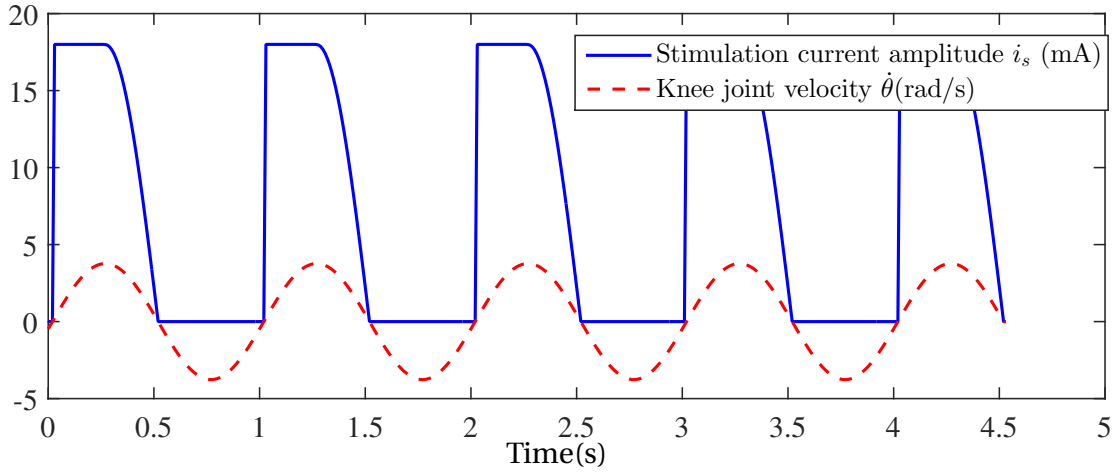

Figure 7.2: Stimulation pattern: amplitude of the current stimulating the quadriceps muscles in synchronization with the knee joint velocity.

7.2.1.3 Stimulation torque estimation

In the proposed hybrid control strategy, the torque resulting from the quadriceps FES is considered as an external disturbance for the the wearer's shank-foot segment/orthosis system (see Figure 7.1). The stimulation torque can be estimated using the Non-linear Disturbance Observer (NDO) described in chapter 5.

7.2.2 Performance evaluation

7.2.2.1 Experimental protocol

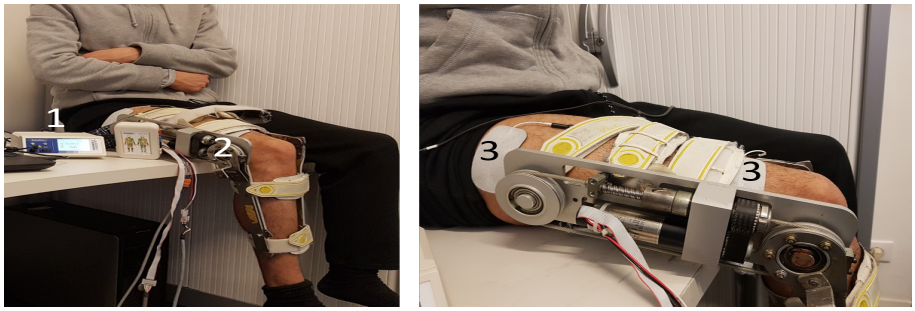

Figure 7.3: Experimental setup. (1) RehaStim 2 stimulator. (2) Knee joint orthosis. (3) Stimulation Electrodes

Two healthy subjects were involved in the experiments; their information are listed in Table. 7.1. Both subjects were able to perform complete knee joint flexion/extension with no spasticity or co-contraction.

Flexion/extension movements are performed in a sitting position while the wearer's shank-foot segment is freely moving in the sagital plane. During the experiments, bipolar adhesive stimulation electrodes are placed over the distal and proximal position of the quadriceps muscles and connected to the RehaStim 2 stimulator (Figure 7.3). A sinusoidal reference trajectory (frequency 0.2Hz and amplitude of 1.2 rad) is used. The subjects participating in the experiments were instructed not to influence voluntarily the wearer's shank-foot segment movement and were not allowed to observe the reference trajectory to reduce any possible anticipation of the movement. Two cases were considered. In the first case, the subject was wearing the orthosis and subject to FES. The amplitude and frequency of flexion/extension movements were determined to fit the human daily living activities and explore the maximum range of motion provided by the orthosis. In the second case, the experiments were conducted using FES only. Following the requirements of the rehabilitation staff at the CHU Mondor (Créteil, France), each experiment lasted 6 minutes. Before experiments, calibration tests of the stimulator were conducted to tune the stimulation parameters (pulse width, frequency and maximal current amplitude) as well as to define threshold, saturation and pain levels. These parameters were determined for the quadriceps muscles group by observing the muscular contraction, the maximum

extension of the knee joint and the feeling of the subject while applying the stimulation.

Table 7.1: Subjects information

	Age	Sex	Height (m)	Weight (Kg)
S1	26	M	1.78	64
S2	27	M	1.90	71

7.2.2.2 Experimental results

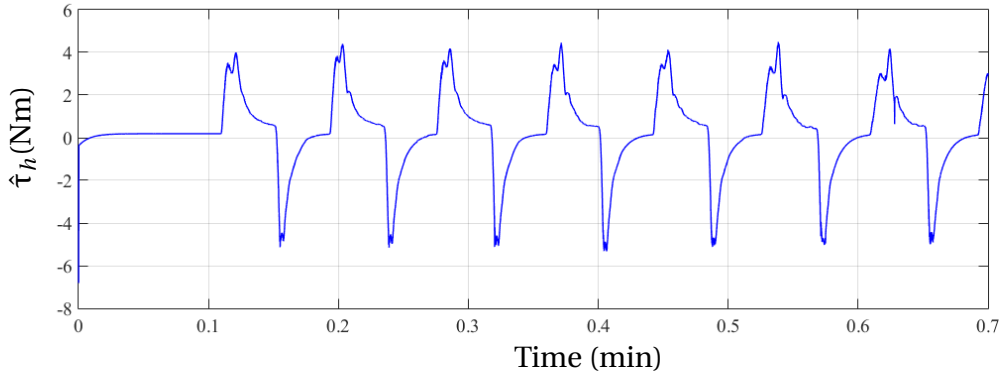

Figure 7.4: Estimated knee joint torque $\hat{\tau}_h$ when using only FES.

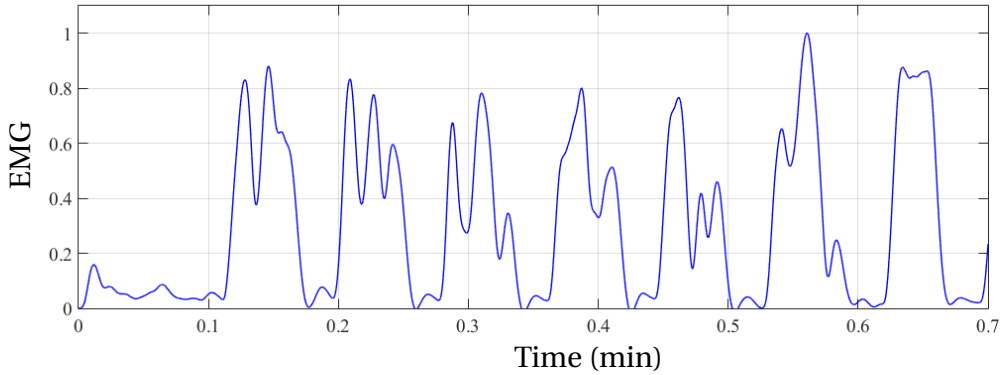

Figure 7.5: EMG activity of the hamstring muscle when using only FES.

To assess the performance of the proposed hybrid impedance control strategy, preliminary experiments have been conducted to evaluate the performance of the Stimulation Torque Estimator (STE) (Figure 7.1). The parameters of the desired impedance model were set as follows: (Id, Bd, Kd) = (0.15, 0.3, 0.1). The parameters of the nonlinear observer were chosen as: k1 = 15, k2 = 1. FES was then applied on the quadriceps muscles

and the activity of the hamstring muscle was recorded using the Delsys ^{TM} EMG sensors to evaluate the flexion/extension of the knee joint. The raw EMG signals were processed using the root mean square envelope method [132]. Figures 7.4 and 7.5 show the estimated stimulation torque and the analyzed hamstring EMG signal normalised with respect to the maximum value of the recorded EMG during the experiment, respectively. Note the profile similarity between the positive part of the estimated wearer's torque and the normalised hamstring EMG signal, confirming therefore the efficiency of the STE in delivering a relatively accurate estimation of the knee joint torque induced by FES.

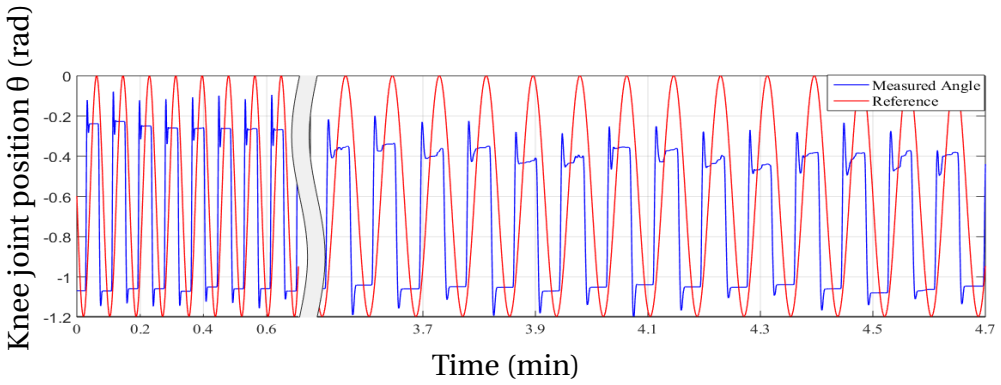

(a)

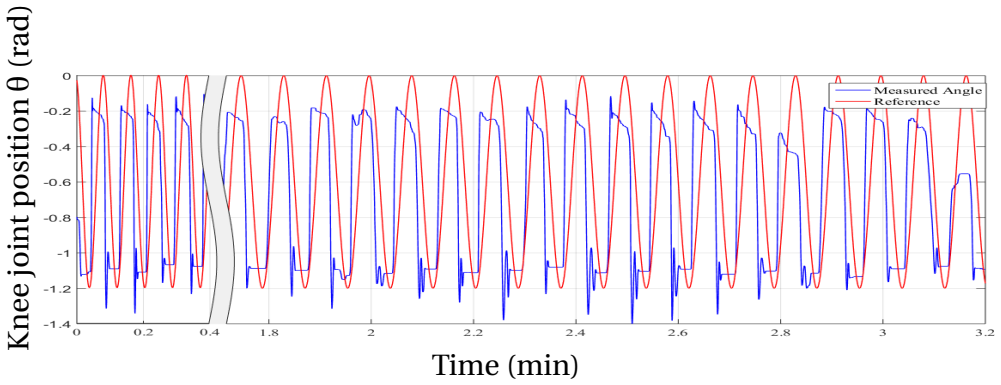

(b)

Figure 7.6: Knee joint position when using only quadriceps FES. (a) Subject 1, (b) Subject 2

To evaluate the muscular fatigue occurrence, subjects have undergone 5 experiment sessions of 6 minutes each, with and without the orthosis assistance, in correspondence with the standardized 6 minutes walking test used in the literature [133, 134]. A sinusoidal trajectory was used as the desired trajectory to generate the stimulation profile as shown in Eq. 7.5. The pulse width and frequency of the stimulation have been set to 150 µs and 40 Hz, respectively. This choice has been advised by the rehabilitation doctor to have the

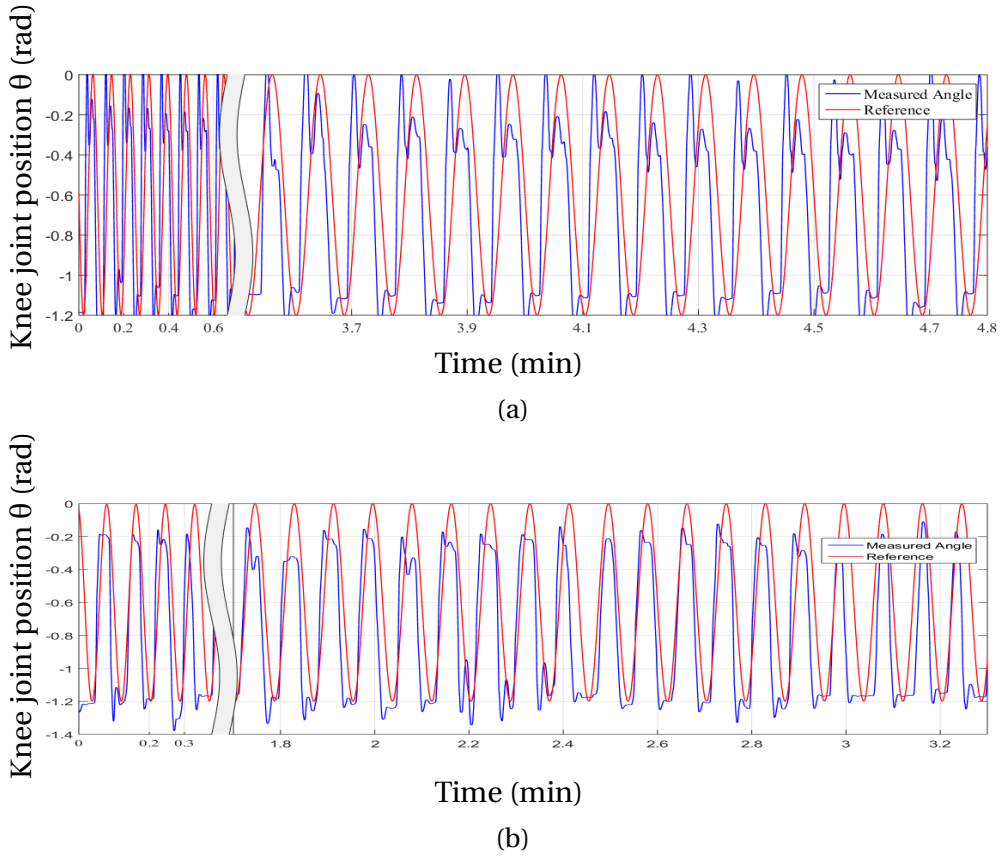

Figure 7.7: Knee joint position when using the FES of the quadriceps muscles and the active orthosis with impedance controller. (a) Subject 1, (b) Subject 2.

best muscular reaction to the stimulation signal.

Figures 7.6, and 7.7 show the knee joint position during the experiments when the orthosis actuator is enabled/disabled, respectively. The purpose is to evaluate the effect of using the proposed hybrid control strategy in delaying the muscular fatigue occurrence. Figure 7.6 show that when using only FES, the subjects were not able to maintain the same knee joint position extension because of the muscular fatigue. After 4.7 min from the beginning of the experiment, the knee joint extension has recorded a decrease of 31.24% for the first subject and 44.44% for the second one, with respect to the maximum extension recorded at the beginning of the experiment. However, when FES and orthosis are jointly used, the extension of the knee joint remains at the same level for the whole experiment period as shown in Figure 7.7.

Figure 7.8-7.9 show the estimated knee joint torque induced via quadriceps FES during the experiments when the orthosis actuator is enabled/disabled, and the orthosis actuator torque, respectively. Figures 7.8 and 7.10 show similar behaviours regarding the

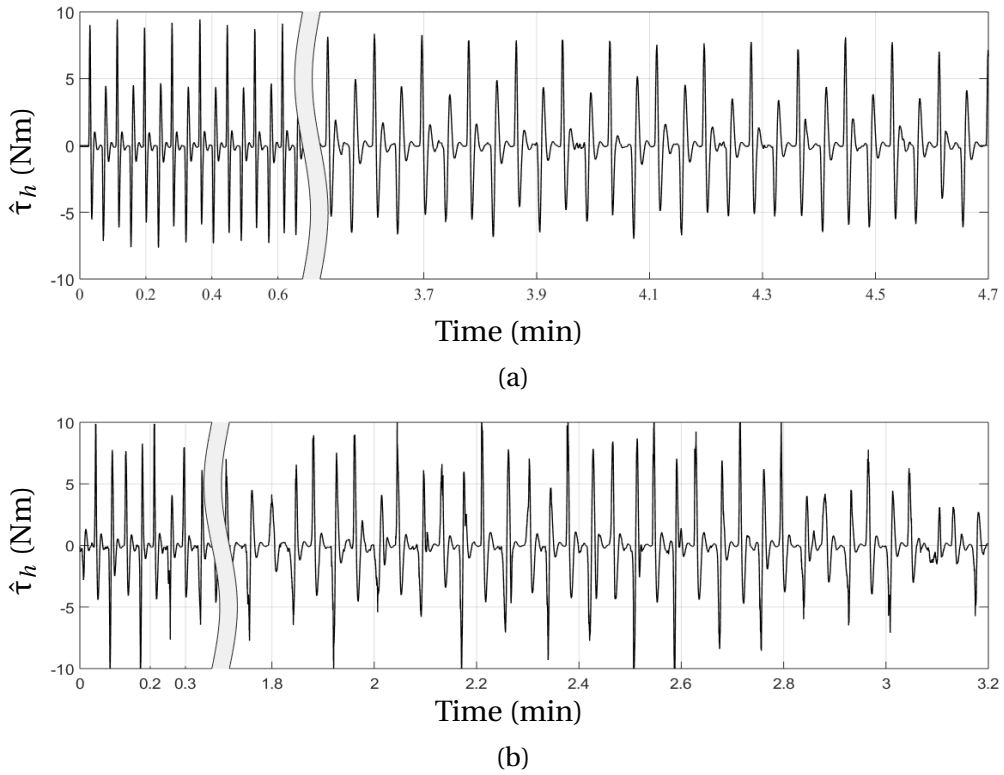

Figure 7.8: Estimated knee joint torque generated through quadriceps FES used alone. (a) Subject 1, (b) Subject 2

estimated knee joint torque since the same stimulation parameters were used in both experiments on the same leg. It is worthy noting a reduction of the maximum knee joint torque due to muscular fatigue. The decrease in the muscular torque is about 27.36% for the first subject and 40.94% for the second one. Notice also that the estimated torque has also a negative part which corresponds to the gravitational torque acting on the knee joint during the flexion phase.

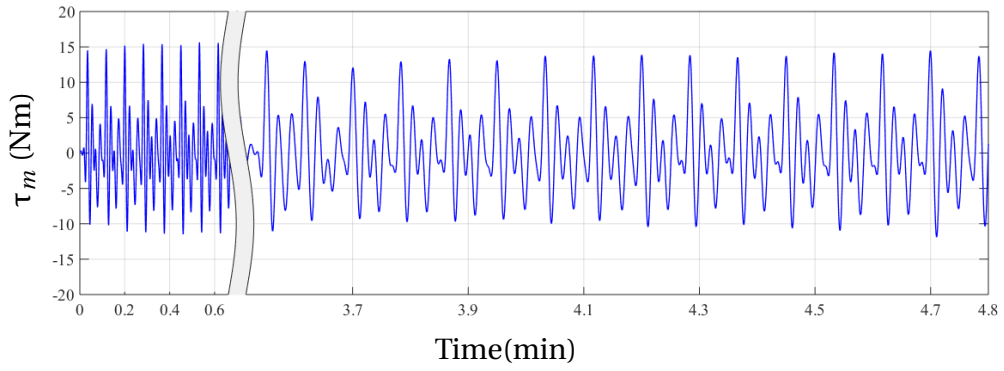

Figure 7.9: Orthosis actuator torque when using jointly FES and the impedance controller.

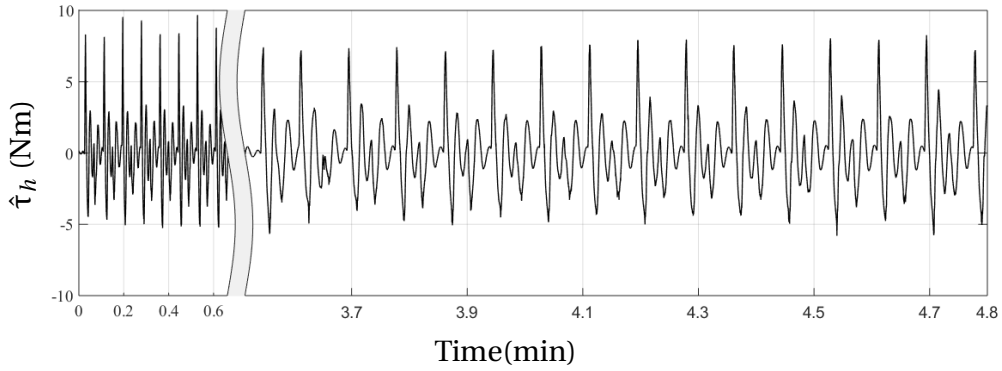

Figure 7.10: Estimated knee joint torque generated through muscular stimulation when using FES and the impedance controller.

7.3 Hybrid impedance control in the case of Sit-To-Stand movements

7.3.1 Description of the control strategy

In this sub-section, an active impedance control strategy taking into account the wearer's effort contributing to the task execution, is developed for the control of the EROWA exoskeleton (see section 3.6, chapter 3). In many cases, actuators of wearable robots are not able to generate the torques needed to achieve a desired task. This is particularly true for tasks requiring great efforts such as STS movements [135]. To deal with this issue, hybrid controllers combining the use of lower limb exoskeletons and FES are mainly exploited. The structure of the proposed hybrid controller consists of three parts: a mid-level controller, a low-level controller and a stimulation controller. The mid-level controller is an impedance controller; the low-level controller is a joint position controller in series with a high gain torque controller; the stimulation controller is monitored by a STS phase detection algorithm. The structure of the proposed hybrid controller is shown in Figure 7.11 and detailed in the following subsections.

7.3.1.1 Exoskeleton control

The mechanical impedance of the wearer/exoskeleton system is defined as the ratio of the joint position q_r to the interaction torque τ_I. The impedance of the wearer's limb Z_h is affected by the exoskeleton impedance Z_e. If the exoskeleton is passive, the

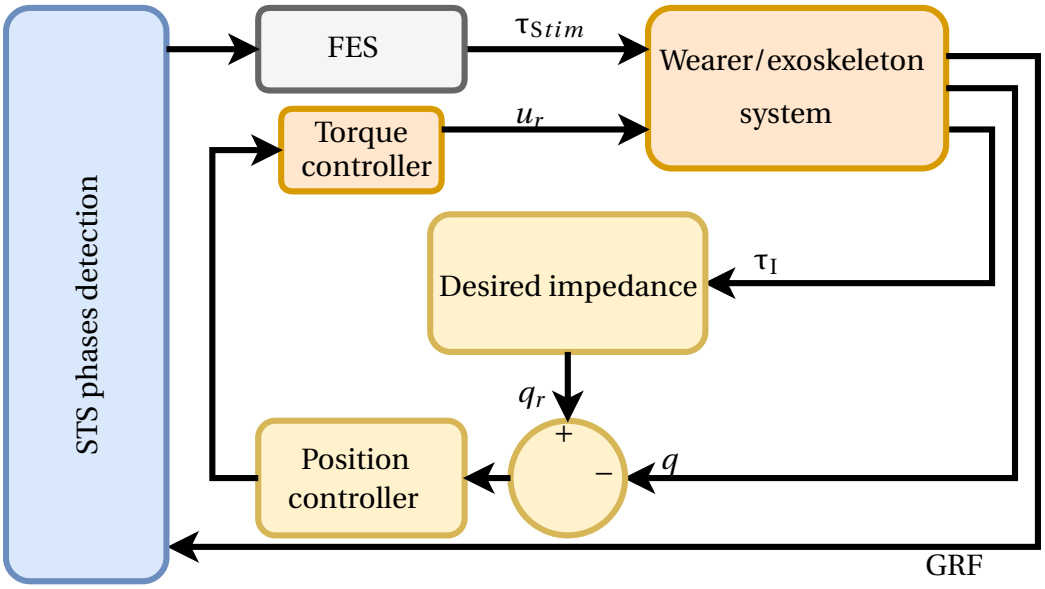

Figure 7.11: Structure of the hybrid impedance control.

impedance of the wearer/exoskeleton system is higher than the one of the wearer's limb ($Z_h + Z_e > Z_h$). To compensate such an impedance increase, the purpose is to reduce the wearer/exoskeleton system impedance to a desired level Z_d. To determine the assistance level that must be provided by the exoskeleton, a desired impedance model is designed based on the wearer's motor ability to perform STS movements. The wearer's efforts needed to perform such movements can be reduced by choosing a relatively small desired impedance Z_d. A linear impedance model for the hip and the knee joints is chosen as follows:

$$Z_d = \frac{q_r}{\tau_I} = \frac{1}{J_d s^2 + B_d s + K_d} \tag{7.6}$$

where J_d, B_d and K_d represent the desired inertia, damping and stiffness parameters, The interaction torque τ_I is obtained by measuring the torsion spring deflection angle of the SEA actuator. Note that the ankle joints are controlled directly by the wearer such that the reference position trajectory of the ankle joint is considered similar to the current ankle joint position (i.e. $q_{r1} = q_1$). The hip and knee reference trajectories q_r are generated using the desired impedance model (Eq. 7.6). To track accurately the joint reference position trajectory, a two-layer cascaded controller is proposed as shown in Figure 7.12. The outer PID position controller generates the desired assistive torque τ_d, which is fed to an inner loop that controls the SEA motor position using a PID controller.

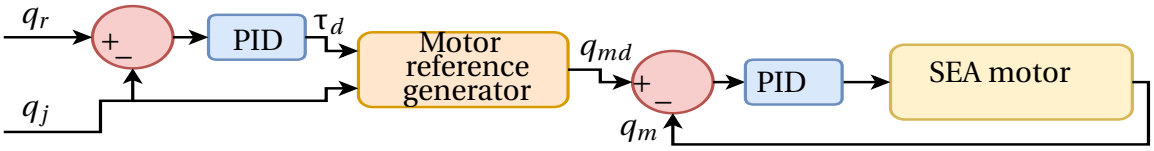

Figure 7.12: Control diagram of the SEA actuator. q_r is the desired joint position obtained from the desired impedance model; q_j is the measured joint position; q_{md} is the desired SEA motor position, q_m is the measured SEA motor position.

7.3.1.2 Stimulation control

Figure 7.13: Pre-extension and extension phases of STS movement.

According to [136] and based on an EMG analysis of the lower limb muscular groups (hip and knee joint flexor and extensor muscles, ankle joint plantar flexion and dorsiflexion muscles) with respect to torque requirements, STS movements without hand assistance are mainly achieved by the quadriceps femoris, the tibialis anterior and the paraspinal muscles. In [135], STS movement is divided into a pre-extension phase and an extension phase; the transfer occurs at the time the thighs are lifted off the chair as shown in Figure 7.13. In the pre-extension phase, the feet are moved backward, the upper body rotates forward and the knees move forward, which causes the ankle dorsiflexion. During the extension phase, the extensor muscles actuating the hips, the knees and the ankles move the body mass vertically. As stated in [136, 137], the peak muscular activity of the hips and the knees extensor muscles occur during the second phase of the STS movement. At that time, the maximum force is approximately four to five times the subject's weight. In the proposed approach, FES is triggered during the extension phase of the STS movement. For this purpose, the time required to reach the maximum value of the GRF

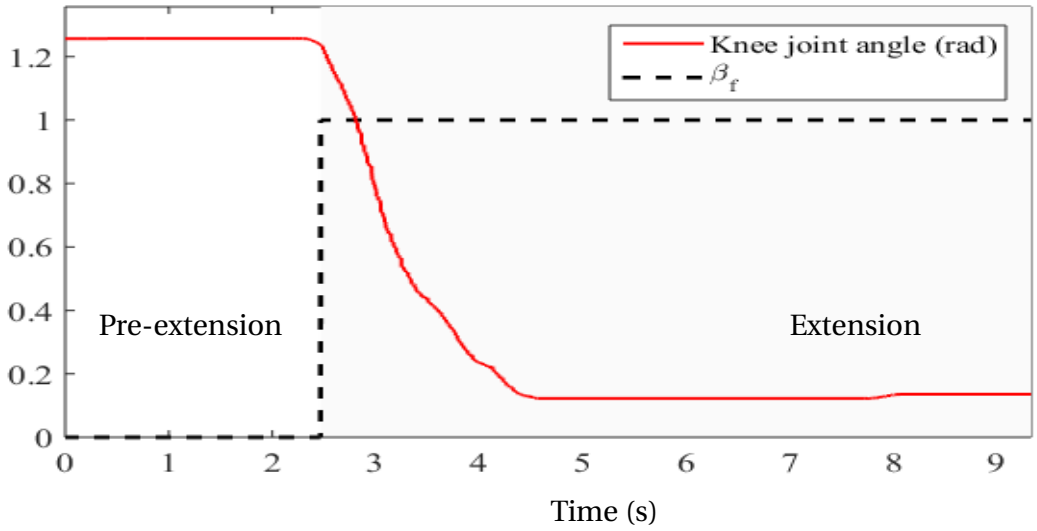

Figure 7.14: STS phases and corresponding knee joint position.

represents a good approximation of the ”Seat-Off” time [129]. Thus, FES is enabled when the "Seat-off" time is detected and applied to the quadriceps extensor muscle during the whole extension phase.

$$\beta_f = \begin{cases} 1 & \text{if } F_{GRF} > F_{GRF,sh} \\ 0 & \text{otherwise} \end{cases} \tag{7.7}$$

β_f represents the variable allowing to enable/disable FES; F_{GRF} is the measured GRF and $F_{GRF,sh}$ is a threshold value calibrated at the beginning of the experiment.

To assess the detection accuracy of the seat-off time, a STS movement is performed. The knee joint position and β_f are given in Figure 7.14. It is clearly shown that β_f switches from 0 to 1 as soon as the activation of knee extensor muscle starts.

Figure 7.15 shows the EMG recording of the vastus lateralis activity as well as the detection of the seat-off time. One can observe that the peak of the quadriceps muscles activity occurs at the beginning of the STS movement extension phase, justifying therefore the choice to stimulate the quadriceps during that phase.

Since FES is applied to the quadriceps muscles, measuring EMG activity of the vastus lateralis muscle is relatively constraining due to the muscle artifacts that can appear in the EMG signals. Many studies have reported the artifact contamination of the muscular EMG activity during FES [138], and the approaches commonly used to extract the voli-

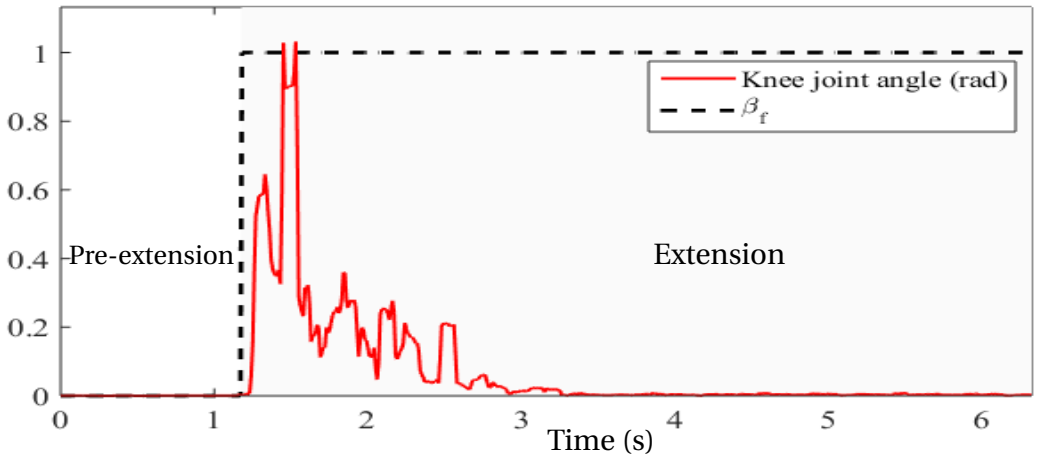

Figure 7.15: STS phase detection and EMG recording of the Vastus Lateralis muscle activity.

tional EMG from recorded EMG require relatively complex computations [139]. Thus, it is easier to exploit the muscles co-activity property to quantify the FES assistance as proposed in [140, 141]. For this purpose, EMG signals corresponding to hamstring muscle activity have been recorded to evaluate the proposed hybrid impedance control strategy.

7.3.2 Performance evaluation

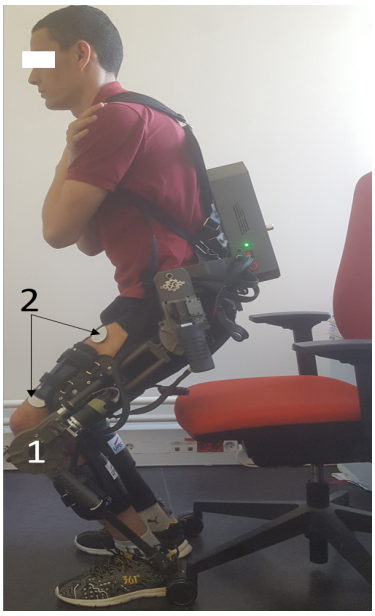

Figure 7.16: Subject performing STS movement with the assistance of the EROWA exoskeleton and quadriceps FES. (1) EROWA Exoskeleton. (2) Electrical stimulation electrodes.

The experiments were performed using the EROWA exoskeleton and the RehaStim 2 stimulator (HASOMED, Germany) as shown in Figure 7.16. The experiments were con-

ducted with a healthy subject (Sex: male; Age: 26; Weight: 63 kg; Heigh: 178 cm). The subject was informed of the experimental protocol, and gave his consent before the experiments. He did not present any muscle spasticity or co-contraction, and was able to perform complete flexion/extension of all the joints involved in STS movement.

The stimulation pulse width and frequency are set to 150 μs and 35Hz, respectively. To detect the STS phases, GRF is measured using FSR sensors (Delsys, Inc.). EMG sensors (Delsys, USA) are placed at the quadriceps muscles group to monitor the muscular activity during the extension phase. The EMG recordings of the Vastus Lateralis muscle activity are used to evaluate first the effectiveness of the impedance control strategy. The raw EMG signals are processed using time domain RMS method [132]. A first experiment was conducted to evaluate the assistance provided by the exoskeleton. The subject was asked to perform five STS movements with and without the exoskeleton assistance both without FES. Figure 7.17 shows the average EMG signal. One can observe that the maximum value of the EMG signal is reduced when the wearer is under the exoskeleton assistance. The average reduction percentage for the five STS movements is about 38%.

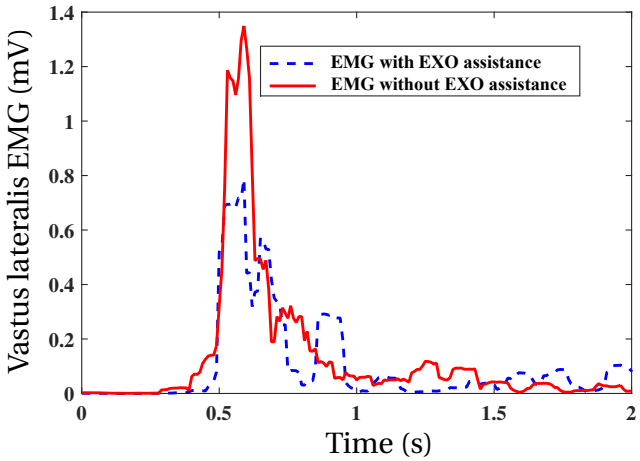

Figure 7.17: EMG of the Vastus Lateralis muscle activity during the extension phase with and without exoskeleton assistance.

Another experiment was conducted to evaluate the assistance provided through FES when performing STS movements while wearing the EROWA exoskeleton. Five STS movements were performed by the subject with and without FES assistance.

Figure 7.18 shows clearly that the average EMG signal of the hamstring muscle during the extension phase without FES assistance is lower than the one with FES assis-

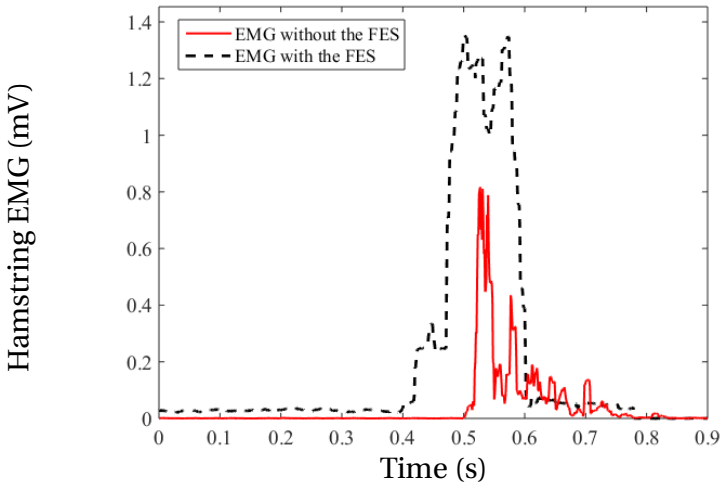

Figure 7.18: EMG of the hamstring muscle activity during the extension phase with and without FES assistance.

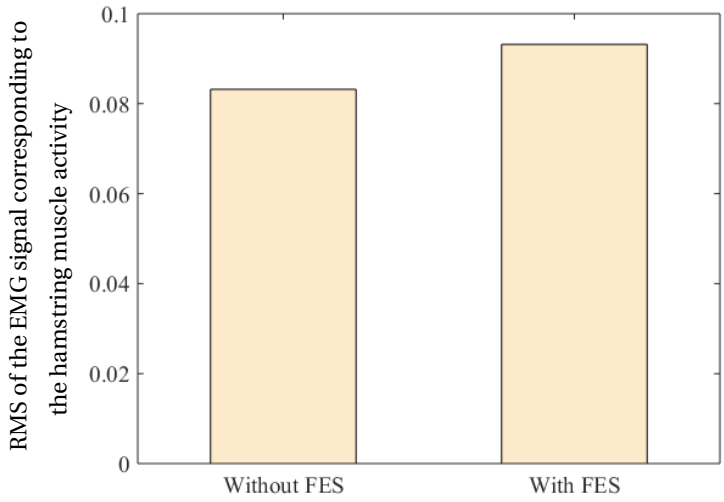

Figure 7.19: RMS of the EMG signal corresponding to the hamstring muscle activity during the extension phase with and without FES assistance.

tance. This is due to the additional contraction of the quadriceps muscles induced by FES. RMS of the EMG signal of the hamstring muscle in the cases with and without FES assistance is shown in Figure 7.19. One can observe that the RMS of the EMG signal increases when FES is enabled. The increase is about 11.96%, which means that the subject is more involved in the achievement of STS movement by developing more efforts via his/her quadriceps muscles. Regarding the assistance torque provided by the exoskeleton with and without FES assistance, note that the need for the exoskeleton assistance is reduced when FES is enabled (Figure 7.20). The RMS of the knee joint torque provided by the exoskeleton actuator is decreased with an average percentage of 26.07% (Figure 7.21).

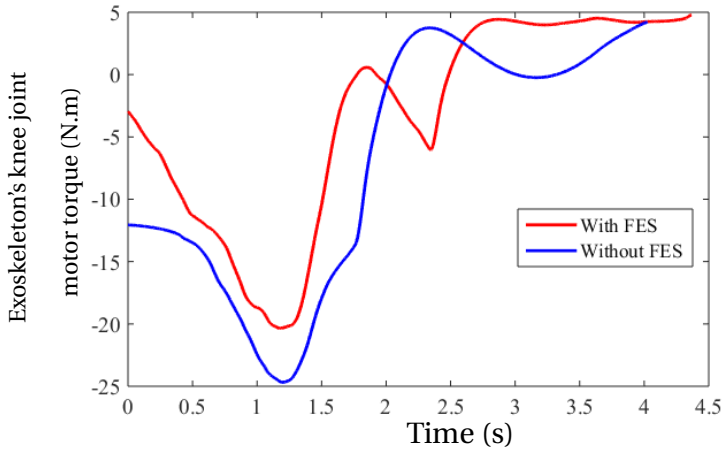

Figure 7.20: Knee joint torque provided by the exoskeleton actuator during the extension phase with and without FES assistance.

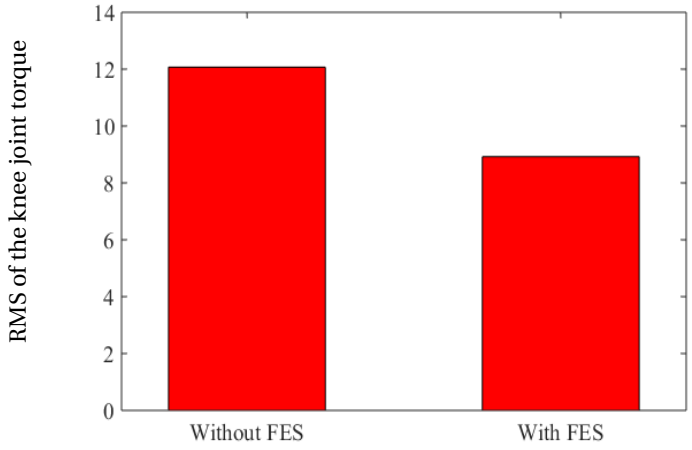

Figure 7.21: RMS of the knee joint torque provided by the exoskeleton actuator during the extension phase with and without FES assistance.

7.4 Conclusion

In this chapter, an AAN hybrid control strategy is presented and two case studies were considered. The first one concerns the use of a knee joint orthosis to ensure flexion/extension movements of the EICOSI. The second case study focuses on the use of the EROWA exoskeleton for STS movements assistance.

The experimental results show the ability of the Stimulation Torque Estimator (STE) in estimating the torque generated through muscular stimulation, and interestingly, the ability of the proposed control strategy to delay the muscular fatigue occurrence. Note that the non-linear disturbance observer is used to avoid the development of a complex musculo-skeletal model or the use of extra force/torque sensors. Experiments have also

showed the benefit of using a hybrid control strategy in comparison to both kinds of assistance used separately : FES and wearable robot. The hybrid approach reduces the required exoskeleton assistance to perform a movement while ensuring a better involvement of the subject.

Chapter 8

General conclusion and perspectives

I think and think for months and years. Ninety-nine times, the conclusion is false. The hundredth time I am right.

Albert Einstein

In this thesis, we proposed different human centered assistive control strategies to assist lower limb movements using orthoses/exoskeletons and Functional Electrical Stimulation (FES). The use of FES allows guaranteeing the subject's involvement in the assistive/rehabilitation process.

The first strategy is a proxy-NDO-based force control of the SEA actuator of the EROWA exoskeleton for three human-robot interaction modes: zero-impedance mode, force tracking mode and high torque mode. A two-mass dynamic model based NDO is exploited into the inner-layer of a conventional PSMC structure to enhance the controller robustness with respect to environmental and modeling uncertainties. In addition to accuracy tracking enhancement, this strategy ensures wearer's safety using a force compliance model depending on the interaction torque between the wearer and the exoskeleton at the knee joint. The proposed control strategy, evaluated through simulations and experiments, achieved a higher tracking accuracy in comparison to PID and PSMC controllers while ensuring wearer's safety facing unexpected situations in terms of interaction torque variation.

The second strategy consists of a hybrid controller of a knee joint hybrid orthosis for flexion/extension movements restoration. The generated stimulation torque, considered as an external disturbance, is estimated using a Non-linear Disturbance Observer (NDO). The torque provided by the wearer is complemented by an adaptive control torque provided by the orthosis. The input-to-state stability of the whole system with respect to the estimated stimulation torque was proved theoretically using a Lyapunov analysis. Simulation and experimental results showed the ability of the STE in estimating the muscle stimulation torque without requiring a relatively complex musculo-skeletal modeling or the use of additional force/torque sensors. They showed also the ability of the proposed hybrid controller to ensure an accurate tracking of the desired trajectory.

The third control strategy is an impedance compensation-based control complemented with a balance reinforcement-based control to assist a subject performing Sit-To-Stand (STS) movements. This strategy allows adaption of the wearer/exoskeleton system impedance to the desired one using a human joint torque observer and a time-varying desired impedance model. Moreover, a Sliding Mode Controller (SMC) is used to provide sufficient power support to ensure an efficient assistance. The balance reinforcement-

based control was developed to prevent from two typical failed STS movements, "seat-back" and "step-forward". The characteristics and robustness of the proposed strategy were theoretically analyzed in simulation. The performance of the proposed control strategy is evaluated in simulation and experiments. The obtained results showed the efficiency of the proposed control strategy to estimate the wearer's joint torques, reduce the wearer/exoskeleton system impedance and provide appropriate power support to the wearer for both human effort reduction and balance reinforcement.

The fourth strategy consists of an AAN hybrid control strategy. Two case studies were considered; the first one concerns the use of a knee joint orthosis to ensure flexion/extension movements of the EICOSI orthosis and the second case study focuses on the use of the EROWA exoskeleton for STS movements assistance. The experimental results showed the ability of the proposed control strategy to delay the muscular fatigue occurrence, and the benefit of using a hybrid control strategy in comparison to both kinds of assistance used separately : FES and wearable robot. The proposed control strategy allows reducing the required exoskeleton assistance to perform a movement while ensuring a better involvement of the subject.

Based on the promising results presented in this thesis, we believe that the proposed control strategies contribute an important step towards efficient control of lower limb exoskeletons for assisting dependent people in their daily living activities. The proposed strategies can be further extended in future research directions. A short-term perspective will consist of investigating other advanced control strategies in the inner-layer structure of the proxy-NDO-based controller. An interesting challenge to address, specific to impedance control strategies, will consist of developing approaches, on the one hand, to identify the proper wearer/exoskeleton system compliance for a given daily living activity, interaction with environment, level of uncertainty, etc., and on the other hand, to determine the optimal impedance parameters.

To better characterize the wearer's movement context, a promising perspective is the development of control strategies exploiting machine-learning-based locomotion modes (level walking, stairs ascent/descent, ramp ascent/descent, etc.) recognition algorithms. This kind of approaches will present the advantages of providing a relatively fast human intention or locomotion mode detection, and efficient control of wearable robots to pro-

vide the wearer the required assistance without latency effects.

A way to improve performance of hybrid FES/Exoskeleton control strategies is to develop enhanced methods to estimate the torque induced by FES and also realistic muscular fatigue estimation models; for these two objectives, machine-learning algorithms are potentially interesting. In practice, even though muscular activity can be easily measured using EMG signals, the use of FES makes these signals unusable due to the artifacts induced by the FES and interference of signals from neighbouring muscles. The development of an EMG signal processing algorithm that allows capturing the signal between stimulation pulse trains is an interesting alternative solution to qualitatively evaluate the FES induced torque estimation obtained from an NDO. Furthermore, using closed-loop FES control strategies, will allow improving the tracking accuracy as well as delaying muscular fatigue occurrence. However, using a closed-loop FES control induces an actuator redundancy issue for which dynamic control allocation approaches are interesting solutions to investigate. These approaches, based on advanced optimization algorithms, allow distributing the assistance torques among the actuators in a way to minimize and delay the occurrence of muscular fatigue; FES is seen as an actuator.

The control strategies proposed in this thesis were mainly evaluated through experiments involving healthy subjects and showed their effectiveness. However, experiments with paretic patients must be conducted to evaluate the potential of the proposed control strategies in a clinical setting. We believe that these control strategies would be very beneficial for rehabilitation purposes, as it can reduce the required human efforts while achieving the same movement by the subject.

Developing effective assessment metrics to evaluate lower limb exoskeletons is also of great importance. The metrics commonly used for evaluating such devices vary considerably from one study to another. Standards protocols for assessing the assistance and rehabilitation aspects of wearable robotic devices are more than important and urgently required for research community.

Appendix A

Robustness with respect to modeling uncertainties

Considering the modeling uncertainties, the wearer/exoskeleton system dynamic model can be represented as follows:

$$\mathrm{M}^*(q)\ddot{q} + \mathrm{C}^*(q,\dot{q})\dot{q} + \mathrm{G}^*(q) = \mathrm{U} = \mathrm{U}_e + \mathrm{U}_h + \mathrm{J}_\mathrm{F}^\mathrm{T}\mathrm{F}, \tag{8.1}$$

where the parameter matrices satisfy:

$$\mathrm{M}^*(q) = \mathrm{M}(q) + \Delta\mathrm{M}(q), \tag{8.2}$$

$$\mathrm{C}^*(q,\dot{q}) = \mathrm{C}(q,\dot{q}) + \Delta\mathrm{C}(q,\dot{q}), \tag{8.3}$$

$$\mathrm{G}^*(q) = \mathrm{G}(q) + \Delta\mathrm{G}(q). \tag{8.4}$$

For both the identified and real wearer/exoskeleton systems, it is reasonable to assume that the parameter matrices have the following properties:

Property 1: The inertia matrices are symmetric and positive definite, i.e.:

$$\begin{aligned} &\xi^\mathrm{T}\mathrm{M}^*(q)\xi = \xi^\mathrm{T}(\mathrm{M}^*(q))^\mathrm{T}\xi > 0 \\ &\xi^\mathrm{T}\mathrm{M}(q)\xi = \xi^\mathrm{T}(\mathrm{M}(q))^\mathrm{T}\xi > 0, \quad \forall q,\xi \in \mathrm{R}^n. \end{aligned} \tag{8.5}$$

Property 2: The matrices $\frac{1}{2}\dot{\mathrm{M}}^*(q) - \mathrm{C}^*(q,\dot{q})$ and $\frac{1}{2}\dot{\mathrm{M}}(q) - \mathrm{C}(q,\dot{q})$ are all skew-symmetric and therefore:

$$\begin{aligned} &\xi^\mathrm{T}(\frac{1}{2}\dot{\mathrm{M}}^*(q) - \mathrm{C}^*(q,\dot{q}))\xi = 0 \\ &\xi^\mathrm{T}(\frac{1}{2}\dot{\mathrm{M}}(q) - \mathrm{C}(q,\dot{q}))\xi = 0, \quad \forall q,\dot{q},\xi \in \mathrm{R}^n. \end{aligned} \tag{8.6}$$

Property 3: Assume that the gravitational potential functions of the real and identified wearer/exoskeleton systems are $\mathrm{P}_{\mathrm{E}}^{*}(q) > 0$ and $\mathrm{P}_{\mathrm{E}}(q) > 0$. The gravitational terms in the corresponding models satisfy then:

$$\mathrm{G}^{*}(q) = \frac{\partial \mathrm{P}_{\mathrm{E}}^{*}(q)}{\partial q}, \quad \mathrm{G}(q) = \frac{\partial \mathrm{P}_{\mathrm{E}}(q)}{\partial q}. \tag{8.7}$$

Property 4: The elastic potential function of the virtual stiffness torque is assumed as $\mathrm{P}_{\mathrm{V}}(q) > 0$. Consequently:

$$\mathrm{R}\tau_{v}(q) = \frac{\partial \mathrm{P}_{\mathrm{V}}(q)}{\partial q}. \tag{8.8}$$

Lemma: The modeling uncertainty terms $\Delta\mathrm{M}(q)$, $\Delta\mathrm{C}(q,\dot{q})$ and $\Delta\mathrm{G}(q)$ also have the similar properties, i.e.:

$$\xi^{\mathrm{T}}\Delta\mathrm{M}(q)\xi = \xi^{\mathrm{T}}(\Delta\mathrm{M}(q))^{\mathrm{T}}\xi > 0, \quad \forall q, \xi \in \mathrm{R}^{n} \tag{8.9}$$

$$\xi^{\mathrm{T}}(\frac{1}{2}\Delta\dot{\mathrm{M}}(q) - \Delta\mathrm{C}(q,\dot{q}))\xi = 0, \quad \forall q, \dot{q}\xi \in \mathrm{R}^{n} \tag{8.10}$$

$$\Delta\mathrm{G}(q) = \frac{\partial(\mathrm{P}_{\mathrm{E}}^{*}(q) - \mathrm{P}_{\mathrm{E}}(q))}{\partial q}. \tag{8.11}$$

Proof 1: This lemma can be easily deduced from (8.2) to (8.4).

Note that the wearer/exoskeleton system dynamic model (8.1) can be rewritten as follows:

$$\mathrm{M}(q)\ddot{q} + \mathrm{C}(q,\dot{q})\dot{q} + \mathrm{G}(q) = \mathrm{U} = \mathrm{U}_{e} + \mathrm{U}_{h} + \mathrm{J}_{\mathrm{F}}^{\mathrm{T}}\mathrm{F} + \mathrm{T}_{d}(q,\dot{q},\ddot{q}) \tag{8.12}$$

where T_{d}, the lumped disturbance including the modeling uncertainties of the wearer/exoskeleton model is defined as follows:

$$\mathrm{T}_{d}(q,\dot{q},\ddot{q}) = -\Delta\mathrm{M}(q)\ddot{q} - \Delta\mathrm{C}(q,\dot{q})\dot{q} - \Delta\mathrm{G}(q). \tag{8.13}$$

Actually, the lumped disturbance $\mathrm{T}_{d}(q,\dot{q},\ddot{q})$ cannot be excluded in the estimated human torque $\hat{\mathrm{U}}_{h}$, since nominal system parameters are used in the nonlinear disturbance observer formulation (6.2). Thus, we have the following approximation in the steady-state

of tracking control:

$$\hat{\mathrm{U}}_h = \mathrm{U}_h + \mathrm{T}_d(q, \dot{q}, \ddot{q}), \tag{8.14}$$

where U_h is the generalized torque obtained from the actual human muscle strength. Therefore, the real desired impedance model used in the control strategy can be expressed as follows :

$$\lambda_1(\mathrm{M}(q)\ddot{q}_r + \mathrm{C}(q, \dot{q})\dot{q}_r) + \lambda_2\mathrm{G}(q) = \mathrm{U}_h + \mathrm{R}\tau_v(q) + \mathrm{T}_d(q, \dot{q}, \ddot{q}). \tag{8.15}$$

The parameters λ_1 and λ_2 are set to define the assistance rates related to the hip and knee joints, respectively and satisfy:

$$\|\lambda_1\|_\infty < 1, \quad \|\lambda_2\|_\infty < 1. \tag{8.16}$$

From (8.15), it can be noted that even when no human input U_h is provided, the reference trajectory q_r might be unstable due to the lumped disturbance. To guarantee the safety of the wearer, the stability of the reference trajectory q should be guaranteed with respect to the model uncertainty. The following theorem gives the sufficient condition.

Proposition. For any $\forall\, q_r \in \mathrm{R}^n$*, if the following inequalities:*

$$\begin{aligned} &\lambda_1\mathrm{M}(q_r) + \Delta\mathrm{M}(q_r) > 0, \\ &(\lambda_2 - \mathrm{I})\mathrm{P}_\mathrm{E}(q_r) + \mathrm{P}_\mathrm{E}^*(q_r) + \mathrm{P}_\mathrm{V}(q_r) > 0 \end{aligned} \tag{8.17}$$

hold, then the equilibrium $q_r - q_{r0}$ *is stable with* $\lambda_2\mathrm{G}(q_{r0}) + \Delta\mathrm{G}(q_{r0}) + \mathrm{R}\tau_v(q_{r0}) = 0$.

Proof 2: Here, we only investigate the situation where there is no human input and the trajectory tracking control has converged. The desired impedance model (8.15) can therefore be represented as follows:

$$\lambda_1(\mathrm{M}(q_r)\ddot{q}_r + \mathrm{C}(q_r, \dot{q}_r)\dot{q}_r) + \lambda_2\mathrm{G}(q_r) = \mathrm{R}\tau_v + \mathrm{T}_d(q, \dot{q}, \ddot{q}). \tag{8.18}$$

By substituting (8.13) into (8.18), we obtain:

$$(\lambda_1\mathrm{M}(q_r) + \Delta\mathrm{M}(q_r))\ddot{q}_r + (\lambda_1\mathrm{C}(q_r, \dot{q}_r) + \Delta\mathrm{C}(q_r, \dot{q}_r))\dot{q}_r) + \lambda_2\mathrm{G}(q_r) + \Delta\mathrm{G}(q_r) = \mathrm{R}\tau_v. \tag{8.19}$$

$q_r - q_{r0}$ represents an equilibrium point of the system (8.19). Let us choose the Lyapunov candidate function as:

$$\mathrm{V} = \frac{1}{2}\dot{q}_r^{\mathrm{T}}(\lambda_1 \mathrm{M}(q_r) + \Delta\mathrm{M}(q_r))\dot{q}_r + (\lambda_2 - \mathrm{I})\mathrm{P_E}(q_r) + \mathrm{P_E^*}(q_r) + \mathrm{P_V}(q_r). \tag{8.20}$$

Thus, we get:

$$\begin{aligned}
\dot{\mathrm{V}} =& \dot{q}_r^{\mathrm{T}}(\lambda_1 \mathrm{M}(q_r) + \Delta\mathrm{M}(q_r))\ddot{q}_r + \frac{1}{2}\dot{q}_r^{\mathrm{T}}(\lambda_1 \dot{\mathrm{M}}(q_r) + \Delta\dot{\mathrm{M}}(q_r))\dot{q}_r \\
&+ \frac{d}{dt}[(\lambda_2 - \mathrm{I})\mathrm{P_E}(q_r) + \mathrm{P_E^*}(q_r) + \mathrm{P_V}(q_r)] \\
=& -\dot{q}_r^{\mathrm{T}}[(\lambda_1 \mathrm{C}(q_r, \dot{q}_r) + \Delta\mathrm{C}(q_r, \dot{q}_r))\dot{q}_r + \lambda_2 \mathrm{G}(q_r) + \Delta\mathrm{G}(q_r) - \mathrm{R}\tau_{\upsilon}] \\
&+ \frac{1}{2}\dot{q}_r^{\mathrm{T}}(\lambda_1 \dot{\mathrm{M}}(q_r) + \Delta\dot{\mathrm{M}}(q_r))\dot{q}_r + [(\lambda_2 - \mathrm{I})\frac{\partial \mathrm{P_E}(q_r)}{dt} + \frac{\partial \mathrm{P_E^*}(q_r)}{dt} + \frac{\partial \mathrm{P_V}(q_r)}{dt}] \\
=& \dot{q}_r^{\mathrm{T}}[\frac{1}{2}(\lambda_1 \dot{\mathrm{M}}(q_r) + \Delta\dot{\mathrm{M}}(q_r)) - (\lambda_1 \mathrm{C}(q_r, \dot{q}_r) + \Delta\mathrm{C}(q_r, \dot{q}_r))]\dot{q}_r \\
&- \dot{q}_r^{\mathrm{T}}[\lambda_2 \mathrm{G}(q_r) + \Delta\mathrm{G}(q_r)] + [(\lambda_2 - \mathrm{I})\dot{q}_r^{\mathrm{T}}\mathrm{G}(q_r) + \dot{q}_r^{\mathrm{T}}\mathrm{G}^*(q_r) + \dot{q}_r^{\mathrm{T}}\mathrm{R}\tau(q_r)] \\
\leq& \ 0.
\end{aligned}$$

Therefore, we can affirm that the equilibrium point is stable. This completes the proof.

Appendix B

Gait cycle description

The description of the gait cycle differs from one author to another but tends towards a single definition [142]. The normal gait cycle is typically defined as starting from the heel strike of one foot and ending at the next heel strike of the same foot. Usually, the gait cycle is divided into two main phases: stance and swing phases. The stance phase defines the period of time when the foot is in contact with the ground and the swing phase is the period of time when the leg is swinging to perform a step. According to the changes of the feet soles interactions with the ground, a gait cycle decomposition involving six gait phases is presented in [143]. As shown in Figure 8.1, the considered gait cycle phases are defined as follows [142]:

- Loading Response (LR): begins at Inicial Contact (IC) of the right heel with the ground (heel strike) and ends with the Toe Landing (TL). The duration interval of that phase is usually from 0% to 10% of the gait cycle.
- Mid-Stance (MS): begins at the end of LR when the foot leaves the ground, and ends when the body center of gravity is directly over the right foot. The duration interval of that phase is usually from 10% to 30% of the gait cycle.
- Terminal Stance (TS): begins at the end of MS and ends when the foot strikes the ground. The duration interval of that phase is usually from 30% to 50% of the gait cycle.
- Pre-Swing (PS): begins from the heel strike one foot and ends with the toe-off of the other foot. The duration interval of that phase is usually from 50% to 60% of the gait

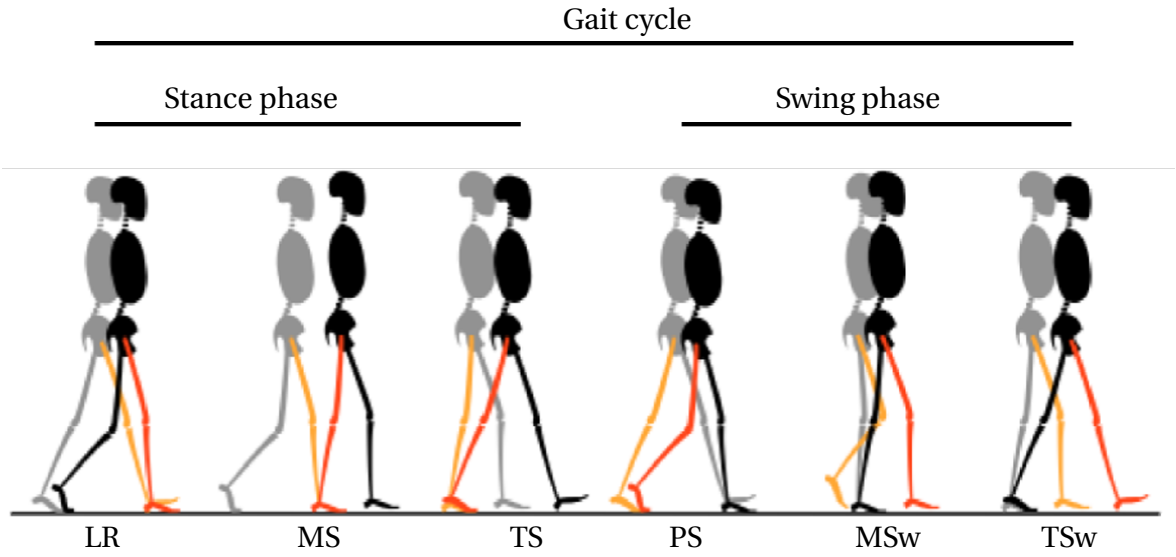

Figure 8.1: Gait phases representation; the black and orange legs represent the left and right legs.

cycle.

- Mid-Swing (MSw): strats with the toe-off of one foot and ends when the tibia of the same foot is in vertical position. The duration interval of that phase is usually from 60% to 87% of the gait cycle.

- Terminal Swing (TSw): begins at the end of MSw and ends when the other foot contacts the ground. The duration interval of that phase is usually from 87% to 100% of the gait cycle.

References

[1] M. R. Tucker, J. Olivier, A. Pagel, H. Bleuler, M. Bouri, O. Lambercy, J. del R Millán, R. Riener, H. Vallery, and R. Gassert, "Control strategies for active lower extremity prosthetics and orthotics: a review," *Journal of neuroengineering and rehabilitation*, vol. 12, no. 1, p. 1, 2015. 6, 8, 14, 15

[2] H. Herr, "Exoskeletons and orthoses: classification, design challenges and future directions," *Journal of neuroengineering and rehabilitation*, vol. 6, no. 1, p. 21, 2009. 6

[3] J. B. Makinson, D. P. Bodine, and B. R. Fick, "Machine augmentation of human strength and endurance hardiman i prototype project," General Electric CO Schenectady NY Specialty Materials Handling Products, Tech. Rep., 1969. 7

[4] H. Kazerooni, J.-L. Racine, L. Huang, and R. Steger, "On the control of the berkeley lower extremity exoskeleton (bleex)," in *Proceedings of the IEEE International Conference on Robotics and Automation ICRA.* IEEE, 2005, pp. 4353–4360. 7, 12

[5] E. Guizzo and H. Goldstein, "The rise of the body bots," *IEEE spectrum*, vol. 42, no. 10, pp. 50–56, 2005. 7, 12

[6] S. C. Jacobsen, M. Olivier, F. Smith, D. F. Knutti, R. T. Johnson, G. Colvin, and W. Scroggin, "Research robots for applications in artificial intelligence, teleoperation and entertainment," *The International Journal of Robotics Research*, vol. 23, no. 4-5, pp. 319–330, 2004. 7

[7] S. Jacobsen, "On the development of xos, a powerful exoskeletal robot," in *Proc. IEEE/RSJ Int. Conf. on Intelligent Robots and Systems, San Diego, CA, 2007*, 2007. 7

[8] M. Ishii, K. Yamamoto, and K. Hyodo, "Stand-alone wearable power assist suit–development and availability–," *Journal of robotics and mechatronics*, vol. 17, no. 5, pp. 575–583, 2005. 8

[9] J. L. Pons, *Wearable robots: biomechatronic exoskeletons*. John Wiley & Sons, 2008. 8

[10] H. Hodson, "Robotic suit gives shipyard workers super strength," *New Scientist*, vol. 2980, no. 4, 2014. 8

[11] M. Fontana, R. Vertechy, S. Marcheschi, F. Salsedo, and M. Bergamasco, "The body extender: A full-body exoskeleton for the transport and handling of heavy loads," *IEEE Robotics & Automation Magazine*, vol. 21, no. 4, pp. 34–44, 2014. 8

[12] S. Marcheschi, F. Salsedo, M. Fontana, and M. Bergamasco, "Body extender: whole body exoskeleton for human power augmentation," in *2011 IEEE international conference on robotics and automation*. IEEE, 2011, pp. 611–616. 8, 16

[13] S. Mohammed, Y. Amirat, and H. Rifai, "Lower-limb movement assistance through wearable robots: state of the art and challenges," *Advanced Robotics*, vol. 26, no. 1-2, pp. 1–22, 2012. 8

[14] J. Mehrholz, S. Thomas, C. Werner, J. Kugler, M. Pohl, and B. Elsner, "Electromechanical-assisted training for walking after stroke," *Cochrane Database of Systematic Reviews*, no. 5, 2017. 8

[15] A. Sale, N. Berardi, and L. Maffei, "Environment and brain plasticity: towards an endogenous pharmacotherapy," *Physiological reviews*, vol. 94, no. 1, pp. 189–234, 2014. 9

[16] A. Esquenazi, M. Talaty, A. Packel, and M. Saulino, "The rewalk powered exoskeleton to restore ambulatory function to individuals with thoracic-level motor-complete spinal cord injury," *American journal of physical medicine & rehabilitation*, vol. 91, no. 11, pp. 911–921, 2012. 9

[17] S. Maeshima, A. Osawa, D. Nishio, Y. Hirano, K. Takeda, H. Kigawa, and Y. Sankai, "Efficacy of a hybrid assistive limb in post-stroke hemiplegic patients: a preliminary report," *BMC neurology*, vol. 11, no. 1, p. 116, 2011. 9

[18] M. Aach, O. Cruciger, M. Sczesny-Kaiser, O. Höffken, R. C. Meindl, M. Tegenthoff, P. Schwenkreis, Y. Sankai, and T. A. Schildhauer, "Voluntary driven exoskeleton as a new tool for rehabilitation in chronic spinal cord injury: a pilot study," *The Spine Journal*, vol. 14, no. 12, pp. 2847–2853, 2014. 9

[19] H. Kawamoto and Y. Sankai, "Power assist method based on phase sequence and muscle force condition for hal," *Advanced Robotics*, vol. 19, no. 7, pp. 717–734, 2005. 9, 11

[20] S. A. Kolakowsky-Hayner, J. Crew, S. Moran, and A. Shah, "Safety and feasibility of using the eksotm bionic exoskeleton to aid ambulation after spinal cord injury," *J Spine*, vol. 4, no. 3, 2013. 10

[21] (2020) Eksonr. [Online]. Available: https://eksobionics.com/eksohealth/eksonr/clinicians/ 10

[22] K. Kong, H. Moon, B. Hwang, D. Jeon, and M. Tomizuka, "Impedance compensation of subar for back-drivable force-mode actuation," *IEEE Transactions on Robotics*, vol. 25, no. 3, pp. 512–521, 2009. 10, 16

[23] K. Kong and D. Jeon, "Design and control of an exoskeleton for the elderly and patients," *IEEE/ASME Transactions on mechatronics*, vol. 11, no. 4, pp. 428–432, 2006. 10

[24] N.-S. Kwak, K.-R. Müller, and S.-W. Lee, "Toward exoskeleton control based on steady state visual evoked potentials," in *2014 International Winter Workshop on Brain-Computer Interface (BCI)*. IEEE, 2014, pp. 1–2. 10

[25] A. Kilicarslan, S. Prasad, R. G. Grossman, and J. L. Contreras-Vidal, "High accuracy decoding of user intentions using eeg to control a lower-body exoskeleton," in *2013 35th Annual International Conference of the IEEE Engineering in Medicine and Biology Society (EMBC)*. IEEE, 2013, pp. 5606–5609. 10

[26] S. Wang, L. Wang, C. Meijneke, E. Van Asseldonk, T. Hoellinger, G. Cheron, Y. Ivanenko, V. La Scaleia, F. Sylos-Labini, M. Molinari *et al.*, "Design and control of the mindwalker exoskeleton," *IEEE transactions on neural systems and rehabilitation engineering*, vol. 23, no. 2, pp. 277–286, 2015. 10, 12

[27] M. Bortole, A. Venkatakrishnan, F. Zhu, J. C. Moreno, G. E. Francisco, J. L. Pons, and J. L. Contreras-Vidal, "The h2 robotic exoskeleton for gait rehabilitation after stroke: early findings from a clinical study," *Journal of neuroengineering and rehabilitation*, vol. 12, no. 1, p. 54, 2015. 10, 16

[28] M. Vukobratovic, D. Hristic, and Z. Stojiljkovic, "Development of active anthropomorphic exoskeletons," *Medical and Biological Engineering*, vol. 12, no. 1, pp. 66–80, 1974. 11

[29] Y. Hasegawa, J. Jang, and Y. Sankai, "Cooperative walk control of paraplegia patient and assistive system," in *Intelligent robots and systems, 2009. IROS 2009. IEEE/RSJ international conference on*. IEEE, 2009, pp. 4481–4486. 11

[30] H. Kawamoto and Y. Sankai, "Power assist system hal-3 for gait disorder person," *Computers helping people with special needs*, pp. 19–29, 2002. 11

[31] T. Sakurai and Y. Sankai, "Development of motion instruction system with interactive robot suit hal," in *Robotics and Biomimetics (ROBIO), 2009 IEEE International Conference on*. IEEE, 2009, pp. 1141–1147. 11

[32] K. Suzuki, G. Mito, H. Kawamoto, Y. Hasegawa, and Y. Sankai, "Intention-based walking support for paraplegia patients with robot suit hal," *Advanced Robotics*, vol. 21, no. 12, pp. 1441–1469, 2007. 11

[33] (2016) Rewalk. [Online]. Available: http://rewalk.com/ 11

[34] G. A. Pratt and M. M. Williamson, "Series elastic actuators," in *Intelligent Robots and Systems 95.'Human Robot Interaction and Cooperative Robots', Proceedings. 1995 IEEE/RSJ International Conference on*, vol. 1. IEEE, 1995, pp. 399–406. 11

[35] J. Pratt, B. Krupp, and C. Morse, "Series elastic actuators for high fidelity force control," *Industrial Robot: An International Journal*, vol. 29, no. 3, pp. 234–241, 2002. 11

[36] J. A. Blaya and H. Herr, "Adaptive control of a variable-impedance ankle-foot orthosis to assist drop-foot gait," *IEEE Transactions on neural systems and rehabilitation engineering*, vol. 12, no. 1, pp. 24–31, 2004. 11

[37] K. Kong, J. Bae, and M. Tomizuka, "A compact rotary series elastic actuator for human assistive systems," *IEEE/ASME transactions on mechatronics*, vol. 17, no. 2, pp. 288–297, 2012. 12, 15, 33, 35

[38] H. Kazerooni and R. Steger, "The berkeley lower extremity exoskeleton," *Journal of dynamic systems, measurement, and control*, vol. 128, no. 1, pp. 14–25, 2006. 12

[39] E. Guizzo, "Sarcos exoskeleton bringing iron man suit closer to reality," *US Army Research Laboratory, ARO in Review, Spectrum IEEE*, 2010. 12

[40] K. Yamamoto, K. Hyodo, M. Ishii, and T. Matsuo, "Development of power assisting suit for assisting nurse labor," *JSME International Journal Series C Mechanical Systems, Machine Elements and Manufacturing*, vol. 45, no. 3, pp. 703–711, 2002. 12

[41] K. Yamamoto, M. Ishii, K. Hyodo, T. Yoshimitsu, and T. Matsuo, "Developement of power assisting suit: Miniaturization of supply system to realize wearable suit," in *The Proceedings of the International Conference on Motion and Vibration Control 6.2*. The Japan Society of Mechanical Engineers, 2002, pp. 848–854. 12

[42] C.-P. Chou and B. Hannaford, "Static and dynamic characteristics of mckibben pneumatic artificial muscles," in *Robotics and Automation, 1994. Proceedings., 1994 IEEE International Conference on*. IEEE, 1994, pp. 281–286. 12

[43] F. Daerden and D. Lefeber, "Pneumatic artificial muscles: actuators for robotics and automation," *European journal of mechanical and environmental engineering*, vol. 47, no. 1, pp. 11–21, 2002. 12

[44] N. Costa and D. G. Caldwell, "Control of a biomimetic" soft-actuated" 10dof lower body exoskeleton," in *Biomedical Robotics and Biomechatronics, 2006. BioRob 2006. The First IEEE/RAS-EMBS International Conference on*. IEEE, 2006, pp. 495–501. 12

[45] D. P. Ferris, K. E. Gordon, G. S. Sawicki, and A. Peethambaran, "An improved powered ankle–foot orthosis using proportional myoelectric control," *Gait & posture*, vol. 23, no. 4, pp. 425–428, 2006. 12, 17

[46] G. S. Sawicki, K. E. Gordon, and D. P. Ferris, "Powered lower limb orthoses: applications in motor adaptation and rehabilitation," in *Rehabilitation Robotics, 2005. ICORR 2005. 9th International Conference on*. IEEE, 2005, pp. 206–211. 12, 17

[47] B. Quinlivan, S. Lee, P. Malcolm, D. Rossi, M. Grimmer, C. Siviy, N. Karavas, D. Wagner, A. Asbeck, I. Galiana *et al.*, "Assistance magnitude versus metabolic cost reductions for a tethered multiarticular soft exosuit," *Sci. Robot*, vol. 2, no. 2, pp. 1–10, 2017. 13

[48] F. A. Panizzolo, I. Galiana, A. T. Asbeck, C. Siviy, K. Schmidt, K. G. Holt, and C. J. Walsh, "A biologically-inspired multi-joint soft exosuit that can reduce the energy cost of loaded walking," *Journal of neuroengineering and rehabilitation*, vol. 13, no. 1, p. 43, 2016. 13

[49] J. Bae, S. M. M. De Rossi, K. O'Donnell, K. L. Hendron, L. N. Awad, T. R. T. Dos Santos, V. L. De Araujo, Y. Ding, K. G. Holt, T. D. Ellis *et al.*, "A soft exosuit for patients with stroke: Feasibility study with a mobile off-board actuation unit," in *2015 IEEE International Conference on Rehabilitation Robotics (ICORR)*. IEEE, 2015, pp. 131–138. 13

[50] A. T. Asbeck, R. J. Dyer, A. F. Larusson, and C. J. Walsh, "Biologically-inspired soft exosuit," in *2013 IEEE 13th International Conference on Rehabilitation Robotics (ICORR)*. IEEE, 2013, pp. 1–8. 13

[51] D. Zhang, V. N. Dubey, W. Yu, and K. H. Low, "biomechatronics: harmonizing mechatronic systems with human beings," *Frontiers in neuroscience*, vol. 12, p. 768, 2018. 13

[52] B. Chen, H. Ma, L.-Y. Qin, F. Gao, K.-M. Chan, S.-W. Law, L. Qin, and W.-H. Liao, "Recent developments and challenges of lower extremity exoskeletons," *Journal of Orthopaedic Translation*, vol. 5, pp. 26–37, 2016. 14

[53] S. K. Banala and S. K. Agrawal, "Gait rehabilitation with an active leg orthosis," in *ASME 2005 International Design Engineering Technical Conferences and Computers and Information in Engineering Conference*. American Society of Mechanical Engineers, 2005, pp. 459–465. 14

[54] B. Weinberg, J. Nikitczuk, S. Patel, B. Patritti, C. Mavroidis, P. Bonato, and P. Canavan, "Design, control and human testing of an active knee rehabilitation orthotic device," in *Robotics and Automation, 2007 IEEE International Conference on*. IEEE, 2007, pp. 4126–4133. 14

[55] V. Arnez-Paniagua, H. Rifaï, Y. Amirat, M. Ghedira, J. Gracies, and S. Mohammed, "Adaptive control of an actuated ankle foot orthosis for paretic patients," *Control Engineering Practice*, vol. 90, pp. 207–220, 2019. 14

[56] V. Arnez-Paniagua, H. Rifaï, Y. Amirat, S. Mohammed, M. Ghedira, and J.-M. Gracies, "Modified adaptive control of an actuated ankle foot orthosis to assist paretic patients," in *2018 IEEE/RSJ International Conference on Intelligent Robots and Systems (IROS)*. IEEE, 2018, pp. 2311–2317. 14

[57] W.-H. Chen, "Disturbance observer based control for nonlinear systems," vol. 9, no. 4, pp. 706–710, 2004. 15, 50, 51, 70, 89

[58] W. Huo, S. Mohammed, Y. Amirat, and K. Kong, "Active impedance control of a lower limb exoskeleton to assist sit-to-stand movement," in *Proc. IEEE Int. Conf. Robot. Autom.*, 2016, pp. 3530–3536. 15, 17

[59] L. Wang, Z. Du, W. Dong, Y. Shen, and G. Zhao, "Probabilistic sensitivity amplification control for lower extremity exoskeleton," *Applied Sciences*, vol. 8, no. 4, p. 525, 2018. 15

[60] M. S. Al-Quraishi, I. Elamvazuthi, S. A. Daud, S. Parasuraman, and A. Borboni, "Eeg-based control for upper and lower limb exoskeletons and prostheses: A systematic review," *Sensors*, vol. 18, no. 10, p. 3342, 2018. 15

[61] H. Kawamoto, S. Lee, S. Kanbe, and Y. Sankai, "Power assist method for hal-3 using EMG-based feedback controller," in *IEEE International Conference on Systems, Man and Cybernetics*, vol. 2. IEEE, 2003, pp. 1648–1653. 15, 17

[62] E. López-Larraz, F. Trincado-Alonso, V. Rajasekaran, S. Pérez-Nombela, A. J. Del-Ama, J. Aranda, J. Minguez, A. Gil-Agudo, and L. Montesano, "Control of an ambulatory exoskeleton with a brain–machine interface for spinal cord injury gait rehabilitation," *Frontiers in neuroscience*, vol. 10, p. 359, 2016. 15

[63] G. R. Papini and C. A. Avizzano, "Transparent force control for body extender," in *2012 IEEE RO-MAN: The 21st IEEE International Symposium on Robot and Human Interactive Communication*. IEEE, 2012, pp. 138–143. 16

[64] R. Riener, L. Lunenburger, S. Jezernik, M. Anderschitz, G. Colombo, and V. Dietz, "Patient-cooperative strategies for robot-aided treadmill training: first experimental results," *IEEE transactions on neural systems and rehabilitation engineering*, vol. 13, no. 3, pp. 380–394, 2005. 16

[65] S. Hussain, S. Q. Xie, and P. K. Jamwal, "Adaptive impedance control of a robotic orthosis for gait rehabilitation," *IEEE Transactions on Cybernetics*, vol. 43, no. 3, pp. 1025–1034, 2013. 16

[66] W. Huo, S. Mohammed, J. C. Moreno, and Y. Amirat, "Lower limb wearable robots for assistance and rehabilitation: A state of the art," *IEEE systems Journal*, vol. 10, no. 3, pp. 1068–1081, 2014. 16

[67] T. Yan, M. Cempini, C. M. Oddo, and N. Vitiello, "Review of assistive strategies in powered lower-limb orthoses and exoskeletons," *Robotics and Autonomous Systems*, vol. 64, pp. 120–136, 2015. 16

[68] W. M. Vagias, "Likert-type scale response anchors," *Clemson International Institute*

for Tourism & Research Development, Department of Parks, Recreation and Tourism Management. Clemson University, 2006. 17

[69] E. Martini, S. Crea, A. Parri, L. Bastiani, U. Faraguna, Z. McKinney, R. Molino-Lova, L. Pratali, and N. Vitiello, "Gait training using a robotic hip exoskeleton improves metabolic gait efficiency in the elderly," *Scientific reports*, vol. 9, no. 1, pp. 1–12, 2019. 17

[70] Y. Ohta, H. Yano, R. Suzuki, M. Yoshida, N. Kawashima, and K. Nakazawa, "A two-degree-of-freedom motor-powered gait orthosis for spinal cord injury patients," *Proceedings of the Institution of Mechanical Engineers, Part H: Journal of Engineering in Medicine*, vol. 221, no. 6, pp. 629–639, 2007. 17

[71] C.-H. Wu, H.-F. Mao, J.-S. Hu, T.-Y. Wang, Y.-J. Tsai, and W.-L. Hsu, "The effects of gait training using powered lower limb exoskeleton robot on individuals with complete spinal cord injury," *Journal of neuroengineering and rehabilitation*, vol. 15, no. 1, p. 14, 2018. 17

[72] S. J. Kang, J. C. Ryu, I. H. Moon, K. H. Kim, and M. S. Mun, "Walker gait analysis of powered gait orthosis for paraplegic," in *World Congress on Medical Physics and Biomedical Engineering 2006*. Springer, 2007, pp. 2889–2891. 17

[73] B. Husemann, F. Müller, C. Krewer, S. Heller, and E. Koenig, "Effects of locomotion training with assistance of a robot-driven gait orthosis in hemiparetic patients after stroke," *Stroke*, vol. 38, no. 2, pp. 349–354, 2007. 17

[74] H. Akahira, Y. Yamaguchi, K. Nakazawa, Y. Ohta, and N. Kawashima, "Effect of dynamic knee motion on paralyzed lower limb muscle activity during orthotic gait: a test for the effectiveness of the motor-assisted knee motion device," *J Nov Physiother*, vol. 1, pp. 2–6, 2012. 17

[75] X. Zhang and M. Hashimoto, "Synchronization based control for walking assist suit-evaluation on synchronization and assist effect," in *Key Engineering Materials*, vol. 464. Trans Tech Publ, 2011, pp. 115–118. 18

[76] O. A. Howlett, N. A. Lannin, L. Ada, and C. McKinstry, "Functional electrical stimulation improves activity after stroke: a systematic review with meta-analysis," *Archives of physical medicine and rehabilitation*, vol. 96, no. 5, pp. 934–943, 2015. 18

[77] M. Ahmed, M. Huq, and B. Ibrahim, "Investigating the effect of mass variation for sliding mode control of functional electrical stimulation aided sit-to-stand in paraplegia," in *2019 IEEE 15th International Colloquium on Signal Processing & Its Applications (CSPA)*. IEEE, 2019, pp. 223–228. 18

[78] W. Huo, V. Arnez-Paniagua, M. Ghedira, Y. Amirat, J.-M. Gracies, and S. Mohammed, "Adaptive fes assistance using a novel gait phase detection approach," in *2018 IEEE/RSJ International Conference on Intelligent Robots and Systems (IROS)*. IEEE, 2018, pp. 1–9. 18

[79] A. J. Del-Ama, A. D. Koutsou, J. C. Moreno, A. De-Los-Reyes, Á. Gil-Agudo, and J. L. Pons, "Review of hybrid exoskeletons to restore gait following spinal cord injury." *Journal of Rehabilitation Research & Development*, vol. 49, no. 4, 2012. 19, 23

[80] J. C. Moreno, S. Mohammed, N. Sharma, and A. J. del Ama, "Hybrid wearable robotic exoskeletons for human walking," in *Wearable Robotics*. Elsevier, 2020, pp. 347–364. 19

[81] K. H. Ha, S. A. Murray, and M. Goldfarb, "An approach for the cooperative control of FES with a powered exoskeleton during level walking for persons with paraplegia," *IEEE Transactions on Neural Systems and Rehabilitation Engineering*, vol. 24, no. 4, pp. 455–466, 2016. 19

[82] N. A. Kirsch, X. Bao, N. A. Alibeji, B. E. Dicianno, and N. Sharma, "Model-based dynamic control allocation in a hybrid neuroprosthesis," *IEEE Transactions on Neural Systems and Rehabilitation Engineering*, 2017. 19

[83] D. Popovic, R. B. Stein, M. N. Oguztoreli, M. Lebiedowska, and S. Jonic, "Optimal control of walking with functional electrical stimulation: a computer simulation

study," *IEEE Transactions on Rehabilitation Engineering*, vol. 7, no. 1, pp. 69–79, 1999. 19, 23

[84] N. Alibeji, N. Kirsch, and N. Sharma, "An adaptive low-dimensional control to compensate for actuator redundancy and FES-induced muscle fatigue in a hybrid neuroprosthesis," *Control Engineering Practice*, vol. 59, pp. 204–219, 2017. 19

[85] R. Riener, J. Quintern, and G. Schmidt, "Biomechanical model of the human knee evaluated by neuromuscular stimulation," *Journal of Biomechanics*, vol. 29, no. 9, pp. 1157–1167, 1996. 19

[86] O. Brend, C. Freeman, and M. French, "Multiple-model adaptive control of functional electrical stimulation," *IEEE Transactions on Control Systems Technology*, vol. 23, no. 5, pp. 1901–1913, 2015. 19

[87] Y. Stauffer, Y. Allemand, M. Bouri, J. Fournier, R. Clavel, P. Métrailler, R. Brodard, and F. Reynard, "The walktrainer—a new generation of walking reeducation device combining orthoses and muscle stimulation," *IEEE Transactions on neural systems and rehabilitation engineering*, vol. 17, no. 1, pp. 38–45, 2009. 19, 21

[88] A. J. del Ama, Á. Gil-Agudo, J. L. Pons, and J. C. Moreno, "Hybrid FES-robot cooperative control of ambulatory gait rehabilitation exoskeleton," *Journal of neuroengineering and rehabilitation*, vol. 11, no. 1, p. 27, 2014. 19, 21

[89] Y. Ren and D. Zhang, "Fexo knee: A rehabilitation device for knee joint combining functional electrical stimulation with a compliant exoskeleton," in *IEEE RAS & EMBS International Conference on Biomedical Robotics and Biomechatronics*, 2014, pp. 683–688. 19

[90] W. Huo, S. Mohammed, and Y. Amirat, "Observer-based active impedance control of a knee-joint assistive orthosis," in *IEEE International Conference on Rehabilitation Robotics (ICORR)*, 2015, pp. 313–318. 19, 116

[91] R. Kobetic, C. S. To, J. R. Schnellenberger, T. C. Bulea, R. G. CO, and G. Pinault, "Development of hybrid orthosis for standing, walking, and stair climbing after spinal

cord injury," *Journal of rehabilitation research and development*, vol. 46, no. 3, p. 447, 2009. 20

[92] D. Popovic, R. Tomovic, and L. Schwirtlich, "Hybrid assistive system-the motor neuroprosthesis," *IEEE Transactions on Biomedical Engineering*, vol. 36, no. 7, pp. 729–737, 1989. 20

[93] W. K. Durfee and J. M. Hausdorff, "Regulating knee joint position by combining electrical stimulation with a controllable friction brake," *Annals of biomedical engineering*, vol. 18, no. 6, pp. 575–596, 1990. 20

[94] G. Obinata, S. Fukada, T. Matsunaga, T. Iwami, Y. Shimada, K. Miyawaki, K. Hase, and A. Nakayama, "Hybrid control of powered orthosis and functional neuromuscular stimulation for restoring gait," in *Engineering in Medicine and Biology Society, 2007. EMBS 2007. 29th Annual International Conference of the IEEE.* IEEE, 2007, pp. 4879–4882. 20

[95] K. H. Ha, H. A. Quintero, R. J. Farris, and M. Goldfarb, "Enhancing stance phase propulsion during level walking by combining FES with a powered exoskeleton for persons with paraplegia," in *International conference of the IEEE Engineering in medicine and biology society (EMBC)*, 2012, pp. 344–347. 20

[96] T. C. Bulea, R. Kobetic, M. L. Audu, and R. J. Triolo, "Stance controlled knee flexion improves stimulation driven walking after spinal cord injury," *Journal of neuroengineering and rehabilitation*, vol. 10, no. 1, p. 68, 2013. 20

[97] T. C. Bulea, R. Kobetic, M. L. Audu, J. R. Schnellenberger, G. Pinault, and R. J. Triolo, "Forward stair descent with hybrid neuroprosthesis after paralysis: Single case study demonstrating feasibility," *Journal of rehabilitation research and development*, vol. 51, no. 7, p. 1077, 2014. 20

[98] S. Gharooni, B. Heller, and M. Tokhi, "A new hybrid spring brake orthosis for controlling hip and knee flexion in the swing phase," *IEEE Transactions on Neural systems and rehabilitation engineering*, vol. 9, no. 1, pp. 106–107, 2001. 21

[99] M. Goldfarb and W. K. Durfee, "Design of a controlled-brake orthosis for fes-aided gait," *IEEE Transactions on Rehabilitation Engineering*, vol. 4, no. 1, pp. 13–24, 1996. 21

[100] A. J. del Ama, J. C. Moreno, A. Gil-Agudo, A. de-los Reyes, and J. L. Pons, "Online assessment of human-robot interaction for hybrid control of walking," *Sensors*, vol. 12, no. 1, pp. 215–225, 2011. 21

[101] H. Vallery, T. Stützle, M. Buss, and D. Abel, "Control of a hybrid motor prosthesis for the knee joint," *IFAC Proceedings Volumes*, vol. 38, no. 1, pp. 76–81, 2005. 21, 22, 23

[102] N. Sharma, V. Mushahwar, and R. Stein, "Dynamic optimization of FES and orthosis-based walking using simple models," *IEEE Transactions on Neural Systems and Rehabilitation Engineering*, vol. 22, no. 1, pp. 114–126, 2014. 21, 22

[103] N. A. Kirsch, N. A. Alibeji, and N. Sharma, "Model predictive control-based dynamic control allocation in a hybrid neuroprosthesis," in *Dynamic Systems and Control Conference*, vol. 46209. American Society of Mechanical Engineers, 2014, p. V003T43A003. 21, 22, 23

[104] N. A. Alibeji, N. A. Kirsch, and N. Sharma, "An adaptive low-dimensional control for a hybrid neuroprosthesis," *IFAC-PapersOnLine*, vol. 48, no. 20, pp. 303–308, 2015. 21, 22

[105] X. Tu, X. Zhou, J. Li, C. Su, X. Sun, H. Han, X. Jiang, and J. He, "Iterative learning control applied to a hybrid rehabilitation exoskeleton system powered by pam and fes," *Cluster Computing*, pp. 1–14, 2017. 21, 23

[106] V. Dietz, "Spinal cord pattern generators for locomotion," *Clinical Neurophysiology*, vol. 114, no. 8, pp. 1379–1389, 2003. 23

[107] L. Zimmerli, A. Duschau-Wicke, A. Mayr, R. Riener, and L. Lunenburger, "Virtual reality and gait rehabilitation augmented feedback for the lokomat," in *Virtual Rehabilitation International Conference, 2009.* IEEE, 2009, pp. 150–153. 23

[108] W. Hassani, S. Mohammed, H. Rifaï, and Y. Amirat, "Powered orthosis for lower limb movements assistance and rehabilitation," *Control Engineering Practice*, vol. 26, pp. 245–253, 2014. 27, XXV

[109] S. Vlad and N. M. Roman, *International Conference on Advancements of Medicine and Health Care Through Technology; 12th-15th October 2016, Cluj-Napoca, Romania: MEDITECH 2016*. Springer, 2017, vol. 59. 26

[110] M. B. I. Reaz, M. S. Hussain, and F. Mohd-Yasin, "Techniques of emg signal analysis: detection, processing, classification and applications," *Biological procedures online*, vol. 8, no. 1, pp. 11–35, 2006. 26

[111] "Electrode placement and functional movement," https://www.axelgaard.com/Education/Knee-Extension, accessed: 2020-06-03. 28, 37, XXV

[112] S. Oh and K. Kong, "High-precision robust force control of a series elastic actuator," *IEEE/ASME Transactions on Mechatronics*, vol. 22, no. 1, pp. 71–80, 2017. 32

[113] T.-J. Yeh and F.-K. Wu, "Modeling and robust control of worm-gear driven systems," *Simul. Model. Pract. Th*, vol. 17, no. 5, pp. 767–777, 2009. 34, 35, 36

[114] J. J. Craig, *Introduction to robotics: mechanics and control*. Pearson Prentice Hall Upper Saddle River, 2005, vol. 3. 38

[115] P. O. Riley, D. E. Krebs, and R. A. Popat, "Biomechanical analysis of failed sit-to-stand," *IEEE Transactions on Rehabilitation Engineering*, vol. 5, no. 4, pp. 353–359, 1997. 40

[116] E. Dombre and W. Khalil, *Robot manipulators: modeling, performance analysis and control*. John Wiley & Sons, 2013. 42

[117] D. A. Winter, *Biomechanics and motor control of human movement*. John Wiley & Sons, 2009. 42

[118] V. Bonnet and G. Venture, "Fast determination of the planar body segment inertial parameters using affordable sensors," *IEEE Transactions on neural systems and rehabilitation engineering*, vol. 23, no. 4, pp. 628–635, 2015. 43

[119] R. Kikuuwe, S. Yasukouchi, H. Fujimoto, and M. Yamamoto, "Proxy-based sliding mode control: a safer extension of pid position control," vol. 26, no. 4, pp. 670–683, 2010. 48, 49, 52, 53, 60

[120] W. Huo, S. Mohammed, and Y. Amirat, "Impedance reduction control of a knee joint human-exoskeleton system," no. 99, pp. 1–16, 2018. 50

[121] A. Mohammadi, M. Tavakoli, H. J. Marquez, and F. Hashemzadeh, "Nonlinear disturbance observer design for robotic manipulators," *Control Eng. Pract.*, vol. 21, no. 3, pp. 253–267, 2013. 51, 89, 90, 91

[122] X. Li, Y. Pan, G. Chen, and H. Yu, "Multi-modal control scheme for rehabilitation robotic exoskeletons," *Int. J. Rob. Res*, vol. 36, no. 5-7, pp. 759–777, 2017. 57

[123] A. Calanca and P. Fiorini, "A rationale for acceleration feedback in force control of series elastic actuators," 2018. 64

[124] J.-J. E. Slotine and W. Li, "On the adaptive control of robot manipulators," *The international journal of robotics research*, vol. 6, no. 3, pp. 49–59, 1987. 71

[125] H. Rifai, S. Mohammed, B. Daachi, and Y. Amirat, "Adaptive control of a human-driven knee joint orthosis," in *IEEE International Conference on Robotics and Automation (ICRA)*, 2012, pp. 2486–2491. 71

[126] S. Buatois, D. Miljkovic, P. Manckoundia, R. Gueguen, P. Miget, G. Vançon, P. Perrin, and A. Benetos, "Five times sit to stand test is a predictor of recurrent falls in healthy community-living subjects aged 65 and older," *Journal of the American Geriatrics Society*, vol. 56, no. 8, pp. 1575–1577, 2008. 94, 95

[127] K. Kong, J. Bae, and M. Tomizuka, "Control of rotary series elastic actuator for ideal force-mode actuation in human–robot interaction applications," vol. 14, no. 1, pp. 105–118, 2009. 96

[128] W. HUO, "Assistive control strategies for lower-limb exoskeletons," Theses, Université Paris-Est, Dec. 2016. [Online]. Available: https://tel.archives-ouvertes.fr/tel-01534826 98

[129] P. O. Riley, D. E. Krebs, and R. A. Popat, "Biomechanical analysis of failed sit-to-stand," *IEEE Transactions on rehabilitation engineering*, vol. 5, no. 4, pp. 353–359, 1997. 101, 126

[130] G. Aguirre-Ollinger, J. E. Colgate, M. A. Peshkin, and A. Goswami, "Active-impedance control of a lower-limb assistive exoskeleton," in *Rehabilitation Robotics, 2007. ICORR 2007. IEEE 10th International Conference on*. IEEE, 2007, pp. 188–195. 115

[131] T. Kesar and S. Binder-Macleod, "Effect of frequency and pulse duration on human muscle fatigue during repetitive electrical stimulation," *Experimental physiology*, vol. 91, no. 6, pp. 967–976, 2006. 116

[132] M. B. I. Reaz, M. Hussain, and F. Mohd-Yasin, "Techniques of emg signal analysis: detection, processing, classification and applications," *Biological procedures online*, vol. 8, no. 1, p. 11, 2006. 120, 128

[133] J. Liu, C. Drutz, R. Kumar, L. McVicar, R. Weinberger, D. Brooks, and N. M. Salbach, "Use of the six-minute walk test poststroke: is there a practice effect?" *Archives of physical medicine and rehabilitation*, vol. 89, no. 9, pp. 1686–1692, 2008. 120

[134] N. M. Salbach, K. K. O'brien, D. Brooks, E. Irvin, R. Martino, P. Takhar, S. Chan, and J.-A. Howe, "Considerations for the selection of time-limited walk tests poststroke: a systematic review of test protocols and measurement properties," *Journal of Neurologic Physical Therapy*, vol. 41, no. 1, pp. 3–17, 2017. 120

[135] J. H. Carr, *Neurological Rehabilitation, 2/e*. Elsevier India, 2014. 123, 125

[136] H. Kagaya, Y. Shimada, K. Ebata, M. Sato, K. Sato, T. Yukawa, and G. Obinata, "Restoration and analysis of standing-up in complete paraplegia utilizing functional electrical stimulation," *Archives of physical medicine and rehabilitation*, vol. 76, no. 9, pp. 876–881, 1995. 125

[137] R. B. Shepherd and A. Gentile, "Sit-to-stand: functional relationship between upper body and lower limb segments," *Human movement science*, vol. 13, no. 6, pp. 817–840, 1994. 125

[138] F. Mandrile, D. Farina, M. Pozzo, and R. Merletti, "Stimulation artifact in surface emg signal: effect of the stimulation waveform, detection system, and current amplitude using hybrid stimulation technique," *IEEE Transactions on neural systems and rehabilitation engineering*, vol. 11, no. 4, pp. 407–415, 2003. 126

[139] S. Qiu, J. Feng, R. Xu, J. Xu, K. Wang, F. He, H. Qi, X. Zhao, P. Zhou, L. Zhang *et al.*, "A stimulus artifact removal technique for semg signal processing during functional electrical stimulation," *IEEE Transactions on Biomedical Engineering*, vol. 62, no. 8, pp. 1959–1968, 2015. 127

[140] B. R. Etnyre and L. D. Abraham, "Antagonist muscle activity during stretching: a paradox re-assessed." *Medicine and Science in Sports and Exercise*, vol. 20, no. 3, pp. 285–289, 1988. 127

[141] A. Serefoglu, U. Sekir, H. Gür, and B. Akova, "Effects of static and dynamic stretching on the isokinetic peak torques and electromyographic activities of the antagonist muscles," *Journal of sports science & medicine*, vol. 16, no. 1, p. 6, 2017. 127

[142] F. Attal, Y. Amirat, A. Chibani, and S. Mohammed, "Automatic recognition of gait phases using a multiple-regression hidden markov model," *IEEE/ASME Transactions on Mechatronics*, vol. 23, no. 4, pp. 1597–1607, 2018. V

[143] J. Perry, J. R. Davids *et al.*, "Gait analysis: normal and pathological function," *Journal of Pediatric Orthopaedics*, vol. 12, no. 6, p. 815, 1992. V

List of figures

List of tables

List of publications

Journals

- Huo, W., **Alouane, M. A.**, Vincent Bonnet, Jian Huang, Yacine Amirat, Ravi Vaidyanathan, a& Samer Mohammed. Impedance Modulation Control of a Lower Limb Exoskeleton to Assist Sit-to-Stand Movements. IEEE Transactions on Robotics. (2020). (Under-Review)

- Huo, W., **Alouane, M. A.**, Amirat, Y., & Mohammed, S. (2019). Force Control of SEA-Based Exoskeletons for Multimode Human–Robot Interactions. IEEE Transactions on Robotics, Vol. 36 No. 2, pp. 570-577, April 2020.

- **Alouane, M. A.**, Rifai, H., Kim, K., Amirat, Y., & Mohammed, S. Hybrid impedance control of a knee joint orthosis, Industrial Robot, Vol. 46 No. 2, pp. 192-201, March 2019.

Peer-review Conferences

- **Alouane, M. A.**, Rifai, H., Amirat, Y., & Mohammed, S. Cooperative Control for Knee Joint Flexion-Extension Movement Restoration. In Proc. Of the IEEE/RSJ International Conference on Intelligent Robots and Systems, IROS 2018, Madrid, Spain, pp. 5175-5180, Oct. 2018.

- **Alouane, M. A.**, Huo, W., Rifai, H., Amirat, Y., & Mohammed, S. (2019). Hybrid FES-Exoskeleton Controller to Assist Sit-To-Stand movement. In Proc. Of the 2nd IFAC Conference on Cyber-Physical & Human-Systems, CPHS 2018, Miami, United States, , pp. 352-357, Dec. 2018.

Book Chapters

- **Alouane, M. A.**, W. Huo, H. Rifai, Y. Amirat, & S. Mohammed. Assistive Control Strategies for a Lower-Limb Exoskeleton (E-ROWA). In Wearable Robotics for Motion Assistance and Rehabilitation, Springer, 2020.